Lancaster University

Lancashire Teaching Hospitals NHS
NHS Foundation Trust

Targeting the gut microbiota to improve patient outcomes following stoma reversal surgery

Ella Southern (BSc Hons)

This thesis is submitted for the degree of
MSc by Research

November 2025

Biomedical and Life Sciences

Declaration

I, Ella Southern, confirm that the work presented in this thesis is entirely my own and has not been submitted in full or in part for the award of a higher degree at any other educational institution. No sections of this thesis have been published. I confirm that information derived from other sources has been cited accordingly.

Abstract

Temporary faecal diversion by loop ileostomy disrupts the sensitive intestinal environment, resulting in significant atrophy and rendering the downstream bowel defunctioned. Upon stoma reversal, 40% of patients experience morbidities such as intestinal inflammation and reduced bowel function associated with poor intestinal restoration. Strategies to improve epithelial repair following loop ileostomy remain underexplored, with probiotics, synbiotics, and mechanical stimulation providing limited improvements. Here, the impact of prebiotic stimulation of the defunctioned ileum was investigated by assessing changes to the epithelial morphology, immune cell populations, and bacterial composition. Two patient cohorts were studied: an unfed group (n=35), who did not receive pre-operative enteral feeding, and a prebiotic-fed group (n=5), who received Orafti® Synergy1 (inulin-oligofructose) diluted in Ensure® nutrient shake via a stoma feeding tube for 2-27 days before reversal. Full-thickness samples were obtained from proximal (functional) and distal (defunctioned) ileal segments at reversal. Tissues were analysed by histology, flow cytometry, and phylum-specific 16S rDNA qPCR. Faecal diversion did not alter macrophage, T helper, or TLR5+ cell frequencies in the lamina propria, but was associated with an increase in CD11c+ dendritic cells, which may reflect an anti-inflammatory response. Morphological analyses revealed that prebiotic feed significantly increased crypt depth in the defunctioned ileum compared with unfed tissue ($p=0.0365$), suggesting increased epithelial cell proliferation. Compared with the unfed bowel, villus height was no longer atrophied, indicating that villus restoration was underway. Interestingly, CD11c+ dendritic cells were reduced after prebiotic feeding, perhaps suggesting a return toward immune homeostasis. Phylum-specific microbial profiling revealed a significant increase in Firmicutes abundance in prebiotic-fed ileum, consistent with a shift toward eubiosis. Future species-level analysis via 16S sequencing is required to confirm microbial restoration and validate the link to epithelial outcomes. Collectively, these findings conclude that enteral prebiotic feeding may partially restore microbiota, promote epithelial renewal, and modulate immune cell populations. This highlights the therapeutic potential of prebiotic stoma feeding in improving mucosal health before ileostomy reversal, with implications for reducing postoperative complications. Future work should explore optimal feeding time and investigate species-level microbial changes by 16S sequencing.

Acknowledgements

I would like to take this opportunity to thank my supervisor, Dr Rachael Rigby, for her support and guidance throughout this project. I would also like to thank my secondary supervisor, Dr John Worthington, for his valuable help with flow cytometry analysis.

Also, I am grateful to the surgical team at Lancashire Teaching Hospitals Trust for their key role in this research project and for allowing me the opportunity to observe the stoma reversal procedure.

A big thanks to Dr Elisabeth Shaw for her training and advice in flow cytometry and histology.

Lastly, I am grateful for my family, friends and my partner for the endless support and motivation throughout this project and always.

Abbreviations

16S rDNA RT-qPCR	16S Ribosomal-DNA Real-Time Quantitative PCR
AMP	Antimicrobial Proteins
APES	3-Aminopropyltriethoxysilane
CSCM	Crypt-specific core microbiota
DAMP	Damage-associated molecular pattern
DC	Dendritic cell
dH_2O	Distilled H_2O
EGFR	Epidermal growth factor receptor
FMT	Faecal Microbiota Transplantation
Fz	Frizzled
GF	Germ free
GI	Gastrointestinal
GPCR	G-protein coupled receptor
H&E	Haematoxylin and Eosin
HDAC	Histone deacetylase
HEV	High endothelial venules
HMP	Human Microbiome Project
IBD	Irritable bowel disease *(usually: Inflammatory bowel disease)*
IDO	Indoleamine-2,3-dioxygenase
IEC	Intestinal Epithelial Cell
IFN	Interferon
Ig	Immunoglobulin
IL	Interleukin
ILC	Innate lymphoid cell
ISC	Intestinal stem cells
LGR5	Leucine-rich repeat-containing G-protein-coupled receptor 5
LP	Lamina propria
LPS	Lipopolysaccharide
LRP	Lipoprotein receptor-related protein
M cell	Microfold cell
MAMP	Microbe-associated molecular pattern
MLN	Mesenteric lymph nodes
MUC2	Mucin 2
NF-κB	Nuclear Factor-κB
NICD	Notch intracellular domain
NK	Natural killer (cell)
NLR	Nod-like Receptor
PAMP	Pathogen-associated molecular pattern
PCNA	Proliferating Cell Nuclear Antigen
PCP	Planar cell polarity
PCR	Polymerase Chain Reaction

PFA	Paraformaldehyde
PP	Peyer's patch
PSA	Polysaccharide A
RORγ^{+}	Retinoic acid receptor-related orphan receptor-γ-positive
SBA	Secondary bile acids
SCFA	Short Chain Fatty Acids
TCF	T-cell factor
TCR	T cell receptor
TGF-β	Transforming Growth Factor-β
TLR	Toll-like receptor
T_{reg}	Regulatory T cell

Contents

1 Introduction

1.1 Intestinal Renewal and Repair

1.1.1 The Intestinal Mucosa

The mucosa represents the innermost layer of the intestine and plays a central role in nutrient absorption and protecting the underlying tissues from the luminal contents. It is organised into three layers: the epithelium, lamina propria (LP), and muscularis (Hickey *et al.*, 2023). The epithelium forms an important biochemical and physical barrier made up of a single layer of intestinal epithelial cells (IECs), separating the luminal contents from the underlying tissues. The main IEC type in the intestine is the absorptive enterocytes, which are columnar epithelial cells specialised for nutrient uptake (Johansson *et al.*, 2011). In the small intestine, the epithelium is structured into protrusions known as villi and the invaginations between them, the crypts of Lieberkühn, allowing optimised surface area for nutrient absorption.

Secretory IECs, including enteroendocrine, goblet, and Paneth cells, make up a large proportion of the epithelial layer, maintaining barrier function and aiding nutrient absorption (Gustafsson and Johansson, 2022). Goblet cells secrete glycosylated mucins such as mucin 2 (MUC2) into the lumen, creating the first line of defence against microbial invasion, the mucus layer (Figure 1.1). Paneth cells release antimicrobial proteins (AMPs) such as defensins, cathelicidins and lysozyme, which kill or inhibit the growth of bacteria (Kim and Ho, 2010). Enteroendocrine cells link the central and enteric neuroendocrine systems by secreting hormones that regulate digestion. The diverse functions of these IEC cell types and the tight junctions joining them collectively form an effective barrier against the environment, while selectively allowing the absorption of nutrients, electrolytes, and water.

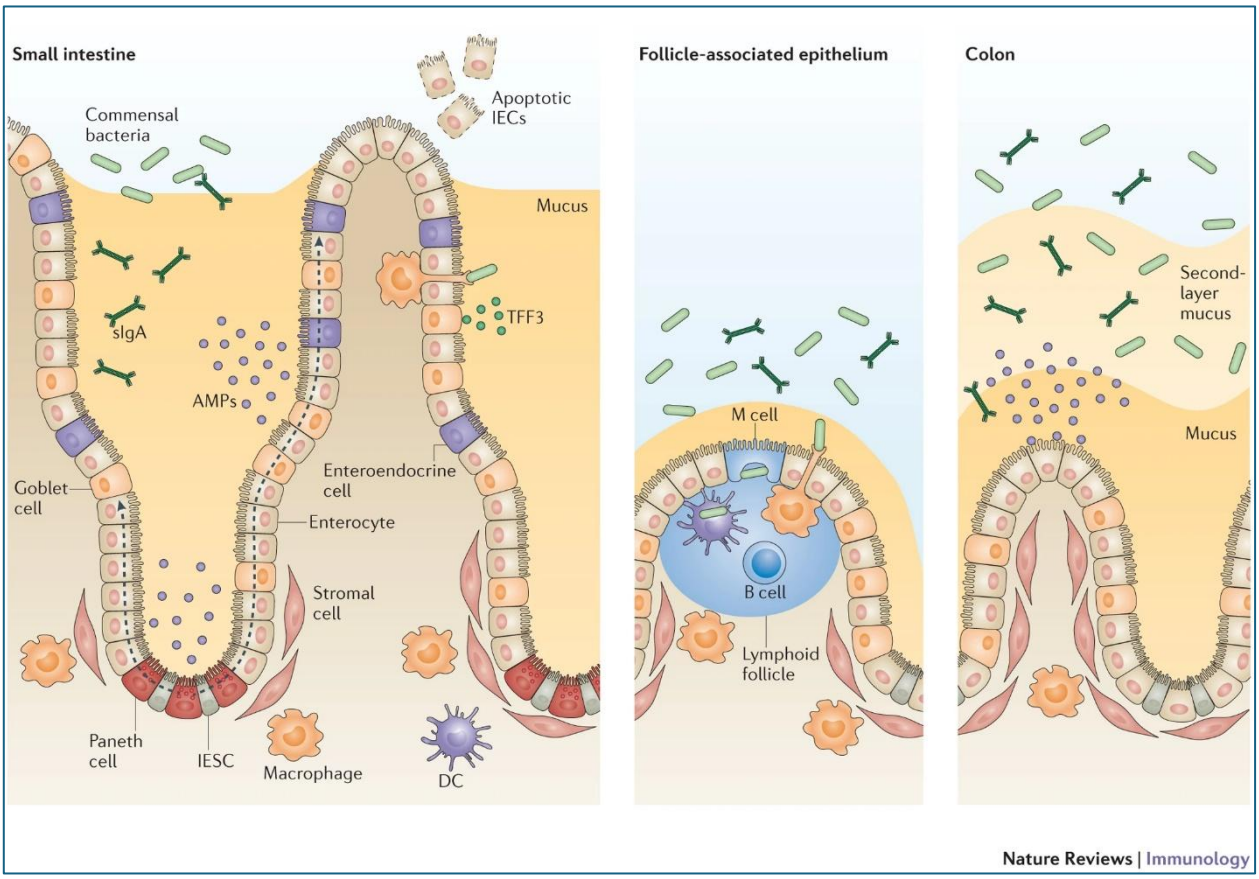

Figure 1.1: ***Structure of the intestinal epithelial barrier (Peterson and Artis, 2014).*** IECs, such as goblet and enteroendocrine cells, line the villi of the small intestine, functioning in nutrient absorption and immune protection. Paneth cells remain in the base of the crypt, where they secrete mucus and AMPs, promoting the exclusion of bacteria from the epithelial surface. Immune follicles in the intestine are also lined with epithelial cells, including specialised microfold (M) cells, which mediate the transport of antigens and live bacteria across the epithelial barrier. The colon epithelium is primarily composed of enterocytes, covered by a double mucus layer specialised for protection against mechanical damage and pathogens. Secretory IgA is released by the epithelial cells into the mucus layer, preventing pathogen attachment and further enhancing barrier function.

Beneath the epithelium is the LP, a layer of connective tissue that provides structural support, vascularisation, and lymphoid drainage. The LP is a critical site for immune responses, acting as a coordination centre for interactions between commensal microbiota, IECs, and immune cells (Ogino and Takeda, 2023). The LP is infiltrated with immune cells, including innate (e.g. macrophages, dendritic cells, innate lymphoid

cells, and neutrophils) and adaptive (e.g. $CD4^+$, $CD8^+$ and regulatory T cells) immune populations.

Overall, the mucosa acts as a dynamic interface between the luminal contents and underlying tissues, facilitating selective nutrient absorption while simultaneously maintaining a physical and immunological barrier against pathogens and damage. The ability of the epithelium to self-renew effectively is crucial in maintaining the integrity of this barrier, protecting against infection, mechanical injury, inflammation and malabsorption.

1.1.2 Intestinal Renewal and Its Protective Function

Regeneration of the intestinal epithelium is a tightly regulated, continuous process of cell turnover that ensures the maintenance of barrier function. IECs are continuously replenished by *Lgr5*$^+$ intestinal stem cells (ISCs) in the base of the crypts, allowing the fastest turnover in the human body, with a turnaround time of just 4-5 days (Foerster *et al.*, 2022). The proliferation, differentiation, and function of these progenitor cells are tightly controlled as they move up the crypt-villus axis, as shown in Figure 1.2. Progenitor cells differentiate into specialised epithelial cell types, including enterocytes, goblet cells, enteroendocrine cells, and Paneth cells, in response to signals from surrounding cells in the ISC niche.

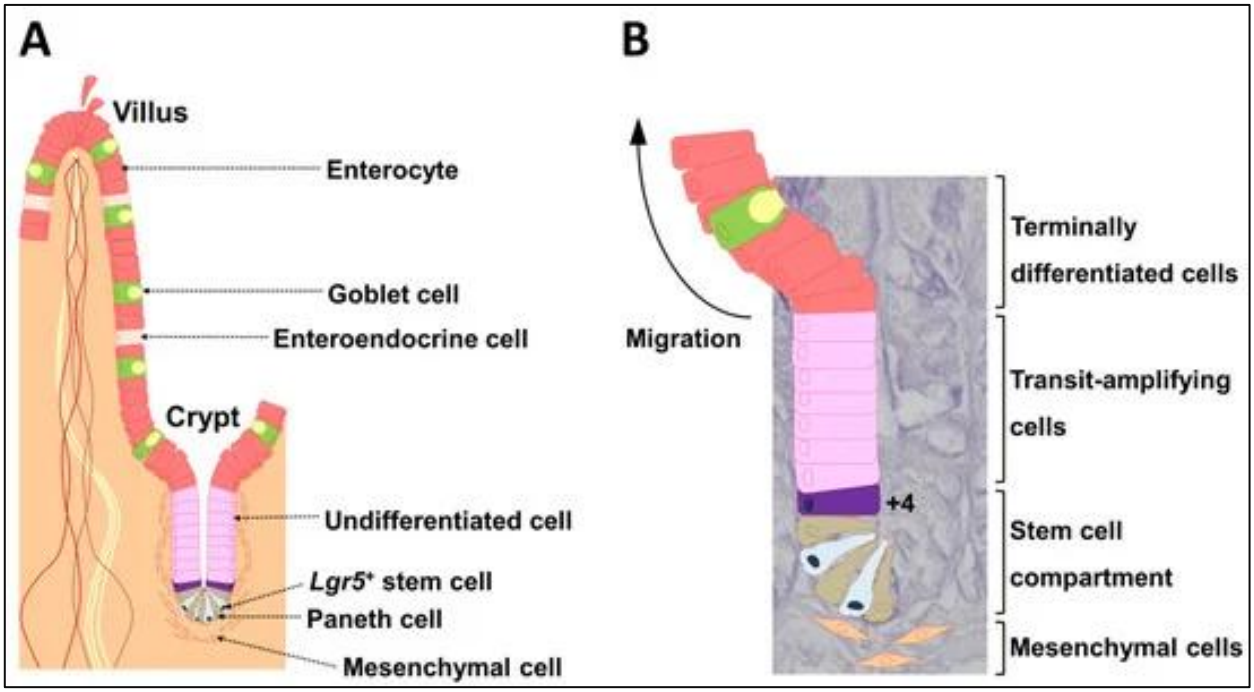

Figure 1.2 – ***The crypt ISC niche (Takahashi and Shiraishi, 2020).*** **A)** Schematic representation of the intestinal crypt-villus axis. *Lgr5*$^{+}$ stem cells reside at the very bottom of the crypt, flanked by Paneth cells and surrounded by subepithelial mesenchymal cells. Starting as *Lgr5*$^{+}$ stem cells in the base of the crypt and resulting in terminally differentiated cells, the IECs become more differentiated moving up the crypt-villus axis. Daughter cells differentiate into discrete populations of cells as they migrate upwards into the gut lumen reaching the villus tip. Apoptotic terminally differentiated cells are removed from the tip of the villus once they have performed their function, allowing space for newly differentiated cells. **B)** The hierarchical organisation of stem cells is demonstrated in a DAPI-stained crypt.

Epithelial regeneration is vital in maintaining the integrity of the gut barrier, allowing nutrient absorption while protecting against toxins and responding to injury. Epithelial injury can occur as a result of mechanical stress or inflammatory pathways involved in the pathogenesis of bowel conditions such as inflammatory bowel disease (IBD). During injury or inflammation, epithelial repair is mediated by rapid migration and proliferation of ISCs and neighbouring cells via growth factors such as epidermal growth factor (EGF), regulated by the NF-kB pathway and toll-like receptor (TLR) signalling. At the early phase of injury, epithelial cells at the wound margin alter their

polarity and migrate to cover the exposed basement membrane through actin cytoskeleton remodelling. TLR activation by recognition of bacterial ligands promotes epithelial migration and production of AMPs, initiating barrier repair and activating epidermal growth factor receptor (EGFR) signalling (Shaykhiev, Behr and Bals, 2008).

The NF-kB pathway is a key driver of wound healing under inflammatory conditions and promotes the expression of survival and proliferation-promoting genes, which further stimulate epithelial turnover (Spehlmann and Eckmann, 2009). Differentiation of epithelial progenitors into specialised cell types must then occur to restore epithelial functionality. Balance is maintained between Paneth and goblet cells through NF-kB, Wnt and Sox9 regulation (Brischetto *et al.*, 2021). This ensures the restoration of a fully functional epithelial layer, maintaining barrier function rapidly following injury.

These signalling pathways can become dysregulated as a result of genetic, molecular and cellular alterations, damaging the gut barrier and often contributing to bowel disease (Sommer *et al.*, 2021). Disrupted barrier function can cause hyperpermeability or 'leaky' gut, exposing the underlying mucosal layers to microbes and toxins from the luminal environment. Upon detection of microbial antigens, mucosal immune cells are recruited, releasing cytokines and possibly triggering inflammatory pathways (Zundler *et al.*, 2019). This occurs in IBD, where defects in the epithelial layer allow infiltration of microbiota, activating dendritic cells (DCs) and macrophages in the LP (Christovich and Luo, 2022). This induces the recruitment of pro-inflammatory T cells, causing tissue injury and chronic inflammation due to hypersensitivity to microbial antigens (Sartor, 2006).

Barrier function must be maintained by tightly regulated cell signalling pathways that promote IEC proliferation and differentiation to allow wound healing while preventing uncontrolled ISC proliferation.

1.1.3 Signalling Pathways that Mediate Regeneration

The rapid and continuous process of self-regeneration in the intestinal epithelium is tightly regulated by signalling pathways such as Wnt/β-catenin, which maintains ISC

activity, and Notch and Hippo pathways, which coordinate differentiation and proliferation. Paneth cells in the crypts control ISCs by expressing ligands such as epidermal growth factor (EGF), transforming growth factor-α (TGFα), Wnt3, and delta-like ligand 4 (DLL4).

The Wnt signalling pathway is a highly conserved cell-signalling mechanism used to control nuclear gene expression to control cell proliferation, differentiation, and migration (MacDonald, Tamai and He, 2009). There are two main pathways of Wnt signalling, both of which occur in the gut epithelium. The canonical Wnt/β-catenin pathway regulates stem cell maintenance, fate determination and proliferation, whereas the non-canonical Wnt pathway occurs independently of β-catenin and is important in cell polarity and migration. The central role of Wnt signalling in the gut is demonstrated by the loss of all secretory cells when Wnt inhibitors such as dickkopf 1 are overexpressed (Pinto *et al.*, 2003). Wnt ligands are secreted from mesenchymal cells in the ISC niche, creating a gradient along the crypt-villus axis, where Wnt-regulated transcription is strongest at the base of the crypt, inducing expression of stem cell lineage markers such as *Lgr5*. The non-canonical Wnt pathway directs the alignment of IECs as they differentiate during tissue regeneration, helping to maintain the integrity of the epithelium. Intestinal barrier function relies on the formation of tight junctions, which are regulated by the Wnt/$Ca2^{+}$ pathway, ensuring that epithelial permeability is optimised (Crosnier, Stamataki and Lewis, 2006). This pathway utilises the regulation of intracellular $Ca2^{+}$ to mediate migration, adhesion, and contraction of IECs, ensuring an integral barrier with highly selective permeability.

A multitude of additional signalling pathways influence intestinal renewal and repair in response to external stimuli. Notch signalling is essential for maintaining the proliferative state of Lgr5+ stem cells in the crypt, as proliferation ceases in the absence of Notch ligands (Van Es *et al.*, 2005). Moreover, TLR, NF-kB, Hippo/YAP, JAK/STAT and EGFR signals have specialised functions in promoting intestinal renewal and maintaining barrier integrity. Upregulation of these pathways by microbial metabolites and immune signals such as pro-inflammatory cytokines is crucial in promoting intestinal repair and maintaining homeostasis.

1.2 Intestinal Immunology

1.2.1 The Intestinal Mucosa as an Organ of Immunology

The intestinal mucosa is constantly exposed to trillions of microbes, digestive enzymes, food-derived antigens and metabolites; therefore, its immune system must be highly specialised to balance tolerance and defence mechanisms effectively (Ahluwalia, Magnusson and Öhman, 2017). This is achieved through a robust immune front comprising a large population of immune cells, including specialised secretory IEC types, macrophages, DCs, and lymphocytes (Allaire *et al.*, 2018). Luminal contents and bacteria interact initially with the mucus layer, which provides an anti-microbial environment containing IgA and antimicrobial peptides, effectively reducing the bacterial load that reaches the epithelium.

As well as forming a physical barrier, IECs have intrinsic anti-microbial properties, acting as part of the mucosal immune system. For instance, paneth cells in the crypt are the primary source of AMPs, including defensins, which form pores in bacterial membranes, lysosymes, which lyse bacterial peptidoglycans, and RegIIIγ, which kills gram-positive bacteria (Bevins and Salzman, 2011). Moreover, IECs express pattern recognition receptors (PRRs) such as TLRs and NOD-like receptors (NLRs), enabling recognition of microbial ligands (Schären and Hapfelmeier, 2021). As well as interacting with the innate immune system, IECs are responsible for transporting secretory IgA into the mucus.

Gut-associated lymphoid tissue (GALT) is a primary lymphoid organ composed of immune cells residing in the LP, intraepithelial lymphocytes, and immune cells located in organised lymphatic tissue. GALT accounts for 70% of the immune system by weight and is organised into isolated lymphoid follicles (ILFs) in the epithelial layer. In the small intestine, specialised ILFs called Peyer's patches (PP) (Figure 1.3) act as a site for immune surveillance, where antigens are transported across the membrane by microfold cells (M cells) and presented by macrophages to activate a lymphocyte response (Mörbe *et al.*, 2021).

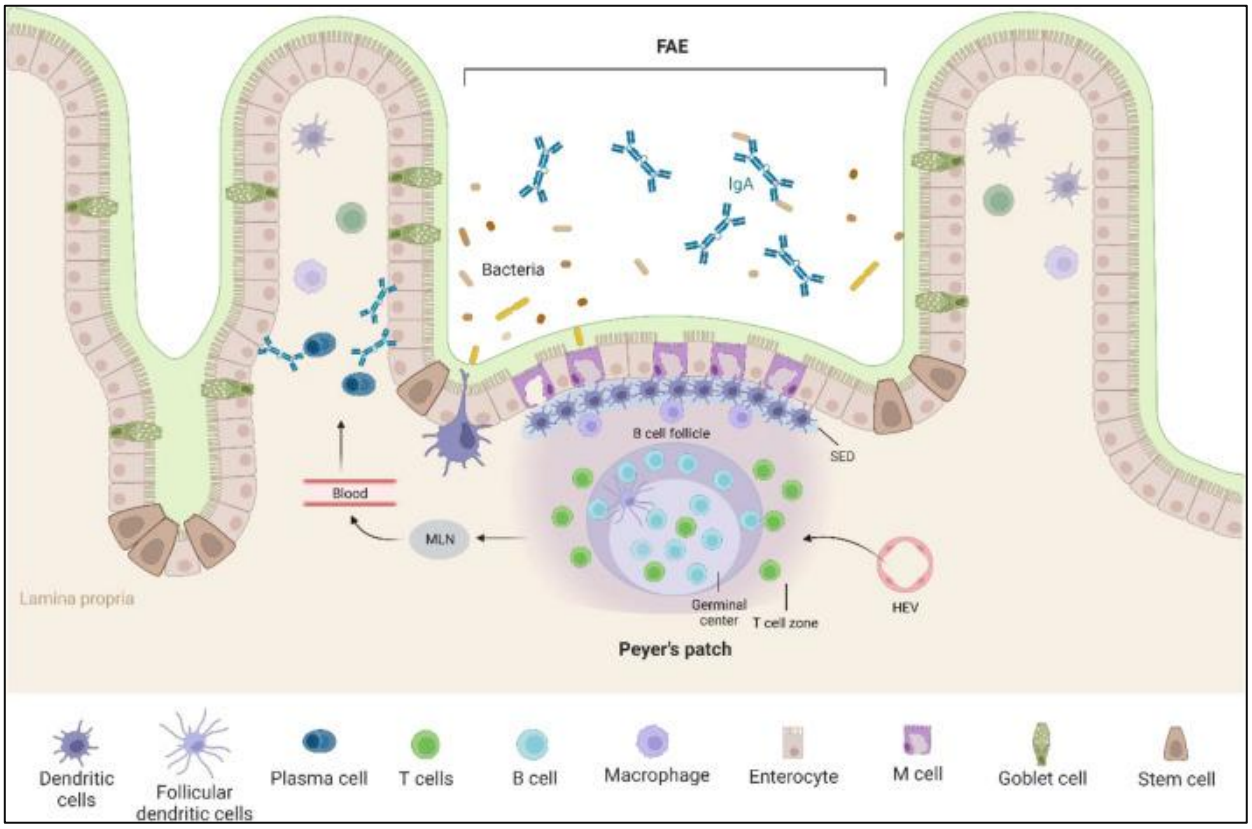

Figure 1.3 - ***Cellular composition of Peyer's patches in the small intestine, a schematic illustration (Park et al., 2023).*** The PP is enclosed by follicle-associated endothelium (FAE), containing specialised antigen-transporting M cells. The subepithelial dome (SED) underlying the FAE houses a dense population of antigen-processing cells such as DCs and macrophages. T and B Lymphocytes enter the PP via high endothelial venules (HEVs) and form large B cell follicles and small T cell zones surrounding them. Interactions between B and T cells at the follicle-T- T cell zone lead to the differentiation and proliferation of B cells in response to a specific antigen. Activated B cells form a population of IgA-secreting cells, producing IgA antibodies that are transported back across the epithelium as secretory-IgA (S-IgA). Generated effector cells leave the PPs via lymphatic vessels and enter the circulation via the mesenteric lymph nodes (MLNs).

The loose connective tissues of the LP contain many circulating IgA plasma cells, T cells, macrophages, DCs, and stromal cells, forming a key microenvironment for immune tolerance and defence. Macrophages are abundant in the LP, exhibiting a tolerogenic phenotype, characterised by high levels of antigen sampling and anti-

inflammatory cytokine production even in response to microbial antigens (Delfini *et al.*, 2022).

In response to pathogenic stimuli, innate lymphoid cells (ILCs), neutrophils, and mast cells are also recruited. Natural killer (NK) cells are a member of the group 1 ILCs with intrinsic and innate cytotoxicity, crucial in the anti-tumour and anti-viral mechanisms in the gut. These large granular lymphocytes work similarly to cytotoxic T cells, without the requirement for prior antigen exposure (Abel *et al.*, 2018). NK cells can distinguish self from non-self, using the absence of MHC-I or the presence of PAMPs/DAMPs, which can activate receptors on the NK cell surface. To target pathogenic or damaged cells, NK cells can use a range of mechanisms, including perforins and granzymes, which form pores in the target cell membrane and induce apoptosis.

Lymphocytes in the LP include $CD4^+$ and $CD8^+$ T cells, plasma cells and memory cells. These adaptive cell types are crucial mediators of the intestinal immune response, ensuring the rapid clearance of invading pathogens while downregulating inflammatory responses under normal conditions to maintain a tolerogenic environment.

1.2.2 Maintaining Immune Tolerance in the Gut

IECs recognise bacterial components via toll-like receptors (TLRs), and deliver their antigens to underlying mucosal immune cells such as macrophages and DCs to induce tolerant, anti-inflammatory signals (McDole *et al.*, 2012). M cells are specialised epithelial cells involved in the uptake of luminal antigens to initiate antigen-specific responses in the PP, such as IgA production. Innate and adaptive immune cells of the LP function collaboratively to provide a quiescent environment that is tolerant to microbiota whilst recognising and defending against pathogenic stimuli.

Luminal contents transported across the epithelium by M cells are sampled by macrophages and DCs in the underlying mucosa. These are important mediators of the immune response to commensal bacteria in the intestinal epithelium, supporting the balance of tolerance and immunity (Ruane and Lavelle, 2011). For instance, subepithelial

macrophages specialise in phagocytosing luminal contents and releasing anti-inflammatory cytokines to maintain quiescence under homeostatic conditions (Cummings *et al.*, 2016). During tissue damage or infection, innate immune populations of the mucosa can adapt various phenotypes through the expression of surface receptors such as CD molecules. For instance, $CD163^+$ macrophages adapt a pro-inflammatory phenotype during tissue damage, promoting epithelial repair. Moreover, CD64 is expressed on monocytes and macrophages under homeostatic conditions, and is upregulated on APCs, such as DCs, during inflammation to increase antibody detection, enabling several defence mechanisms such as phagocytosis and antibody-dependent cell-mediated cytotoxicity (ADCC) (Tamoutounour *et al.*, 2012). This makes CD64 a useful biomarker of bacterial infections, IBD, and sepsis, with high levels indicating the presence of an active inflammatory response (Agarwal, 2020).

Barrier integrity of the intestinal mucosa is also regulated by ILCs, a small group of hematopoietic cells commonly found at epithelial surfaces. Rather than expressing antigen-specific receptors, ILCs respond to cytokine signalling from other immune cells and can recognise non-specific PAMPs and DAMPs (Spits and Cupedo, 2012). ILC3 cells, together with $CD4^+$ T cells, are the main source of IL-22 in the gut, which is an important cytokine in epithelial-mediated immune responses such as wound repair (Lamkanfi and Dixit, 2012). Recognition of IL-22 by IECs maintains the gut barrier by stimulating the production of antimicrobial peptides RegIII-β and RegIII-γ, as well as promoting epithelial regenerative homeostasis (Zheng *et al.*, 2008). Moreover, ILCs are regulators of $CD4^+$ T cell responses to gut microbiota. Studies have shown that mice deficient in $ROR\gamma^+$ ILC3s had dysregulated adaptive immune responses to commensal bacteria and low-grade systemic inflammation (Hepworth *et al.*, 2013).

Regulatory T cells (T_{regs}) maintain intestinal homeostasis by suppressing inappropriate immune responses to gut bacteria and dietary antigens. The major T_{reg} population in the gut is comprised of $CD4^+$ T cells that express Foxp3, a forkhead transcription factor protein involved in the suppression of autoimmune responses by restricting the transcription of inflammatory cytokines (Kim, 2009). Naïve $CD4^+$ T cells differentiate into induced $Foxp3^+$ T_{reg}s upon T cell receptor (TCR) stimulation from innate cells such

as DCs and are upregulated in the presence of TGF-β and IL-2, and the absence of inflammatory cytokines that induce effector T cell responses (Chen *et al.*, 2003).

$CD103^+$ DCs are involved in the capture and processing of antigens to stimulate the development of induced T regulatory (iT_{regs}) cells, mediating tolerance (Coombes *et al.*, 2007). Unlike natural T_{regs} (nT_{reg}), they are antigen-specific, mediating immune tolerance towards a specific ligand, which is essential in maintaining immune homeostasis. Moreover, in the gut-associated lymphoid tissues (GALT), $CD103^+$ DCs are important generators of gut-tropic $CD8^+$ T cell subsets characterised by the upregulation of receptors CCR9 and $\alpha_4\beta_7$ (Johansson-Lindbom *et al.*, 2005). These are effector T cells that actively migrate towards a specific location within the gut tissues to perform their cytotoxic function. This process relies on the conversion of dietary vitamin A to retinoic acid, which occurs selectively in the small intestine. This process creates a tolerant environment as T_{reg}s migrate back to the mucosa, where they secrete IL-10 to suppress inflammatory pathways (Kurashima, Goto and Kiyono, 2013). If homeostasis between T_{regs} and effector T cells, such as Th17 cells, is lost, microbiota-reactive inflammatory pathways may occur, which can contribute to inflammatory bowel disease (Xu *et al.*, 2019).

1.2.3 Microbes Regulate Immune Tolerance

Studies in GF mice first revealed the role of the microbiota in intestinal T cell homeostasis, as GF animals had impaired T_{reg} function with reduced Foxp3 expression (Östman *et al.*, 2006). Gut microbiota may regulate immune tolerance directly by producing molecules that influence T_{reg}s, or indirectly by mediating IEC or immune cell signals. The gut microbiota is crucial in the development of the immune system in early life, and GF animals present with smaller MLNs, PPs and reduced populations of immune cells such as plasma cells, $CD4^+$ T cells and $CD8^+$ T cells (Takiishi, Fenero and Câmara, 2017). Gut microbiota can activate T_{reg}s directly via microbial antigens such as cell surface molecules, or by releasing metabolites or by products that indirectly influence the host immune system.

Specific recognition of microbial antigens by T cell receptors (TCRs) expressed by T_{regs} and their precursors is required in some instances. *Bacteroides fragilis* modulates T_{regs} via its capsular polysaccharide A (PSA), which acts as a unique T cell antigen that is able to mediate $CD4^+$ T cell proliferation in vitro (Mazmanian *et al.*, 2005). PSA is internalised and processed by $CD11c^+$ DCs in the MLN and presented on MHC-II to activate T_{reg} expansion via TLR2 binding. In this study, colonisation of GF mice with *B.fragilis* alone was sufficient to promote immune tolerance and correct immunological defects seen in the complete absence of a gut microbiome. Capsule polysaccharides from other commensal species have also been reported as inducers of $ROR\gamma^+$ T_{regs} via alternative mechanisms. For example, cell surface β-glucan/galactan (CSGG) polysaccharides derived from *Bifidobacterium bifidum* interact with TLR2-expressing DCs to induce T_{reg} cells via a TLR-mediated process (Verma *et al.*, 2018). Moreover, recent findings unveiled a unique mechanism used by *Escherichia coli* capsule components to induce $ROR\gamma^+$ T_{reg} cells (Sassone-Corsi *et al.*, 2022). Mice monocolonised with *E.coli* deficient in capsule-synthesis genes had impaired clonal expansion and differentiation of $ROR\gamma^+$ T cells, however capsule-less mutants were still able to induce IgA secretion, and were highly IgA coated. This could indicate that sequestering of potentially harmful bacteria into IgA^+ intraluminal casts is an alternative mechanism used to shield the immune system and maintain homeostasis without activating $T_{regs.}$

Alternatively, microbiota can induce T_{regs} via the release of metabolites or by-products. For instance, commensal *Clostridia* species release transforming growth factor-β (TGFβ) and indoleamine-2,3 dioxygenase (IDO) that stimulate colonic T_{regs} (Atarashi *et al.*, 2011). This study generated gnobiotic mice by inoculating GF mice with 46 strains of *Clostridium*. Compared to GF mice, these *Clostridium*-colonised animals accumulated significant populations of T_{regs} in the colon, providing an environment rich in TGF-β and IL-10. Short chain fatty acids (SCFAs) have also been proposed as T_{reg} cell regulators, thought of as small molecular mediators that act via inhibition of histone deacetylases or via GPRs (Arpaia *et al.*, 2013). This may induce histone or Foxp3 acetylation, but results supporting this hypothesis have not been entirely reproducible (Tao *et al.*, 2007). Alternative microbial metabolites such as secondary bile acids (SBAs) initiate

the differentiation of T_{reg} populations via transcriptional regulation. For instance, the SBA 3β- hydroxydeoxycholic acid (isoDCA) was shown to induce Foxp3 by suppressing immunostimulatory properties of DCs, promoting tolerance (Campbell *et al.*, 2020).

Overall, studies have demonstrated the impact of isolated bacterial components, rather than live bacteria, on immune tolerance via the induction of T_{reg} populations. This could indicate the possibility of using microbe-derived components to treat microbiota-related gastrointestinal disorders including colitis and Chron's disease.

1.3 The Gut Microbiota

1.3.1 Overview of the Gut Microbiota

Microorganisms inhabit nearly all surfaces of the human body and have developed a mutualistic relationship with their host over millions of years. One of the most densely populated microbial communities is found in the human gastrointestinal (GI) tract, housing over 100 trillion microorganisms collectively known as the gut microbiota (Thursby and Juge, 2017). This diverse microbial population plays a crucial role in shaping the functions of the immune, metabolic and nervous systems. The population density and types of microbes vary in different anatomical regions of the gut, increasing in abundance and diversity with progression through the GI tract. The colon is particularly rich in bacteria, with concentrations reaching up to 10^{11} cells per millilitre, rendering it one of the most microbially dense environments on Earth (Rinninella *et al.*, 2019).

In recent years, the gut microbiome has received increasing attention, with many studies suggesting its involvement in health and disease (Fan and Pedersen, 2021). An imbalance in the composition of the gut microbiota, known as dysbiosis, has been linked to obesity, diabetes, liver disease, cancer and neurological disorders (Cani, 2018). Microbial dysbiosis is caused by environmental alterations, lifestyle changes, or infection and alters the ratio between beneficial and harmful bacteria in the gut. The ongoing Human Microbiome Project (HMP) uses metagenomics to examine the composition and distribution of bacterial components in the human body and the

factors influencing their evolution. HMP studies have identified microbial genes involved in human metabolic pathways, including the production, consumption, and distribution of nutrients. To maintain systematic and intestinal homeostasis, the gut microbiota must be diverse and balanced.

1.3.2 Composition and Plasticity of the Intestinal Microbiota

Of the 100 trillion bacteria in the gut, the two dominant phyla, Bacteroidetes and Firmicutes, represent 90% of gut microbiota, with Actinobacteria, Proteobacteria, Fusobacteria, and Verrucomicrobia accounting for the remainder (Rinninella *et al.*, 2019). At least 160 species of bacteria can be found in the gut of a healthy individual, varying hugely between individuals based on environmental and genetic factors (MetaHIT Consortium *et al.*, 2010).

Firmicutes are the largest phylum in the gut, containing at least 200 genera of Gram-positive bacteria such as *Lactobacillus*, *Bacillus*, *Clostridium*, and *Enterococcus*. *Clostridium* and *Lactobacillus* are the dominant genera in the intestinal microbiota (Lynch and Pedersen, 2016). Bacteroidetes consist of Gram-negative, rod-shaped bacteria of genera such as *Bacteroides* and *Prevotella*. The Actinobacteria phylum is less abundant and mainly represented by the *Bifidobacterium* genus.

The gut microbiota composition varies widely amongst individuals and within their lifetime, responding to endogenous and exogenous factors including host genetics, diet, antibiotic use and disease. This begins in utero, when foetuses are exposed to maternal microbiota in the amniotic fluid via the placenta (Cariño *et al.*, 2022). Infants born via vaginal delivery are first exposed to the mother's microbiota, which colonises the previously sterile gut, as well as the baby's skin and mouth. Those delivered by cesarean section are not directly exposed to the maternal vaginal microbiota but instead are inoculated by microbes from the hospital environment (Penders *et al.*, 2006). The infant gut microbiota is further influenced by diet (breast versus formula feeding), antibiotic exposure and various environmental factors such as the presence of pets or siblings. In early life, the gut microbiota rapidly diversifies, playing a key role in

the development of the immune system, including protection against pathogens and establishing self-tolerance (Milani *et al.*, 2017).

Microbiota composition and functionality are impacted by host genetics and physiology, environmental exposure, age, drug usage and more. Diet is known to have a strong influence on the composition of intestinal microbiota and plays a key role in the evolution of the microbiota throughout our lifetimes. Gut microbiota composition is incredibly dynamic, with short-term dietary alterations modifying its properties within days (David *et al.*, 2014). For instance, consumption of high levels of dietary fibre from plants has been shown to result in a diverse intestinal microbial community, therefore benefiting human health (Perler, Friedman and Wu, 2023).

1.3.3 Metabolic Functions of the Gut Microbes

Gut microbes play an important role in many metabolic pathways in the gut, producing metabolites essential for human health but otherwise absent due to a lack of host digestive enzymes. These include fermentation of complex carbohydrates, polyphenol metabolism, deconjugation of bile acids, and synthesis of vitamins.

Microbial breakdown of proteins and fibre produces various metabolites, including neuroactive compounds, sulphide-containing molecules, polyamines, and short-chain fatty acids (SCFAs). Gut bacteria also produce neurotransmitters such as GABA, norepinephrine, dopamine, and serotonin, which play a crucial role in modulating the gut-brain axis. Given the physiological activity of these metabolites, the composition and function of the gut microbiota significantly influence host health. Certain metabolites, such as phenol and indole, have been linked to the development of inflammatory bowel disease (IBD), colorectal cancer, and kidney disease (Nicholson *et al.*, 2012).

Lipid metabolism involves microbial modulation of dietary fat digestion, with certain microbial metabolites such as SCFAs influencing fat storage and energy homeostasis. Therefore, diets high in fat have been shown to impact the composition of the gut microbiota, impacting barrier function and inflammatory pathways (Murphy, Velazquez

and Herbert, 2015). Bile salts, initially synthesised in the liver, are modified by gut bacteria through deconjugation and conversion of primary bile acids into secondary bile acids such as deoxycholic acid and lithocholic acid. This is mainly performed by anaerobic bacteria of the genera *Bacteroides*, *Eubacterium* and *Clostridium*, and products are passively absorbed in the colon for transportation back to the liver (Selwyn *et al.*, 2015). Microbes also metabolise dietary polyphenols, secondary metabolites formed in a variety of plants, into bioactive compounds with anti-inflammatory and cardioprotective properties by regulating host signalling pathways such as NF-kB (Marín *et al.*, 2015). Moreover, essential vitamins, such as vitamin K and B-group vitamins (e.g. B2, B9, and B12), are synthesized by gut bacteria. These are vital in the blood clotting cascade, DNA synthesis, and energy metabolism, and cannot be obtained by host metabolism or diet (LeBlanc *et al.*, 2013). Additionally, microbial detoxification processes protect us against toxicity by metabolising xenobiotics, enabling excretion or inactivating their noxious properties by pathways such as glycoconjugation (Shamjana *et al.*, 2024).

Fermentation of dietary fibres by colonic microbes such as Bacteroides and Bifidobacterium results in the production of gases, organic acids, alcohols, and short-chain fatty acids (SCFAs), which are an important energy source for colonic epithelial cells (Macfarlane and Macfarlane, 2012). These SCFAs include acetate (60%), an important energy source for peripheral tissues, propionate (25%), a gluconeogenic substrate in the liver, and butyrate (15%), a primary energy source for epithelial cells in the colon. SCFAs are absorbed in the colon via passive diffusion or active transport, meeting about 10% of the systemic energy demand (Duncan *et al.*, 2007). Butyrate is a particularly important SCFA, which regulates energy homeostasis by stimulating enteroendocrine cells and reduces the effect of harmful metabolites of bile acids and phenols. Overall, microbial metabolites play a crucial role in host physiology, particularly in the intestine, where they interact with the epithelium and mucosal immune system.

1.4 Role of the Gut Microbiota in Intestinal Renewal and Immunology

1.4.1 Microbial Metabolites and Intestinal Repair

Primary studies in GF mice demonstrated the role of microbes in promoting normal intestinal structure and function. IEC proliferation and mucin production is reduced in GF mice, resulting in a thin epithelial layer and mucous barrier (Gordon and Pesti, 1971). Intestinal epithelial homeostasis in the gut relies on communication between the gut microbiota, the mucosal immune system and the epithelium.

Microbial metabolites such as SCFAs, lactate, indoles, bile acids, and succinate each play a role in maintaining ISCs and regulating epithelial renewal and repair. Due to their specialised roles in promoting proliferation and maintaining the crypt stem cell niche, the microbial composition in the crypt is distinct from the mucosa. Alterations in this crypt-specific core microbiota (CSCM) have been reported in colon cancer, highlighting its importance (Saffarian *et al.*, 2019). Microbial products are important in regulating a range of signalling pathways via interaction with host cell receptors such as G-protein coupled receptors (GPCRs) to control ISC function.

Maintenance of the ISC niche is highly dependent on gut microbes and their metabolites interacting with components such as mesenchyme and immune cells. The effects of SCFAs are mediated through their ability to act as ligands for GPCRs and histone deacetylases (HDACs) (Donohoe *et al.*, 2011). Butyrate is the key energy source for epithelial cells and maintains ISC function, as well as modulates epigenetic processes such as histone acetylation, which influences the expression of genes involved in proliferation and repair (Markandey *et al.*, 2021). In intestinal organoids using mice cells, butyrate increases the numbers of $Lgr5^{+}$ stem cells by inhibiting HDAC (Yin *et al.*, 2014). The effects of butyrate on proliferation vary depending on the intestinal segment, with some studies suggesting that it may suppress colonic stem cell proliferation and that differentiated colonocytes metabolise butyrate to prevent it from reaching progenitors in the crypt and impacting homeostasis (Kaiko *et al.*, 2016). Propionate is the product of fucose metabolism by *Akkeermansia muciniphila*, a commensal bacterium that stimulates goblet cell production to support the mucus

layer. The stemness of ISCs is promoted by propionate via a Gpr41/43-dependent signal which ultimately encourages the Wnt/β-catenin pathway to maintain proliferation (Duan *et al.*, 2023). Moreover, acetate has been shown to support the growth of organoids by inhibition of β-oxidation of fatty acids when acetyl-CoA concentration is low (Figure 1.4).

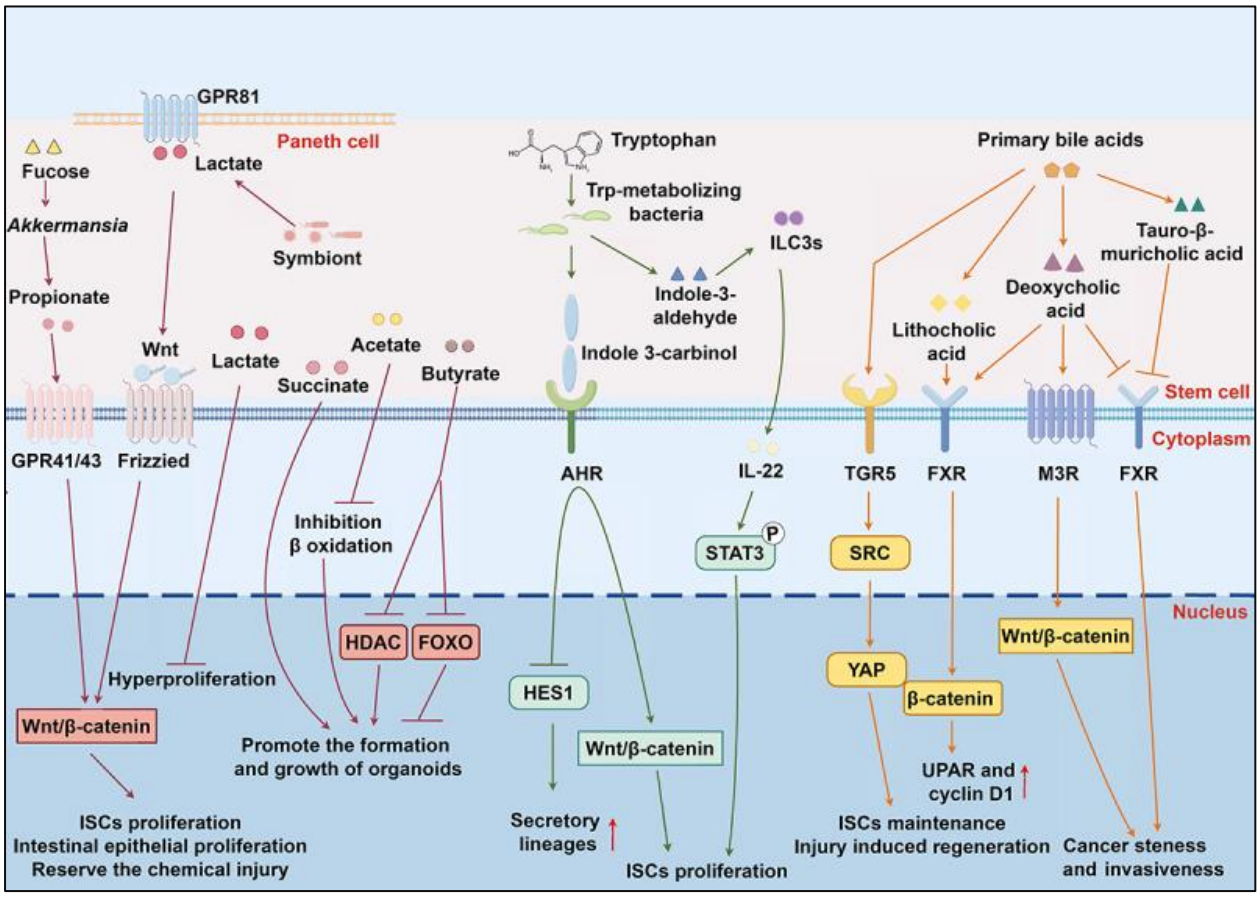

Figure 1.4 - ***Schematic overview of the key effects of microbial metabolites on ISCs and signalling pathways that maintain intestinal homeostasis (Wu et al., 2024).*** Microbiota-derived metabolic products such as SCFAs, lactate, indoles, and secondary bile acids, play a crucial role in promoting epithelial renewal and regulating ISC proliferation through pathways such as Wnt/β-catenin.

Intermediates such as lactate and succinate are also involved in the regulation of the ISC niche. *Lactobacillus*-derived lactate enhances intestinal proliferation in the small intestine and the cecum by activation of Wnt/β-catenin signalling upon GPR81 binding

(Lee *et al.*, 2018). Pre-feeding of mice with lactate protects them from chemotherapy and radiation-induced gut damage, indicating its impact on wound healing and highlighting the importance of *Lactobacillus*.

Indole and its derivatives are produced by the microbial metabolism of tryptophan (Trp), and are important mediators of IEC physiology, immune homeostasis and ISC differentiation by interacting with the aryl hydrocarbon receptor (AhR) on host cells (Agus, Planchais and Sokol, 2018). Microbiota such as *Escherichia coli* and *Serratia marcescens* express tryptophanase, allowing them to metabolise Trp from dietary protein into indoles and derivatives such as indole-3-acetaldehyde, indole-3-aldehyde and indole-3-acetic acid, which activate AhR signalling. AhRs are highly expressed in $Lgr5^+$ ISCs, controlling proliferation (Park *et al.*, 2016). ISC differentiation into secretory lineages (e.g. goblet cells) is promoted by indole-3-carbinol, which activates Wnt/β-catenin signalling and upregulates expression of lineage-specific genes Muc2 and lysozyme (Park *et al.*, 2018). Moreover, indole-3-aldehyde activates ILC3 cells, stimulating the production of IL-22, which promotes epithelial repair through STAT3 signalling (Hou *et al.*, 2018).

Additionally, secondary bile acids (SBAs) such as deoxycholic acid (DCA) and lithocholic acid (LCA) produced by microbiota are important regulators of host metabolism and barrier function via interactions with host receptors (Ferrebee and Dawson, 2015). SBAs promote epithelial regeneration after injury by activating Takeda GPCR 5 (TGR5) signalling, resulting in the activation of Src and Yap proteins and expression of their target genes (Sorrentino *et al.*, 2020). However, high levels of bile acids may have a carcinogenic effect, with DCA and LCA increasing colon cancer stemness and the invasive ability of colonic IECs by activating signalling pathways involved in proliferation and migration (Pai, Tarnawski and Tran, 2004). A balanced diet maintains a basal level of bile acids and gut microbiota, therefore maintaining normal ISC function.

Intestinal homeostasis relies on the balanced microbial environment in the mucosa and the crypts, maintaining epithelial renewal through metabolic signalling pathways and interactions with host immune receptors.

1.4.2 Immune Recognition of Microbiota Promotes Intestinal Renewal

Gut epithelial cells and antigen-presenting immune cells express numerous PRR types, including TLRs and NOD-like receptors (NLRs), which recognise both commensal and pathogenic MAMPs (Mu, Yang and Zhu, 2015). Foundational research in mice deficient in MyD88, an adaptor molecule essential for TLR signalling, found that intestinal renewal was significantly defective (Rakoff-Nahoum *et al.*, 2004). In the absence of TLR signalling, MyD88$^{-/-}$ animals showed severe mortality and morbidity upon exposure to dextran sulfate sodium (DSS) which induces colitis in mice. Whereas the wildtype mice were able to repair the intestinal damage and had a 100% survival rate and much lower morbidity, highlighting the importance of TLR signalling in intestinal renewal.

Most epithelial lineages express TLRs, and expression is tightly regulated to ensure controlled innate immune recognition (Semin *et al.*, 2021). Distribution of TLRs varies among the intestinal tract, with TLR2, TLR5 and TLR9 mainly restricted to the small intestine, and TLR2, TLR4, and TLR5 upregulated in colonic epithelium. The expression of these TLRs is regulated by the presence of gut microbiota, with GF mice presenting reduced levels of TLR expression compared to conventionally raised mice, particularly of TLR2 (Hörmann *et al.*, 2014). Epithelial TLR signalling is involved in enhancing barrier integrity and promoting immune tolerance towards microbiota (Burgueño and Abreu, 2020). Upon recognition of commensal bacteria by TLRs, the immune system responds by producing anti-inflammatory cytokines such as TGF-β, IL-10 and IL-22, which is important in maintaining the IEC barrier. Mice deficient in the ability to produce these cytokines present with intestinal inflammation and reduced in barrier integrity (Keir *et al.*, 2020). The TLR2/IL-10 pathway is particularly important in the maintenance of gut homeostasis, with TLR2 recognition lipoproteins, peptidoglycan and lipoteichoic acid promoting IL-10 expression. The immunosuppressive effect of IL-10 has a positive impact on the intestinal barrier and maintaining an immunotolerant environment (Kuugbee *et al.*, 2016).

Regulation of crypt dynamics is dependent on TLRs. For instance, TLR1 activation upon recognition of microbial-derived ligands helps preserve the architecture of the crypt, influencing crypt-specific epithelial renewal. TLR1-deficient mice had aberrant crypt morphology due to an increase in dysregulated cell proliferation at the base, resulting in a weakened barrier function and allowing increased penetration by commensal bacteria (Kamdar *et al.*, 2018). Moreover, depletion of MyD88 or TLR2 is associated with a loss of trefoil factor 3 (TFF3) expression which is necessary for the maturation of goblet cells, causing impaired mucosal repair and epithelial function (Podolsky *et al.*, 2009). Notch expression in the stem cell niche is also mediated by TLR4 activation, highlighting the role of TLRs in the maintenance of stemness and ISC function in the crypt. However, the role of TLR4 in IEC differentiation can also have opposing effects, as studies in TLR4 $^{-/-}$ mice have shown that TLR4 decreases the rate of goblet cell differentiation and worsens the severity of experimental necrotising enterocolitis (NEC) compared to the knockout (Sodhi *et al.*, 2012). This may indicate the role of microbial-TLR interactions in pathogenesis and inflammation as well as homeostasis. Maintenance of the mucus layer may also depend on microbe-TLR interactions, as deletion of TLR1 and TLR5 results in impaired MUC2 production by goblet cells, and a loss of mucus layer integrity. GF mice show similar effects, with a defective mucus layer highlighting the role of bacterial colonisation on the development and maintenance of the mucus layer (Johansson *et al.*, 2015).

Bacterial ligand binding to TLRs activates downstream signalling molecules through the MyD88 pathway or MyD88-independent signal transduction. Activation of TLR signalling stimulates various cellular pathways such as the NF-kB and MAPK pathways, with the ultimate result being upregulated cytokine expression (Figure 1.5). In the epithelium, IEC recognition of microbial components is necessary to promote regeneration under homeostatic conditions and during injury, where pro-inflammatory cytokines are produced to promote wound healing. When barrier integrity is compromised, recognition of microbes by LP immune cells, such as macrophages, induces an inflammatory response.

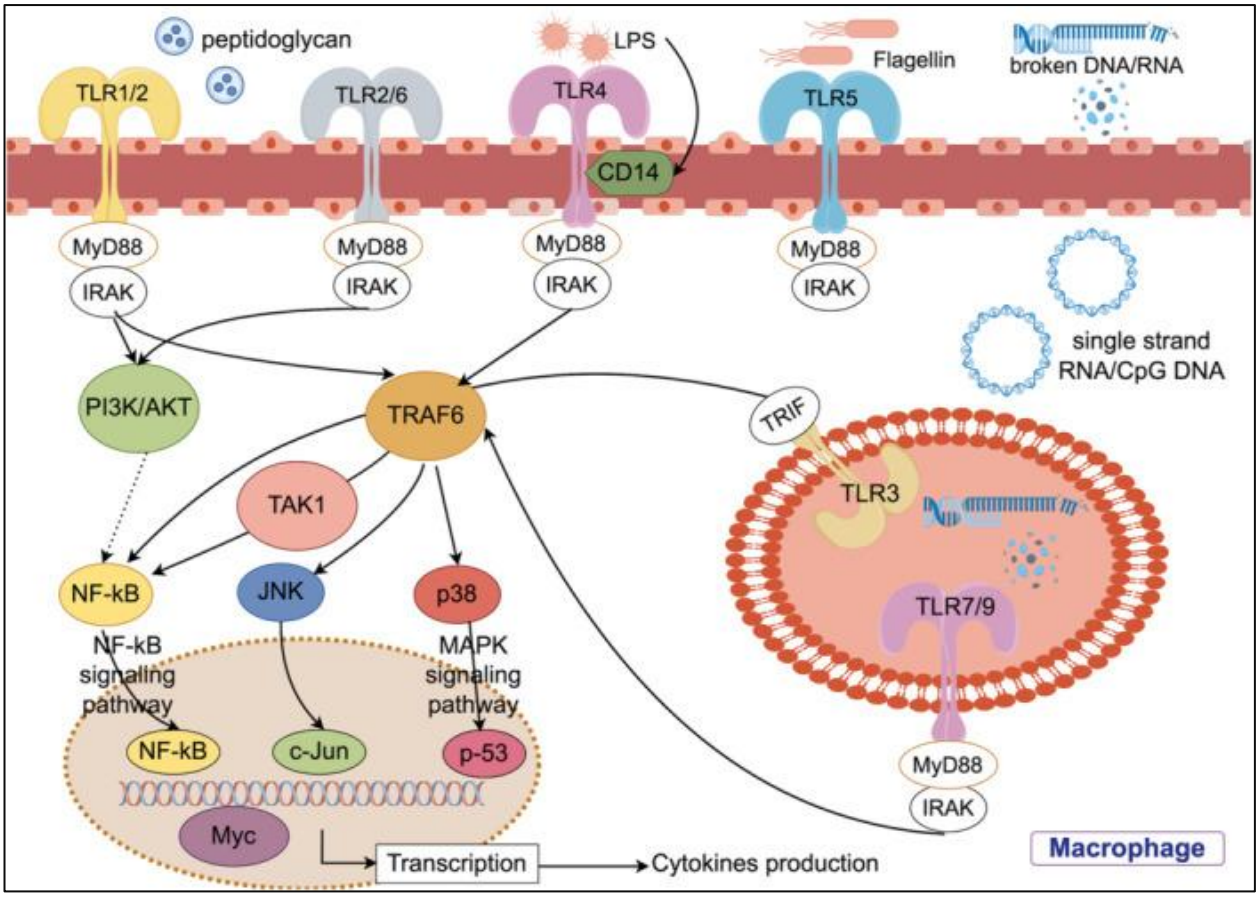

Figure 1.5 - ***TLR signalling in gut epithelial and immune cells.*** Microbial components act as ligands for TLRs: Gram-positive bacterial lipoproteins and peptidoglycan stimulate TLR2, gram-negative lipopolysaccharides (LPS) bind TLR4, flagellins bind TLR5, and ssRNA and damaged DNA components stimulate TLR7 and TLR9. Upon ligand binding, downstream signalling molecules are recruited via MyD88 to activate multiple cascades such as NF-kB, MAPK or JNK pathways. This promotes transcription factors which upregulate cytokine production, mediating the response to microbiota. In epithelial cells, this promotes the production of anti-inflammatory cytokines that maintain barrier function.

Interactions between TLRs and the gut microbiota can become harmful under non-homeostatic conditions, such as in infection or dysbiosis (imbalanced gut microbiota composition). Dysbiosis-associated microbe-TLR crosstalk may be involved in the development of obesity, IBD and colorectal cancer (Chen *et al.*, 2024). Therefore, eubiotic conditions are crucial in promoting gut homeostasis through coordination of

anti-inflammatory pathways involving the intestinal immune system, IECs and gut microbiota in a feedback loop.

1.5 Dysbiosis and Intestinal Dysfunction

1.5.1 Microbial Dysbiosis

Gut dysbiosis refers to a disease-promoting imbalance in the composition or diversity of the gut microbiota. The microbial ecosystem in the gut relies on a network of interactions between different species via their metabolites and secreted by-products. This is known as cross-feeding and means that certain commensals cannot survive without the metabolites from another species. Therefore, the loss of one population of beneficial bacterium could have catastrophic consequences and lead to dysbiosis.

An increasing number of diseases are being associated with intestinal dysbiosis, including inflammatory bowel diseases, but also metabolic disorders, autoimmune diseases, and neurological conditions (Tremlett *et al.*, 2017). The role of dysbiosis in disease states has been demonstrated by microbial transplantation studies, where the gut microbiota of a diseased animal is transplanted into a healthy one to observe the impact on health. Dysbiosis has been linked to inflammatory bowel disease (IBD and Chron's), promoting chronic inflammation and impairing barrier repair and integrity.

1.5.2 Dysbiosis and Intestinal Pathologies

Dysregulation of immune signals such as the NF-kB pathway during microbial dysbiosis may induce inflammation and contribute to the pathogenesis of inflammatory bowel disease (IBD) which can predispose the development colorectal cancer (CRC)(Morrison *et al.*, 2022).

IBD, including Chron's disease and ulcerative colitis, is a complex chronic condition with genetic and environmental influences. Although a definitive causal relationship between dysbiosis and IBD has not been determined, several studies have documented

alterations in the composition of the gut microbiota in IBD patients compared to healthy participants (Ni *et al.*, 2017). Microbial diversity and the relative abundance of beneficial taxa is often reduced in IBD, leading to the overgrowth of potentially pathogenic bacteria that are usually in low abundance. In high quantities, these bacteria may damage the gut barrier via microbial products such as enterotoxins, increasing intestinal permeability and inducing inflammation (Becker, Neurath and Wirtz, 2015). Specific bacterial genera inhibit gut inflammation by reducing the production of pro-inflammatory cytokines and stimulating anti-inflammatory cytokines to enhance immune quiescence. For instance, loss of *Facecalibacterium prausnitzii* exacerbates inflammation by reduced production of IL-10, altering the homeostatic balance between pro and anti-inflammatory signals (Hiippala *et al.*, 2018). Disruption of immune quiescence may upregulate inflammatory responses to gut microbiota, particularly when barrier integrity is compromised, and microbial products may breach the epithelium. In an ex vivo study on IBD mucosa, addition of an *E.coli* culture stimulated the release of pro-inflammatory cytokines (Manichanh *et al.*, 2012). Increased levels of pro-inflammatory cytokines such as TNF-α and IL-6 also disrupt intestinal repair mechanisms, further contributing to the pathologies seen in dysbiosis-related disease states.

Dysbiosis alters the composition of microbial metabolites, leading to dysregulated epithelial renewal. Moderate levels of butyrate support epithelial renewal and T_{reg} induction; however, excessive or insufficient quantities may disrupt proliferation via dysregulated modulation of Wnt/β-catenin and histone deacetylase (HDAC) signalling (Fu, Lyu and Wang, 2023). Therefore, the depletion of carbohydrate-fermenting commensals during dysbiosis is associated with intestinal inflammation due to reduced butyrate levels (Machiels *et al.*, 2014). This is just one reinforcement of the role of gut microbiota in intestinal health and provides evidence that dysbiosis impacts the regenerative ability of the intestinal epithelium. Together, dysbiosis-induced mechanisms establish a cycle where epithelial injury, inflammation, and microbial imbalances worsen each other and contribute to disease.

Dysbiosis-induced defects in intestinal renewal and immune homeostasis highlight the potential of the gut microbiota as a therapeutic target for bowel conditions.

1.5.3 Therapeutic Implications

Emerging therapeutic concepts such as faecal microbiota transplantation (FMT), use of prebiotics and probiotics, and metabolite-based therapies have shown promising results in restoring microbial balance and promoting gut homeostasis (Rose *et al.*, 2021).

Dietary alterations may provide a non-invasive and easily accessible therapeutic strategy for improving microbial diversity in the gut. Diet plays a key role in determining the composition of the gut microbiota - mice fed on a 'Western diet' high in sugar and fats display a dysbiosis manifesting as a reduction of Bacteroidetes and overgrowth of Firmicutes, disrupting intestinal homeostasis (Turnbaugh *et al.*, 2009). Increasing uptake of fermentable fibers (prebiotics) from fruits, vegetables, and whole grains may support SCFA producing bacterial populations, promoting improved intestinal health (Zmora, Suez and Elinav, 2019). Limiting saturated fats and proteins may contribute to a healthy gut microbiota by reducing the growth of pathobionts associated with high-fat and high-protein diets (Zeng *et al.*, 2019). Moreover, foods with anti-inflammatory properties such as those high in antioxidants and polyphenols also promote homeostasis. Polyphenols from plant-based foods enhance Bifidobacterium and Lactobacillus, increasing the concentration of butyrate and contributing to eubiosis. Additionally, dietary probiotics such as yogurt, kefir and kimchi introduce live commensals to the gut, however the ability of probiotics to colonise the host GI tract remains controversial (Suez *et al.*, 2019). Over-the-counter probiotic and prebiotic supplements have the potential to reduce inflammation and promote epithelial renewal and barrier function via increased SCFAs and anti-inflammatory cytokines (Sniffen *et al.*, 2018). However, their efficacy depends on strain specificity and the type/severity of dysbiosis, with some studies reporting limited success in patients with severe dysbiosis (Martyniak *et al.*, 2021).

Moreover, supplementation of metabolites such as SCFAs or their precursors may directly address dysbiosis-related deficiencies and promote epithelial repair

(Mayorgas, Dotti and Salas, 2021). This type of therapy is known as postbiotic treatment, defined as non-viable bacterial products that offer an alternative to live probiotics. Postbiotics may promote immunoregulation, prevent infection, aid in lipid metabolism, and even have anti-cancer properties via antioxidant activity (Klemashevich *et al.*, 2014). Although existing clinical trials have shown promising results, future work aims to elucidate the biological mechanisms of these metabolites and refine administration methods (Żółkiewicz *et al.*, 2020). Overall, the gut microbiota provides an attractive target for the treatment of GI disorders, as dysbiosis is commonly associated with dysregulated wound healing and inflammation in the intestine.

1.6 Introducing the loop ileostomy procedure

1.6.1 Loop Ileostomy and Why It Is Performed

Loop ileostomy is a type of ostomy: a group of surgical procedures that form an anastomosis (stoma) between a segment of the bowel and the skin of the abdominal wall. This results in the diversion of the faecal stream to protect a downstream anastomosis, inflamed distal bowel, malignancy, or bypass an obstruction. 'Ileostomy' refers to the diversion of the ileum, the final portion of the small intestine, meaning that the entire colon is bypassed (Figure 1.6). This is commonly performed following colorectal surgery, such as the removal of a tumour and rejoining of the bowel, to protect the colonic anastomosis and promote healing (Aljorfi and Alkhamis, 2020). Stoma formation results in a functional limb of the ileum that receives nutrients from the faecal stream and a defunctioned limb that does not.

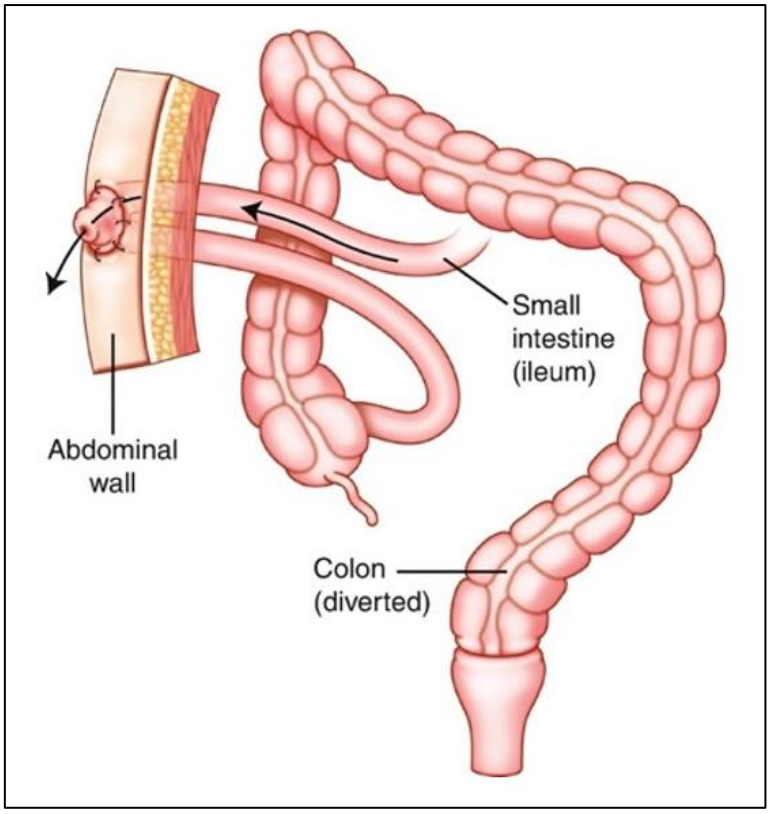

Figure 1.6 – ***Schematic representation of the loop ileostomy formation procedure (Macdonald's Surgical Procedures, 2025).*** A loop of the small intestine is pulled through a small opening in the abdomen and dissected to form 2 openings of bowel (proximal and distal) that are attached to the abdominal wall using surgical stitches. Faeces exit via the proximal bowel and are collected in an ileostomy pouch, and the downstream intestine is diverted.

Loop ileostomy is temporary and is reversed once the underlying condition has improved significantly, and the patient is generally healthy. Reversal surgery involves the rejoining of the proximal and distal limb, allowing the faecal stream to travel through the tract and exit through the anus.

1.6.2 The Impact of Faecal Diversion on the Distal Bowel

Following stoma reversal surgery, up to 40% of patients experience substantial morbidity due to side effects and complications. Common side effects include erratic bowel function such as diarrhoea and incontinence, and surgical wound infection.

More serious complications include defective peristalsis (ileus), intestinal inflammation (ileitis), or anastomotic leakage at the surgical site (El-Hussuna, Lauritsen and Bülow, 2012). The pre-operative risk factors associated with post-stoma-reversal complications are not well understood, but studies have suggested that the surgical closure technique and the time between stoma formation and closure might be involved (Sherman and Wexner, 2017).

Diversion colitis (DC) refers to the downstream inflammation of the colon following faecal diversion and is a common postoperative complication in stoma patients. Microbial dysbiosis contributes to the development of DC, with significantly decreased bacterial diversity shown in the diverted colon of DC patients, with a particular reduction in SCFA-producing bacteria due to reduced dietary fibre availability (Sam *et al.*, 2024). The defunctioned limb is also at higher risk of infection, with *Clostridium difficile* infection affecting approximately 4% of patients following ileostomy reversal (Harries *et al.*, 2017). This occurs due to the loss of protective commensals, overgrowth of pathogenic species and reduced barrier integrity in the distal bowel.

Loop ileostomy leads to atrophy, fibrosis and dysfunction of the distal bowel due to prolonged inactivity, depriving it of nutrients and therefore gut microbiota. In response to nutrient deprivation, IECs downregulate cell growth and proliferation, resulting in an atrophied appearance that can be observed upon histological examination (Beamish *et al.*, 2017). The loss of enteral nutrition in the diverted intestine results in loss of microbiota, impacting on intestinal structure, function and immune state (Williams *et al.*, 2007). Reduced stimulation from metabolites such as SCFAs reduces IEC proliferation, causing villous shortening and crypt dysfunction. Atrophic mucosa is more susceptible to injury and inflammation, leading to the complications observed after stoma reversal. The absence of gut microbiota is linked to these pathologies, as patients with post-surgical complications often exhibit a reduction in total bacterial load (TBL) (Beamish *et al.*, 2023). Increasing degrees of bacterial deficit in the ileum were correlated with an increased risk of post-surgical complications, with the most life-threatening complication of anastomotic leak occurring in the patient with the highest reduction of TBL (97.2% loss). These findings suggest that replenishing the

microbiota of the defunctioned limb before reversal surgery may stimulate epithelial renewal and reduce the risk of developing complications.

1.6.3 Targeting the Microbiota to Improve Epithelial Health in the Distal Bowel

Preoperative stimulation of the defunctioned limb may improve patient outcomes after loop ileostomy reversal surgery. Mechanical stimulation was attempted, where a thickened saline solution was inserted into the distal bowel daily before reversal surgery (2 weeks) to promote normal muscle contraction and prevent postoperative ileus (Abrisqueta *et al.*, 2014). Compared to the control group, patients who received efferent limb stimulation reported more favourable outcomes, including quicker normalisation of bowel function and reduced signs of ileus. Other studies have reported similar results with mechanical stimulation, showing improvements in patient bowel function, including better continence and stool consistency (Rombey *et al.*, 2019). However, mechanical stimulation fails to address the loss of commensal bacteria following faecal diversion, so there is still a risk of mucosal atrophy, inflammation, and impaired barrier function.

Promoting microbial restoration before reanastomosis may improve epithelial renewal in the distal bowel, reversing villous atrophy and restoring homeostasis. Treating the distal loop with SCFAs in solution (e.g. propionate and butyrate) may be beneficial in stimulating IECs and establishing an anti-inflammatory environment before reversal surgery (Fernández López *et al.*, 2019). However, replenishing the microbiota itself may be more beneficial in ensuring the maintenance of intestinal homeostasis and providing alternative functions such as immune tolerance. Treatment of the distal bowel with probiotics led to a reduction in surgical time due to the thickening of the efferent loop; however, it did not decrease the incidence of ileus post-operative complications such as ileus (Rodríguez-Padilla *et al.*, 2021). This may suggest that a prebiotic supplement would be more beneficial, as the distal bowel displays a decreased TBL rather than deficits of certain commensal species (Beamish *et al.*, 2017). Some groups hypothesise that the administration of prebiotics may improve epithelial function in the

defunctioned limb, and could be used alongside mechanical stimulation or probiotic treatment to improve patient outcomes (Marcelino *et al.*, 2023).

1.7 Project introduction and aims

This study aims to improve post-operative outcomes for stoma-reversal patients by stimulating the distal bowel with a prebiotic mixture before reversal. The impact of prebiotic feeding on the distal bowel was measured using flow cytometry, histology, and qPCR, summarised in Figure 1.7.

The first aim of this project was to determine the impact of faecal stream diversion on immune cell populations in the lamina propria. Historical flow cytometry data from an existing study by the Rigby group on untreated patients were analysed to identify alterations in immune populations between the functional and defunctioned bowel. $CD103^+$ DCs, $CD11c^+$ DCs, $C64^+$ APCs, $CD163^+$ macrophages, and $TLR5^+$ cells were analysed. The hypothesis was that there would be no significant differences in immune cell frequencies between the functional and defunctioned portions.

Secondly, the prebiotic-fed tissues were analysed by histological techniques to determine whether the prebiotic stimulated intestinal repair. Morphological measurements of crypt depth and villus height were taken, as well as measuring goblet cell and proliferative cell frequencies within the crypt. The hypothesis was that there would be significant improvements in epithelial health after prebiotic feeding, characterised by increased crypt depth and villus height when compared to the unfed patient group. Goblet and proliferative cell frequencies should be similar between the prebiotic-fed bowel.

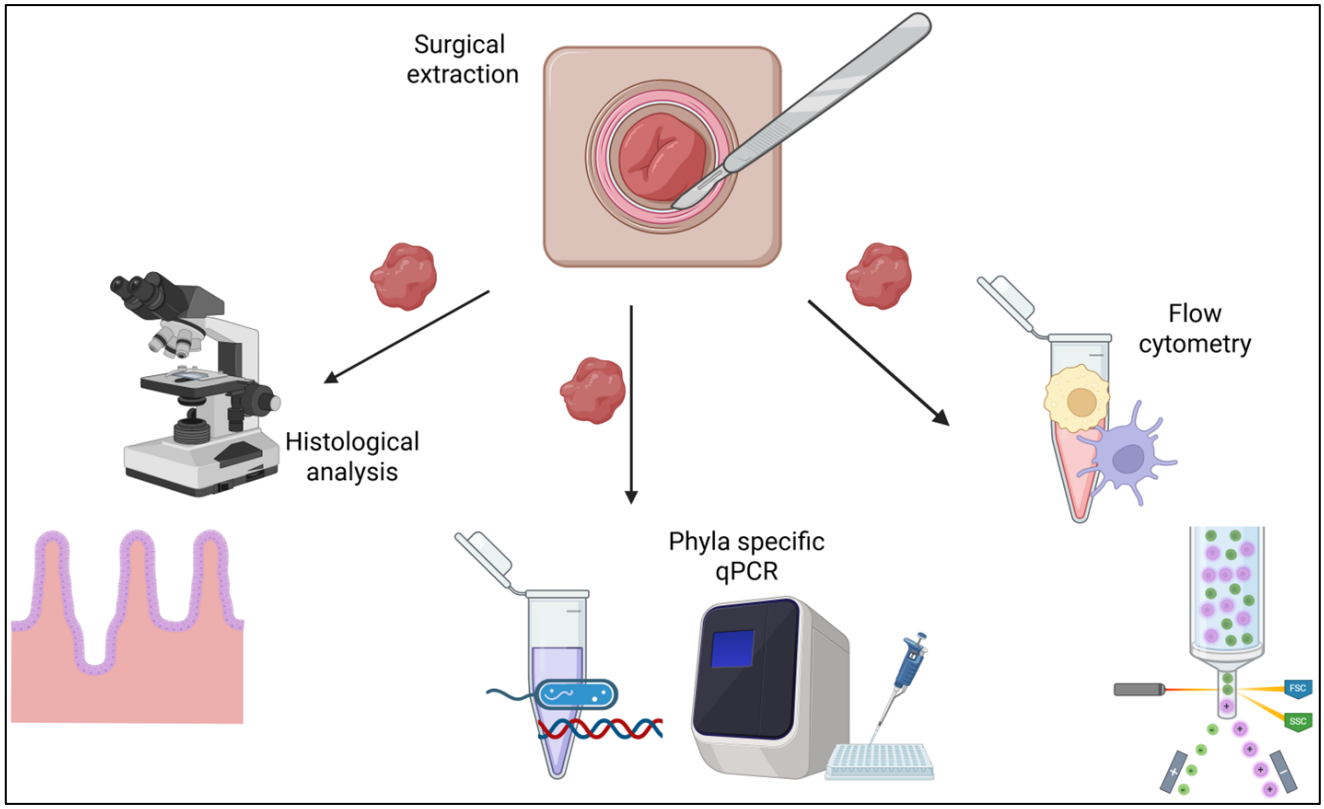

Figure 1.7 - ***Research summary schematic produced in Biorender.*** Upon excision of excess stoma tissue from the surgical site, the functional and defunctioned tissue is dissected into smaller sections for histological analysis, qPCR, and flow cytometry. A full-thickness section is fixed in paraformaldehyde (PFA), embedded in paraffin wax, sectioned and stained accordingly for histology protocols. For bacterial phyla-specific qPCR, a section of the ileum is dissected into small pieces for digestion and DNA extraction. Finally, single cells are isolated for flow cytometry analysis by digesting some tissue and following the cell isolation protocol.

The next goal was to assess changes in immune cell populations after prebiotic feeding. The percentage frequencies of T helper cells, macrophages, and $CD11c^+$ DCs were compared between the unfed and prebiotic-fed patients to identify the impact of prebiotic feeding on immune cells in the LP.

Lastly, the final aim was to use phylum-specific qPCR on isolated bacterial DNA from digested patient tissue to investigate the relative abundances of main bacterial phyla in the functional and defunctioned bowel. Future directions of this study include 16S

sequencing to confirm qPCR results and investigate species-level alterations in microbial composition.

2 Materials and methods

2.1 Materials

2.1.1 Reagents

Table 2.1. - ***Reagents and products list with supplier details.***

Reagent	Supplier	Catalogue Number
QIAmp® UCP Pathogen Mini Kit	Qiagen	50214
Bovine Serum Albumin (BSA)	Sigma Aldrich	A3294
Triton X-100	Sigma Aldrich	T8787
Goat serum	Sigma Aldrich	G9023
PAP pen	Sigma Aldrich	Z377821
SYBR® Green JumpStart™ Taq ReadyMix™	Sigma Aldrich	S4438
Tri-sodium citrate dihydrate	Sigma Aldrich	S1804
3-Aminopropyltriethoxysilane (APES)	Sigma Aldrich	440140

2.1.2 Antibodies

Table 2.2 - ***Antibodies used for immunofluorescence with details of supplier and working concentrations.***

Antibody	Manufacturer	Catalogue No.	Source	Concentration	Working Dilution
Anti-PCNA (PC10)	Life Technologies	13-3900	Mouse	500 µg/mL	1:100
Anti-mouse Alexa-Fluor 488 IgG	Life Technologies	A-11001	Goat	2 mg/mL	1:400
Normal Mouse IgG	Santa Cruz	Sc-2025	Mouse	200 µg/0.5 mL	1:20
Hoechst 33342 Nucleic Acid Stain	Life Technologies	H3570		10 mg/mL	1:1000

2.1.3 qPCR primers

Table 2.3 - ***Phyla-specific qRT-PCR primer sequences.***

	Forward primer sequence	Reverse primer sequence
Universal	5'-AAACTCAAAKGAATTGACGG-3'	5'-CTCACRRCACGAGCTGAC-3'
Bacteroidetes	5'-CRAACAGGATTAGATACCCT-3'	5'-GGTAAGGTTCCTCGCGTAT-3'
Firmicutes	5'-TGAAACTYAAAGGAATTGACG-3'	5'-ATTACCGCGGCTGCTGGC-3'
γ-Proteobacteria	5'-TCGTCAGCTCGTGTYGTGA-3'	5'-CGTAAGGGCCATGATG-3'
Actinobacteria	5'-TACGGCCGCAAGGCTA-3'	5'-TCRTCCCCACCTTCCTCCG-3'

2.1.4 Buffers and solutions

Table 2.4 – ***The composition of buffers and solutions used.***

Solution	Protocol for 1L
4% Paraformaldehyde	40g paraformaldehyde was added to 800 mL 1x PBS heated to 50 ºC. pH was increased by adding NaOH dropwise until dissolved. Solution was filtered and the final pH adjusted to 6.9 with HCl before *q.s.* to 1L with PBS.
Sodium Citrate Buffer (10mM Sodium Citrate, 0.05% Tween 20, pH 6.0)	2.94 g of tri-sodium citrate dihydrate was added to 900 mL dH_2O and mixed to dissolve. pH was adjusted to 6.0 with HCl, and 0.5 mL of Tween 20 added. Solution was mixed well and *q.s.* to 1L with dH_2O.

2.2 Research Ethics

Two studies with separate patient cohorts were included in this report: a cohort of patients who did not undergo stoma feeding (N=35) and a cohort that received prebiotic stimulation of the efferent limb before reversal surgery (N=5). Ethical approval was obtained from the North West Research Ethics Committee for the two studies (13/NW/0695) and (22/WM/0222) respectively, conducted following the Health Research Authority guidelines.

Cohorts consisted of eligible and consenting patients undergoing loop ileostomy reversal surgery at Lancashire Teaching Hospitals Trust (LTHT).

2.3 Patient Eligibility and Recruitment

To be deemed eligible, patients have been 18 years or older, of either sex, and able to self-administer the prebiotic mixture (for stoma feeding patients only). Patients with

ongoing bowel pathologies, such as IBD, and those who had received antibiotic treatment within the last three months were excluded from the study. For patient anonymity, tissue samples were assigned a unique identifier: for the unfed cohort, BCRGXXX and for the fed cohort, SFSXXX.

This study included 5 patients who underwent prebiotic feeding before reversal surgery. Patient demographics are detailed in Table 2.5.

Table 2.5 – ***Patient demographics.***

Patient code	Sex	Age	BMI	Days with stoma	Prebiotic feeding days
SFS002	Male	67	29	881	26
SFS004	Male	47	30	793	2
SFS005	Female	45	25	2030	7
SFS007	Male	25	23	994	6
SFS009	Male	46	37	308	18

2.4 Prebiotic feeding

A feeding tube was inserted into the opening of the defunctioned bowel by a stoma nurse. Patients then self-administered a mixture of Orafti® Synergy1, an oligofructose-enriched inulin-derived prebiotic powder, diluted in Ensure® complete nutrient shake, increasing the amount of prebiotic each day up to 10g, leading to reversal surgery. The period of prebiotic feeding time varied from 2 to 27 days, due to the self-administering nature of the treatment.

2.5 Surgical Sample Acquisition

During loop ileostomy reversal surgery, a small section of intestinal tissue was removed from the end of each limb (proximal/distal) and collected in sterile histopots containing Minimum Essential Media (MEM). Specimens were transported from the surgical theatre at LTHT to the research laboratory at Lancaster University and processed within 2 hours of collection.

2.6 Sample Processing

2.6.1 Cell Isolation for Flow Cytometry

Approximately 250mg of gut tissue from each biopsy was washed in Hanks' balanced salt solution (HBSS) and cut into 5mm sections. The epithelium was removed by incubating the tissue in 1mM dithiothreitol (DTT) and 1mM EDTA in HBSS for 20 minutes at 37 ºC with shaking. The supernatant was discarded before transferring gut tissue into falcon tubes containing 10 mL of gut digest media (50 mL HBSS, 10% FCS [Gibco], 0.5 mg/mL Dispase [Gibco], and 0.5 mg/mL Collagenase [Gibco]) and incubated in a shaking incubator for 60 minutes at 37 ºC. Digestion medium was passed through a 100 mM cell strainer, and suspensions were collected.

The filtrate was centrifuged at 400 x g for 5 m. After centrifugation, the supernatant was removed and the pellet resuspended in 8 mL of 3% Percoll, before centrifugation at 600 g for 20 m. The supernatant (containing mucus and debris) discarded, the pellet, containing mononuclear cells, was washed with 4 mL PBS.

Cells were pelleted through centrifugation for 5 m at 400 x g. The supernatant was removed, and the pellet resuspended in FACs staining buffer (1% BSA in PBS) and stored on ice. Cell counts were performed using a haemocytometer to determine the approximate concentration of cells in each suspension. Cell suspensions were transferred into FACS tubes at a concentration of 1 x 10^6 cells/mL.

2.6.2 Bacterial DNA Extraction

Gut tissue was dissected into small sections to aid release of associated microbiota. The QIAamp DNA Microbiome kit (Qiagen) was used to extract bacterial DNA as per the manufacturer's instructions.

2.6.3 Fixation and Sectioning

Upon excision from the stoma site, full-thickness ileal sections were fixed in 4% PFA solution for 24 h. Samples were placed into cassettes and dehydrated through increasing ethanol concentrations (70-100% for 1 h each) followed by 2 x 1 h incubations in xylene and paraffin wax. Samples were then embedded in paraffin wax and cooled on ice overnight. Sections of 7 uM thickness were prepared using a Microtome (Leica) and mounted onto APES-coated microscope slides and left to dry overnight.

2.7 Histological Analysis

2.7.1 Haematoxylin and Eosin (H&E) Staining

Sections were deparaffinised in xylene for 2 x 5 min, then rehydrated in graded alcohol solutions (100-70%) for 2 x 1 min each. Slides were then rinsed in running tap water and dH2O before immersing in Haematoxylin (Sigma Aldrich) for 3 min with gentle agitation. Slides were washed in warm running water for 15 min, then stained with Eosin for 30 sec with gentle agitation. After rinsing in running tap water for 1 min, sections were dehydrated in increasing alcohol concentration (70-100%) for 2 x 5 min each, followed by 2 x 5 min in xylene. Slides were mounted using histomount and coverslips, then allowed to dry overnight before imaging.

2.7.2 Morphological Analyses

H&E-stained sections were imaged using a Motic microscope fitted with MotiCam at 10X magnification. Suitably orientated sections were analysed using Image J software to measure villus height and crypt depth (Figure 2.1). Measurements were converted from pixels to uM and the percentage change in villus height and crypt depth between the functional and defunctioned sections was calculated.

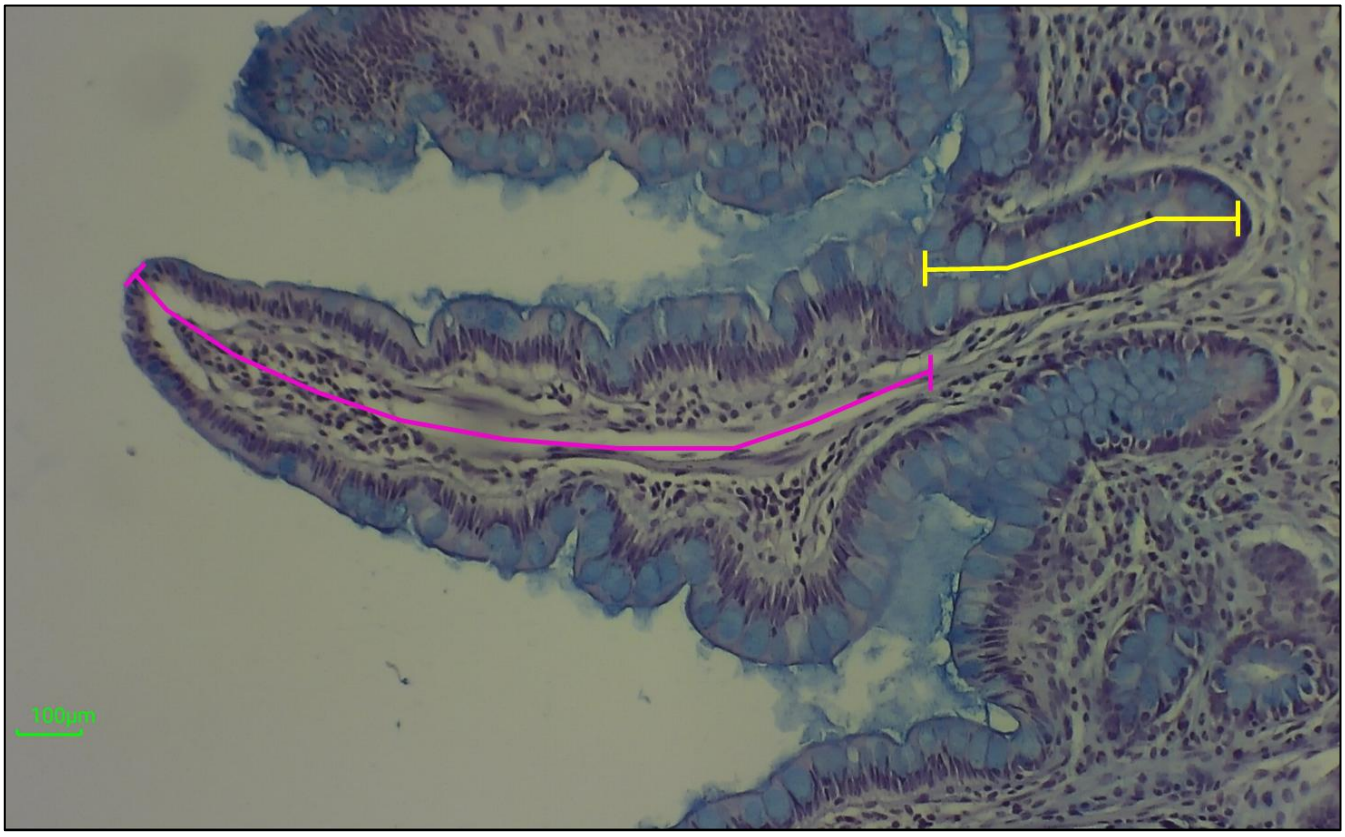

Figure 2.1 – ***Representative demonstration of crypt depth and villus height measurements.*** Villus height = pink, Crypt depth = yellow. Measurements were taken in the ImageJ software by drawing a segmented line from the base of the crypt to the epithelial surface (crypt depth) and from the epithelial surface to the tip of the villus (villus height). The actual distance was calculated by measuring the scale bar (bottom left) and scaling the number of image pixels to the distance in µM.

2.7.3 PAS-Alcian Blue Staining

Sections were deparaffinised in xylene for 2 x 5 min and rehydrated in graded alcohol (100-70%) for 2 x 1 min each. Slides were washed in running water and rinsed in dH2O, then immersed in Alcian blue stain for 5 min. Slides were washed for 3-5 minutes, then oxidised in periodic acid for 7 min. Following another 3-5 min wash step, slides were submerged in Schiff's reagent for 15 min, before rinsing with agitation for 10 min. Samples were counterstained with haematoxylin for 30 sec, followed by dehydration in graded alcohol (70-100%) for 2 x 4 min each, and xylene 2 x 5 min. Samples were mounted using histomount and coverslips and kept at room temperature until imaging.

2.8 Immunofluorescence PCNA Analysis

2.8.1 Deparaffinisation and Rehydration:

Tissue-coated slides were passed through a series of Xylene and decreasing ethanol concentrations to deparaffinise and rehydrate:

1.	Xylene	2x3 minutes
2.	100% ethanol	1x5 minutes
3.	95% ethanol	1x5 minutes
4.	70% ethanol	1x5 minutes

Slides were then rinsed and kept in running water until antigen retrieval.

2.8.2 Antigen Retrieval

Slides were subjected to heat-induced epitope retrieval using a pressure cooker. Slides were placed in a chamber containing 2L of warmed sodium citrate buffer and pressure cooked for 1-1.5 minutes. Following heating, slides were removed from the buffer and placed in TBS for 15 minutes to recover.

2.8.3 Permeabilisation and Blocking

Following antigen retrieval, slides were washed in TBS + 0.025% Triton X-100 for 5 minutes and permeabilised in TBS + 0.25% Triton X-100 for 10 minutes with gentle agitation. Finally, they were washed with TBS + 0.025% Triton X-100 twice for 2 minutes.

Excess solution was removed from around the tissue and a 2 mm PAP hydrophobic marker was used to draw around the sample. Slides were blocked with 10% goat normal serum in TBS + 3% bovine serum albumin (BSA) for 2 hours at room temperature.

2.8.4 Antibody Staining

Recombinant mouse monoclonal anti-PCNA was diluted to a concentration of 1:100 with 1% BSA in TBS and pipetted onto the tissue. Negative controls were stained with normal mouse IgG diluted to 1:20. Slides were incubated at 4 ºC in a humidified chamber overnight.

Slides were washed twice in TBS + 0.025% Triton X-100 for 5 minutes with gentle agitation. Alexa fluor (AF) 488 goat anti-mouse was diluted to 1:400 in TBS + 1% BSA and pipetted onto the control and experimental tissue before incubating at room temperature in the dark for 2 hours.

Following incubation, slides were washed in TBS + 0.025% Triton X-100 twice for 5 minutes with gentle agitation. Co-staining was completed using Hoechst 33342 diluted at 1:10000 for 5 minutes at room temperature. Slides were briefly washed with TBS

before mounting with Vectashield. Cover slips were placed over the tissue and sealed with nail polish. Once dry, slides were kept in the dark at 4 ºC and imaged within 1 week of staining.

2.8.5 Analysis of Stained Slides

Stained slides were imaged on the Zeiss LED microscope at a total magnification of 10x (objective lens at 20x, and 0.5x AxioCam) and wavelength of 488 nm to image proliferative cells (green fluorescence).

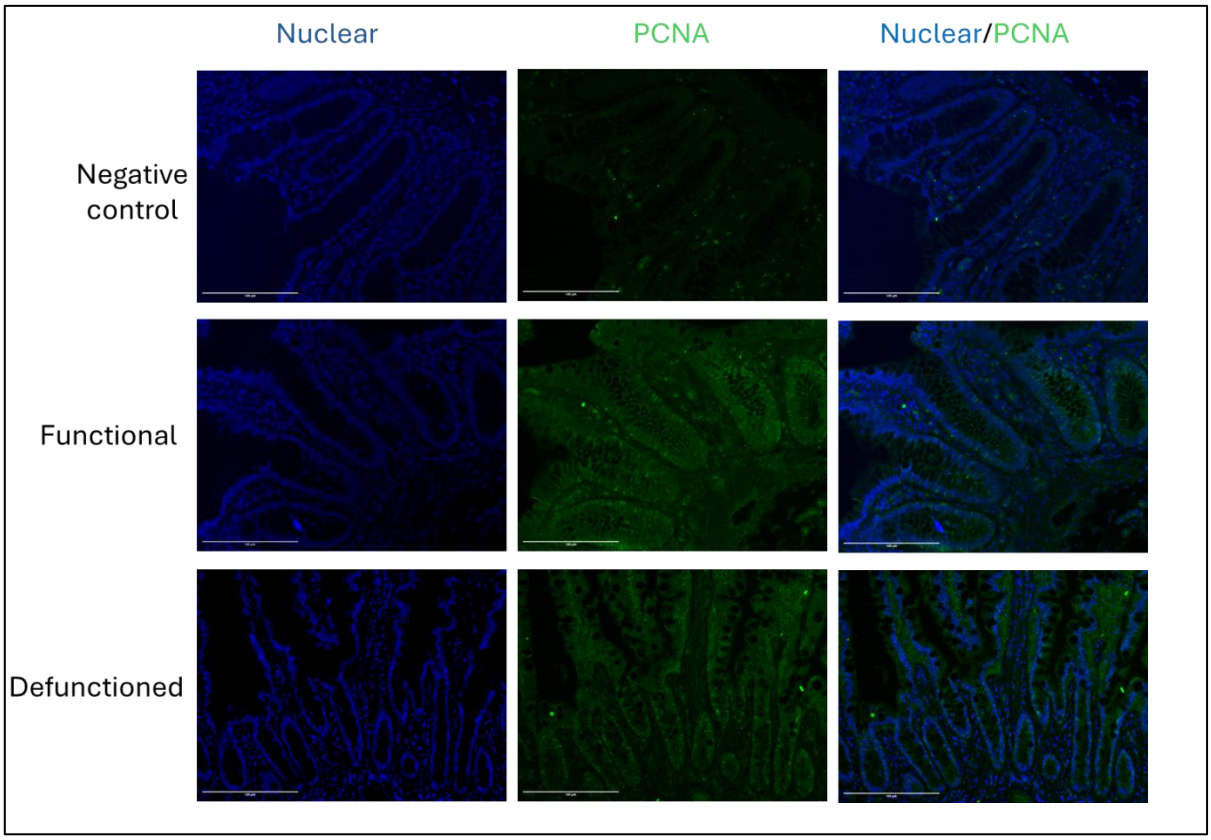

Figure 2.2 - ***Proliferative cell nuclear antigen (PCNA) immunofluorescent staining of intestinal tissue.*** Representative immunofluorescent PCNA labelling (green) of human ileum to measure crypt cell proliferation. Nucleated cells are coloured blue, counterstained with Hoescht 33342. Images were obtained at 20X magnification.

Cell counts were completed using ImageJ software, and the number of PCNA-positive cells per 100μM of crypt was determined.

2.9 Flow Cytometry

2.9.1 Antibody Staining

Fc block (2 uL) was added to each tube and incubated on ice for 30 m. Surface antibodies were added at concentrations of 3 uL of 0.2 mg/mL or 1.2 uL of 0.5 ug/mL and incubated on ice for 30 m in the dark.

Intracellular antibodies were added at concentrations of 6 uL of 0.2 mg/mL and 2 uL of 0.5 ug/mL and incubated on ice for 30 m in the dark. Cells were permeabilised using FIX & PERM (Invitrogen). Cells were then fixed in 1% paraformaldehyde (PFA) in PBS and kept in the dark at 4 ºC until acquisition within 48 hours.

2.9.2 Analysis

Samples were acquired on a Cytoflex flow cytometer, and the data collected were analysed using the FlowJo software.

All samples were first gated for singlets, as shown in Figure 2.3A, to exclude any debris or clumps of cells, followed by gating for live cells based on a live/dead dye (APC-Cy7)(Figure 2.3B).

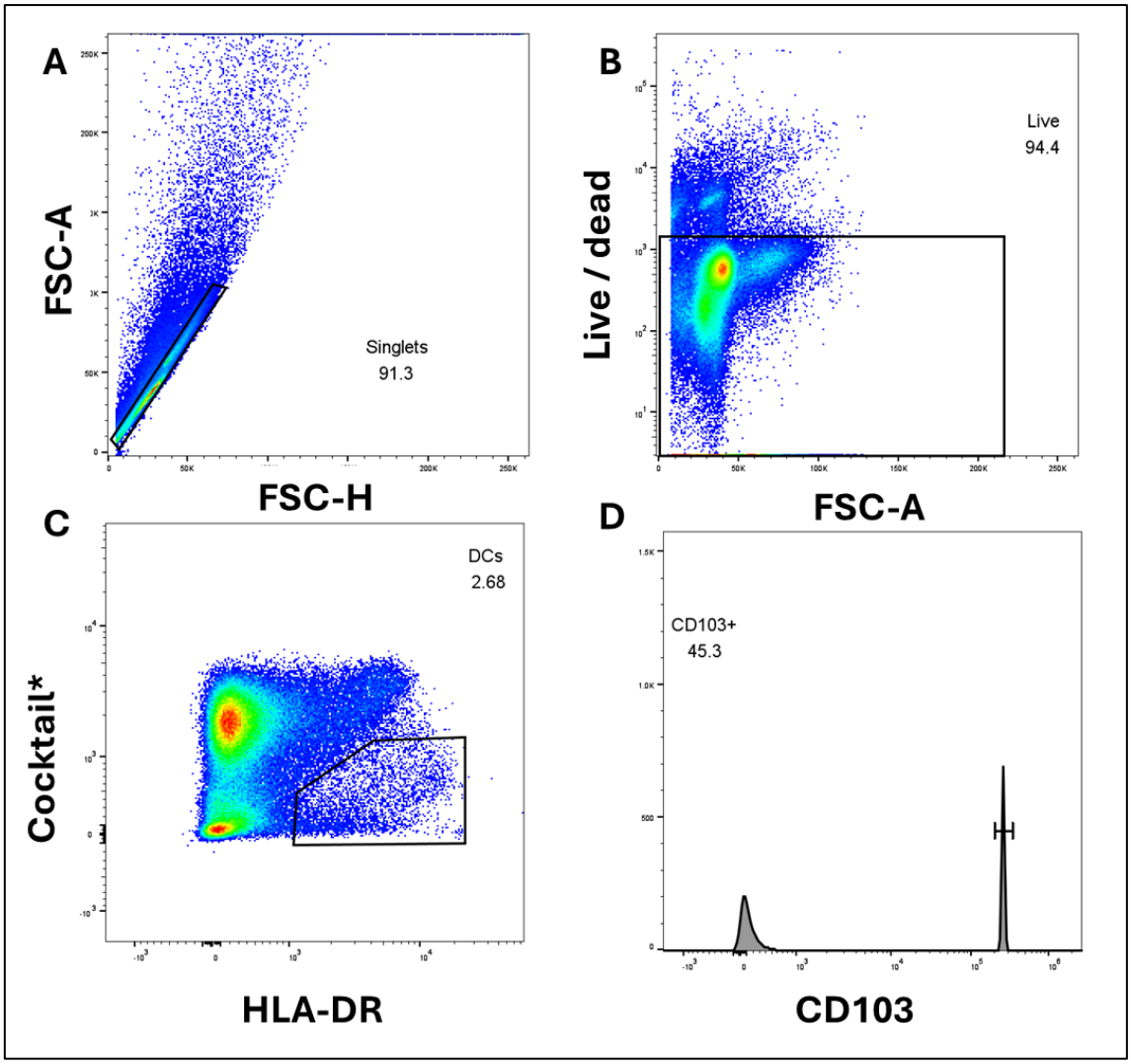

Figure 2.3 - ***Example of gating strategy applied in the flow cytometry analysis of intestinal immune populations.*** **A)** Using FlowJo software, all samples were gated for singlets (FSC-A / FSC-H) to exclude debris and clumps. **B)** Live cells were isolated using a live/dead dye, with the unstained cells being live. **C)** To isolate the DC population, the HLA-DR$^+$, Cocktail$^-$ population was identified and gated on (Cocktail = mixture of CD3, CD14, CD19, CD20, and CD56). **D)** The CD103$^+$ subset was then selected from the dendritic cell population.

Cell-specific gating strategies were applied to isolate DCs (Figure 2.3C), macrophages, and T cell populations, before gating based on the expression of specific markers such as CD molecules (Figure 2.3D).

2.10 Phyla-specific 16s rDNA qPCR

The relative abundance of predominant microbial phyla (Firmicutes, Bacteroidetes, Actinobacteria and g-Proteobacteria) was compared using phylum-specific universal 16S rDNA primers (Table 2.3).

The qPCR reaction was performed in a 96-well plate with a 10 uL reaction volume containing 5uL SYBR Green JumpStart Taq ReadyMix (20 mM Tris-HCl, pH 8.3, 100 mM KCl, 7 mM MgCl2, 0.4 mM of each dNTP, stabilisers, 0.05 unit/mL Taq DNA Polymerase, JumpStart Taq antibody, and SYBR Green I) (Sigma Aldrich), 30-50 ng template DNA, and 0.5 uL of each forward and reverse primer, and 3 uL PCR grade water. PCR was performed using the BioRad CFX Opus 96, programmed with the following parameters:

Data were normalised to total bacterial content using universal primers and the relative abundance of each phylum determined using the ΔΔ-Ct method ($2^{-\Delta\Delta CT}$).

2.11 Statistical analyses

All statistical analyses were carried out using GraphPad Prism software. Wilcoxon signed-rank tests were used for comparisons between the functional and defunctioned ileum within the same patient. The Mann-Whitney U test was used to compare the two patient cohorts (unfed vs fed). Confidence limits of 95% were used ($p<0.05$*, $p<0.01$**).

3 Results

3.1 Investigating the effect of bowel defunctioning on immune populations in the unfed intestine

3.1.1 Faecal Diversion did not impact dendritic cell or macrophage populations

As part of previous research in non-prebiotic-fed patients, flow cytometry was used to identify subtypes of macrophages (MΦ) and DCs of interest. Samples were stained for resident $CD103^+$ DCs, involved in the immune response to commensal bacteria, and $CD64^+$ antigen-presenting cells (APCs). Here, the acquired data were analysed to assess the balance between tolerance and immunity in the functional and defunctioned bowel upon stoma reversal, to make comparisons with the prebiotic-fed bowel.

The total DC population was identified by the expression of HLA-DR, a component of MHC-II, and the absence of CD3, CD14, CD19, CD20, and CD56, determined using a 'Cocktail' of these antibodies. Within this $HLA\text{-}DR^+$ Cocktail- population, the $CD103^+$ DC subset was determined (Figure 3.1A).

The frequency of CD103+ DCs was recorded as a percentage of the total DC population within the functional and defunctioned bowel (Figure 3.1B). There seemed to be a greater proportion of CD103+ DCs present in the defunctioned bowel, with a mean increase of 34.95%; however, this difference was not statistically significant ($p = 0.0938$).

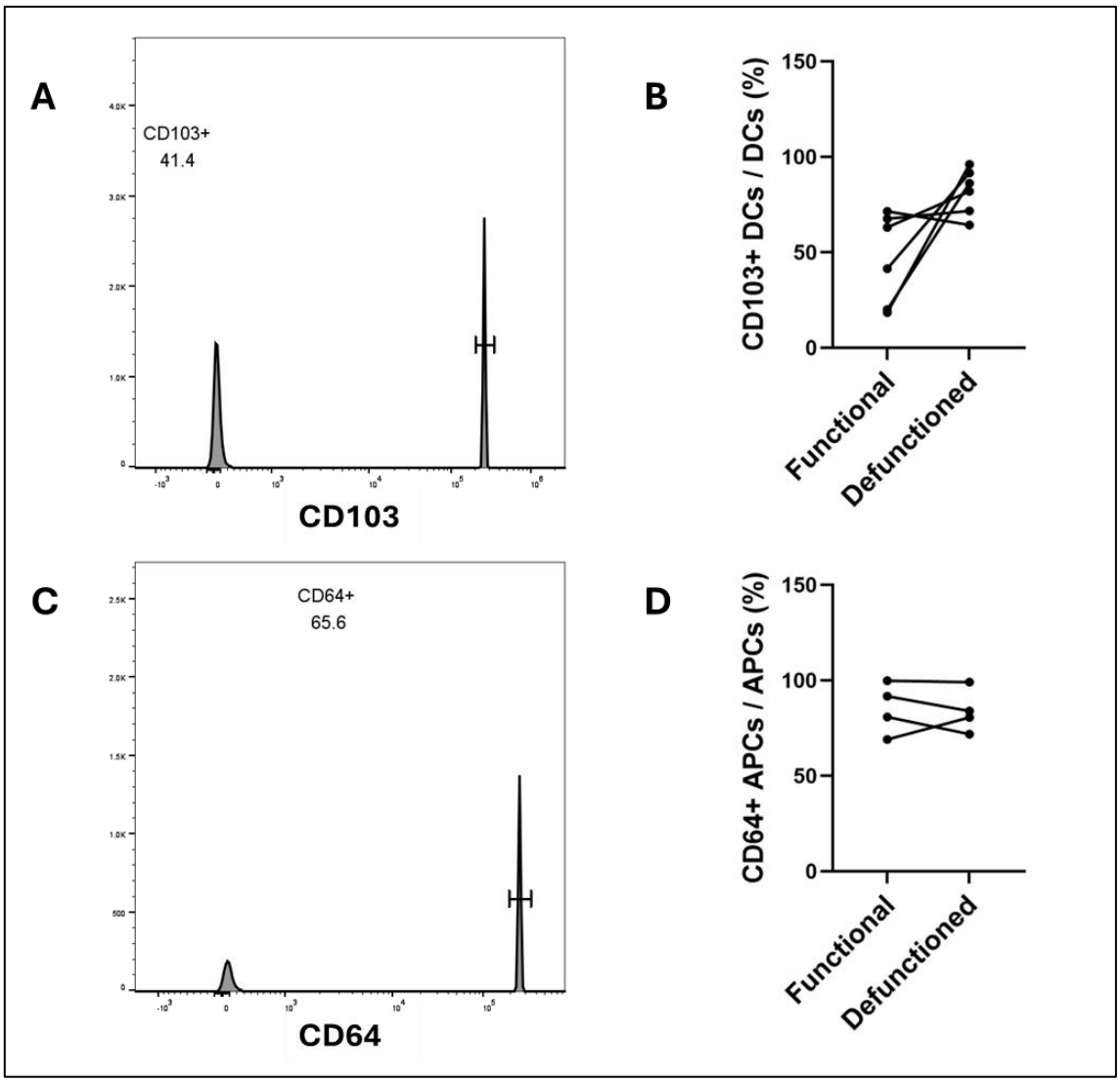

Figure 3.1 - ***Frequency of CD103⁺ DCs and CD64⁺ APCs in the functional and defunctioned segments upon stoma reversal.*** Single cell suspensions were prepared from the mucosa of excess stoma tissue. Cocktail = CD3, CD14, CD19, CD20, and CD56 antibody mixture. **A)** Gating strategy for CD103⁺ DCs within the HLA-DR⁺ population. **B)** Percentage frequency of CD103⁺ DCs in the functional vs defunctioned limb (N=6) (p=0.0938). **C)** Gating strategy for CD64⁺ APCs within the HLA-DR⁺ population. **D)** Percentage frequency of CD64⁺ APCs in the functional and defunctioned segments (N=4) (p=0.875). Data were presented +/- SEM. All data were analysed using Wilcoxon signed-rank testing with 95% confidence limits ($p < 0.05$*, $p < 0.01$**).

CD64 expression within the HLA-DR⁺ antigen-presenting subset was analysed as a measure of inflammation (Figure 3.1C). The frequency of CD64⁺ APCs was highly similar

between the functional and defunctioned limb, providing no evidence of an inflammatory response (p=0.875) (Figure 3.1D).

The percentage of tissue resident CD163⁺ macrophages was identified within the HLA-DR⁺ CD14⁺ macrophage population (Figure 3.2B) and quantified as a percentage of the total macrophage count (Figure 3.2C).

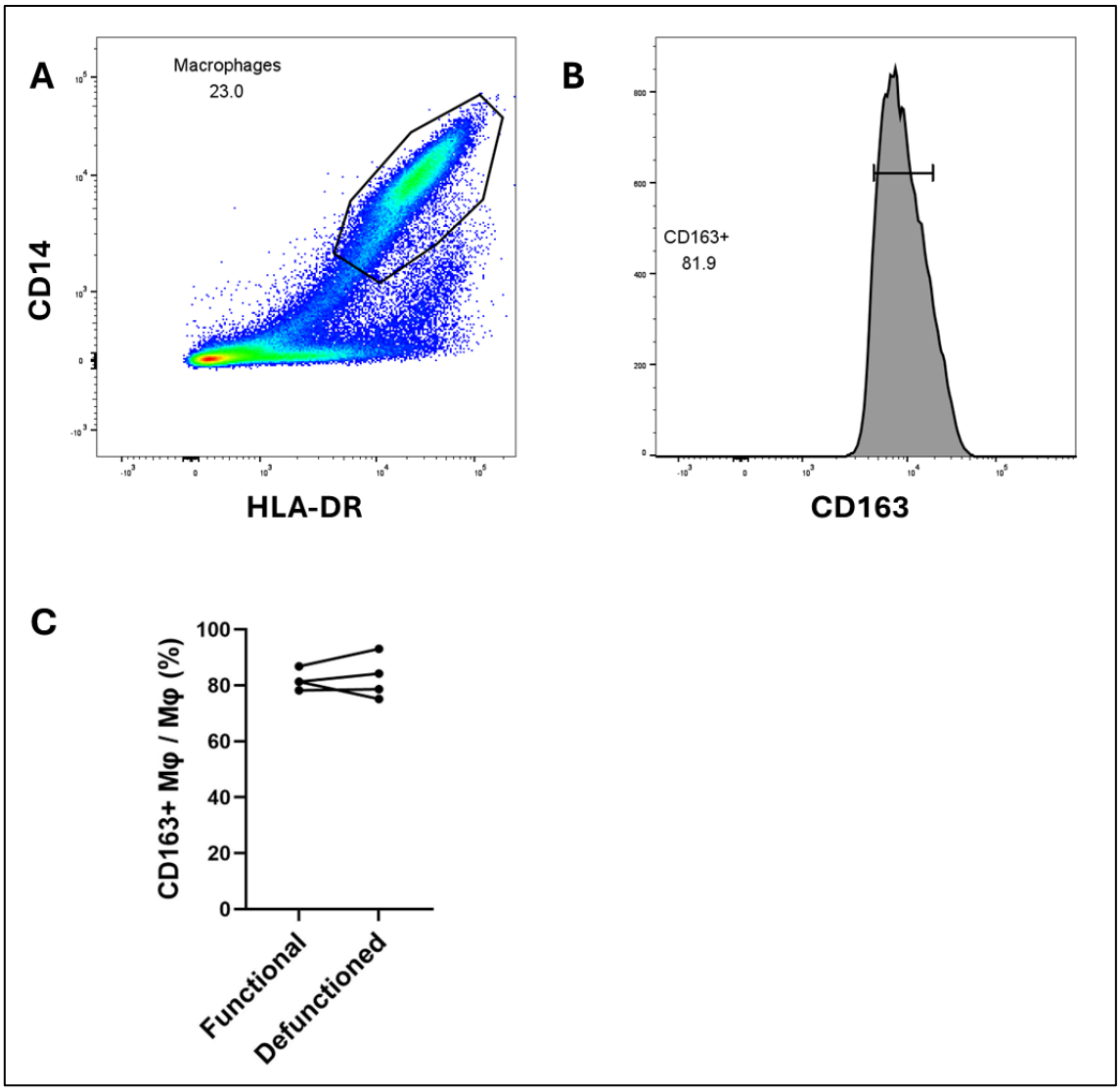

Figure 3.2 - ***Frequency of tissue resident (CD163) macrophages in the intestinal tissue at stoma reversal.*** Single cell suspensions were prepared from the mucosa of excess stoma tissue. **A)** Macrophage gating based on HLA-DR+ CD14+ **B)** Tissue resident macrophages were gated based on CD163⁺ cells within the HLA-DR⁺ group. **B)** The percentage frequency of CD163⁺ macrophages out of the total CD14⁺HLA-DR⁺ macrophage population was determined within

the functional and defunctioned tissue (N=5) (P=0.750). Data were presented +/- SEM. All data were analysed using Wilcoxon signed-rank testing with confidence limits of 95% ($p<0.05$*, $p<0.01$**).

The frequency of $CD163^+$ macrophages was similar between the two segments (p=0.750), suggesting the absence of an ongoing pro-inflammatory tissue repair response upon stoma reversal (Figure 3.2B).

3.1.2 Levels of TLR5 expression were maintained following faecal diversion

Due to the reduced availability of bacterial ligands, it was hypothesised that immune cells in the defunctioned bowel may downregulate their expression of surface receptors such as TLRs. Here, TLR5, the receptor for bacterial flagellin, was quantified to estimate alterations in surface receptors in response to dysbiosis.

TLR5 expression was measured within the DC and macrophage populations to assess the impact of faecal diversion on TLR levels. The TLR5-expressing DC population was identified within the $HLA\text{-}DR^+$ $Cocktail^-$ DC population (Figure 3.3A), and the frequency of $TLR5^+$ DCs was recorded as a percentage of the total DC population (Figure 3.3B). Interestingly, TLR5 expression appeared to be greater in the defunctioned bowel; however, this difference was not significant (p=0.0547) at N=8.

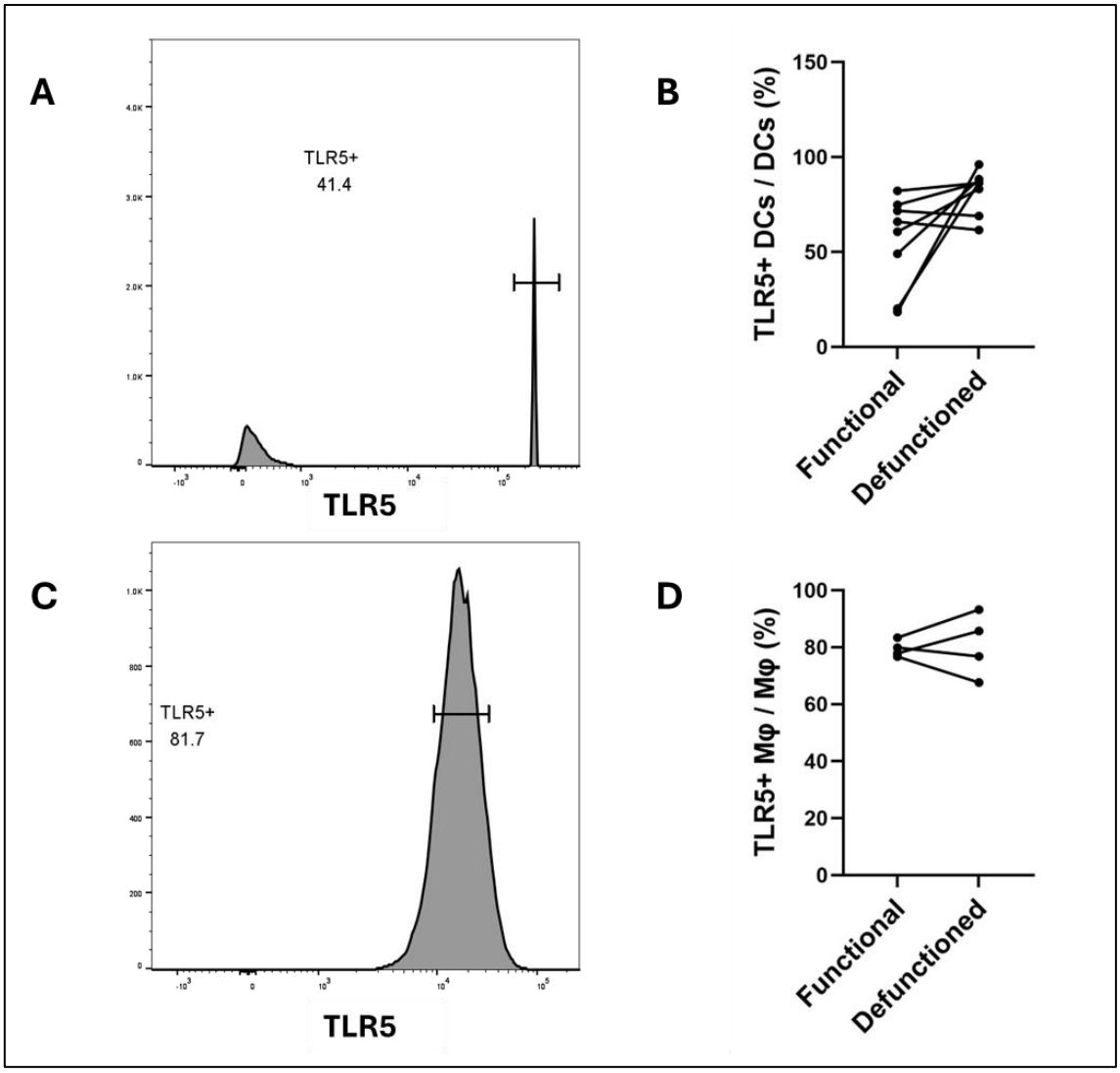

Figure 3.3 - ***Determination of TLR5 expression within macrophage and dendritic cell populations.*** Single cell suspensions were prepared from the mucosa of excess stoma tissue (proximal and distal). **A)** Gating for TLR5$^+$ cells within the DC population (HLA-DR$^+$ Cocktail-). **B)** Percentages of TLR5$^+$ DCs out of the total DC count in the functional and defunctioned bowel (p=0.0547) (N=8). **C)** Gating for TLR5+ cells within the CD14$^+$ HLA-DR$^+$ macrophage population. **D)** The frequencies of TLR5$^+$ macrophages as a percentage of the total MΦ count were recorded for the functional and defunctioned patient samples (N=4) (p=0.875).

Within the CD14$^+$ HLA-DR$^+$ macrophage population, TLR5-expressing macrophages were gated (Figure 3.3A). TLR5 expression was high in both the functional and defunctioned limb, with no significant difference between the two segments (p=0.875) (Figure 3.3B).

3.1.3 An increase in CD11c$^+$ dendritic cells was observed in the defunctioned ileum

CD11c$^+$ DCs are a major subset of myeloid DCs involved in the maintenance of immune homeostasis in the gut. Analysis of CD11c$^+$ DCs by flow cytometry revealed a significant increase in the defunctioned bowel upon stoma reversal (Figure 3.4).

The CD11c$^+$ subset was identified within the HLA-DR$^+$ Cocktail$^-$ total DC population (Figure 3.4A) and frequency recorded as a percentage (Figure 3.4B).

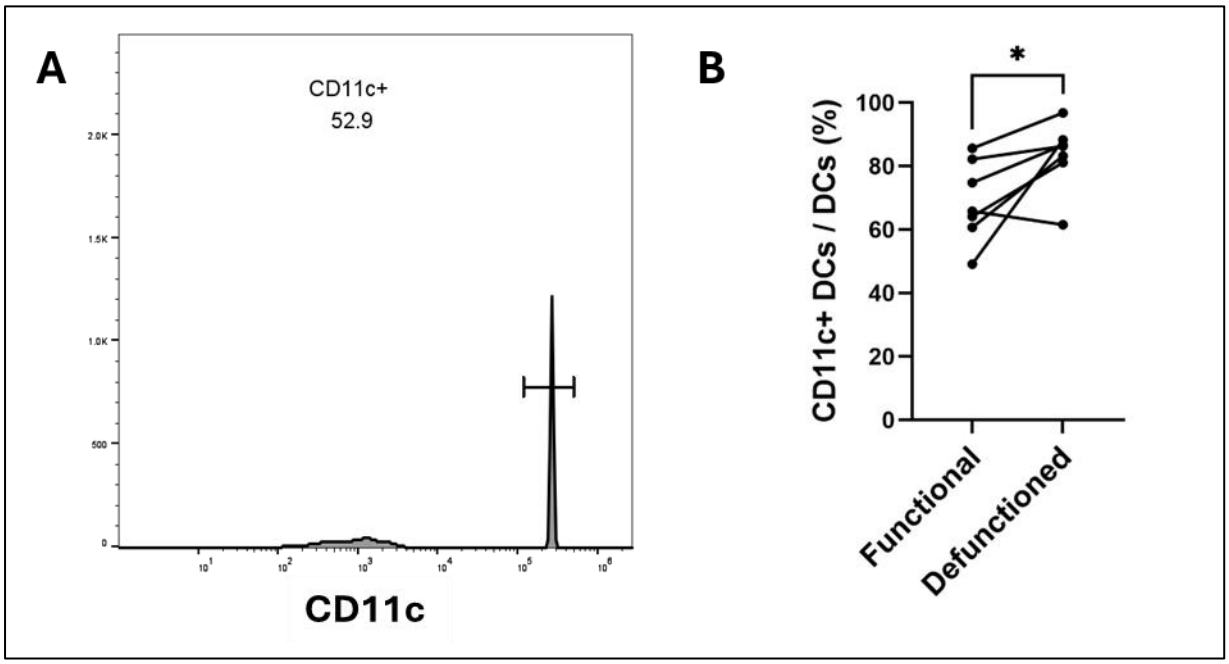

Figure 3.4 - ***Analysis of CD11c$^+$ DCs in proximal and distal ileum upon stoma reversal.*** Single cell suspensions were prepared from the mucosa of excess stoma tissue (proximal and distal). **A)** The CD11c+ subset was gated within the total DC population (HLA-DR$^+$, Cocktail$^-$), using histogram analysis. **B)** Frequency of CD11c$^+$ DCs as a percentage of the total DC count identified within the proximal (functional) and distal (defunctioned) patient tissues (p=0.0469) (N=7).

Interestingly, Figure 3.4B indicates that $CD11c^+$ DCs were significantly increased in the defunctioned bowel after faecal stream diversion ($p=0.0469$). However, it is difficult to determine the immunological impact of this on the defunctioned bowel, as CD11c+ DCs have various phenotypes involved in both anti- and pro-inflammatory responses.

3.2 Assessing the impact of prebiotic feeding on epithelial morphology

3.2.1 Prebiotic feeding restored crypt depth, but villi remained atrophied

H&E-stained sections of functional (Figure 3.5A) and defunctioned (Figure 3.5B) ileum from patients who had undergone prebiotic feeding before stoma reversal were analysed to assess the impact of feeding on intestinal morphology. Crypt depth and villus height were measured using ImageJ software, and the mean depth/height for a minimum of 10 crypts/villi was recorded for each tissue sample. The functional and defunctioned were compared to assess whether the prebiotic feeding altered intestinal morphology within the same patient (Figure 3.5C). The percentage change in crypt depth between the two segments was compared between the unfed and prebiotic-fed cohorts to assess the impact of feeding on the defunctioned intestine (Figure 3.5D).

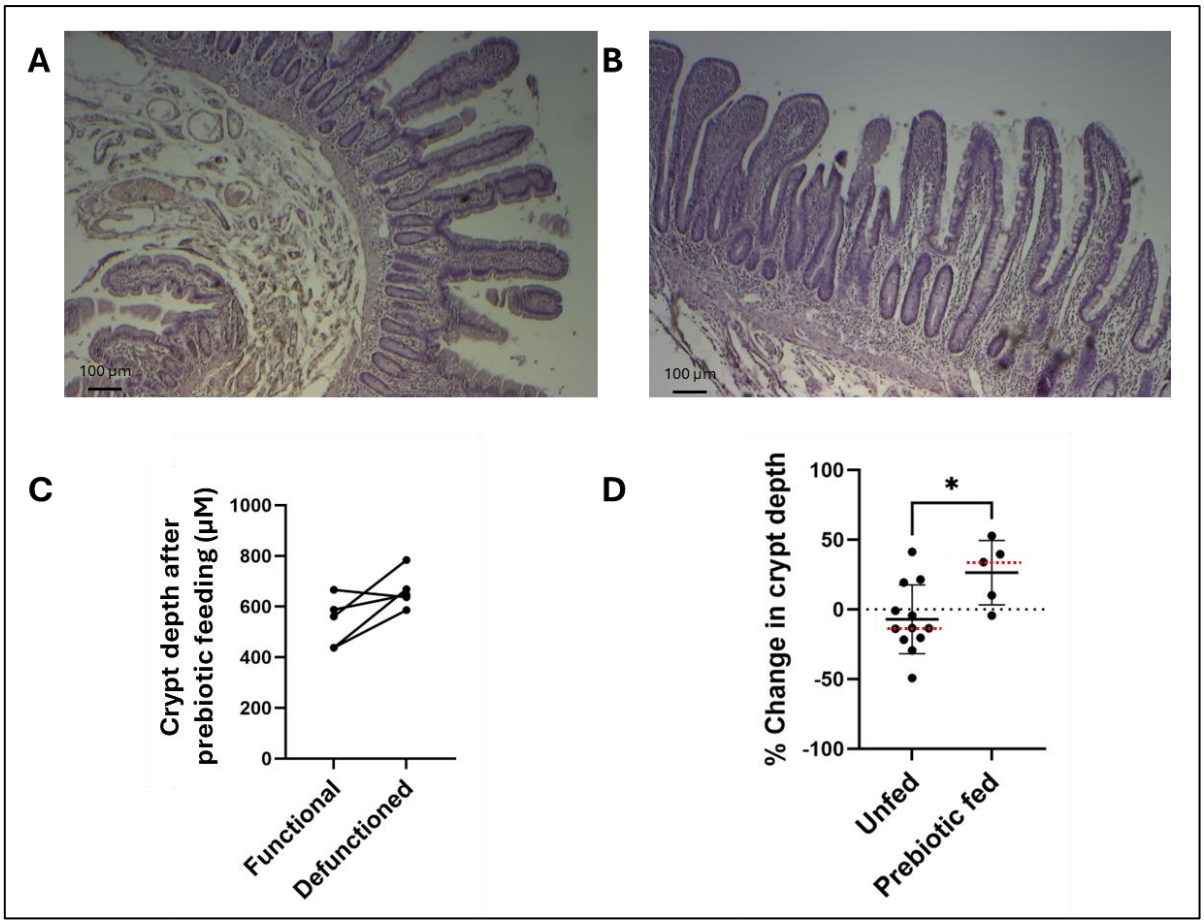

Figure 3.5 - ***Histological analyses of crypt depth in functional and defunctioned ileum with and without prebiotic feeding.*** PAS-Alcian blue-stained sections were imaged using a Moti connect microscope camera at 10X magnification, and analysed using Image J. **A)** Representative section of functional tissue from stoma reversal. **B)** Prebiotic-fed distal ileum within the same patient. **C)** Mean crypt depth (µM) in proximal vs distal ileum after prebiotic feeding (p=0.1250). **D)** Percentage change in crypt depth between proximal and distal bowel in unfed vs prebiotic-fed patients. The mean and SD are shown in black, and the median values are highlighted by the dashed red line (p=0.0365).

Following prebiotic feeding, the depth of crypts in the distal ileum had a tendency to increase when compared to the functioning limb, but at n=5 this did not reach statistical significance (p=0.1250).

Interestingly, compared to the unfed patient group, crypt depth was significantly greater in the prebiotic-fed patients (p=0.0365) upon comparing the functional and defunctioned ileum. This suggests that prebiotic feeding stimulates crypt stem cell proliferation, leading to deeper crypts in the distal bowel, perhaps indicating an improvement in epithelial renewal.

Villus height measurements from functional (Figure 3.6A) and defunctioned (Figure 3.6B) tissues were analysed using the same methodology. Following prebiotic feeding, the villi remained slightly atrophied in defunctioned ileum, with an average reduction of 11% in villus height. However, this atrophy was non-significant (p=0.438) (Figure 3.6C), compared with unfed (Beamish, 2017).

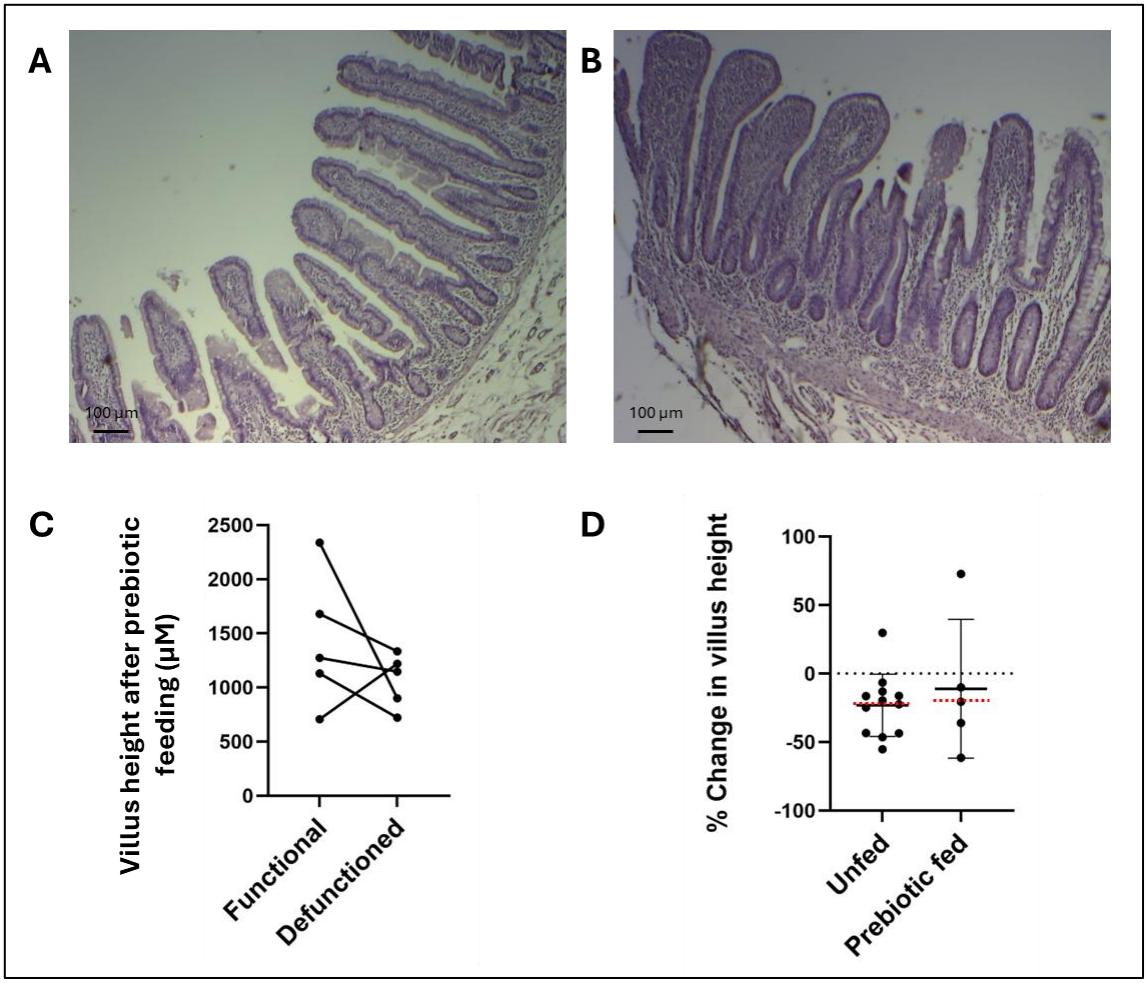

Figure 3.6 - ***Histological analyses of villus height in stoma tissue with and without prebiotic feeding.*** H&E-stained sections were imaged using a Moti Connect microscope camera at 10X magnification and analysed using ImageJ. **A)** Section of the proximal ileum upon stoma reversal. **B)** Prebiotic fed distal ileum. **C)** Mean villus height (µM) in proximal vs distal ileum after prebiotic feeding (p=0.438). **D)** Percentage change in villus height between functional and defunctioned limbs in unfed vs prebiotic-fed patients. Mean and SD are represented in black, and mean values are highlighted by red dashed lines (p=0.879).

The percentage change in villus height between the two intestinal segments was similar between the unfed and prebiotic-fed cohorts (p=0.879), suggesting that the prebiotic feeding did not resolve villus atrophy within the feeding period.

3.2.2 Feeding time may correlate to the extent of epithelial repair

Findings from morphological analysis of the intestinal epithelium suggested that the prebiotic feeding time may not be sufficient to allow for restoration of villus height. It was hypothesised that there may be a correlation between the prebiotic feeding time (days) and the increase in crypt depth/villus height.

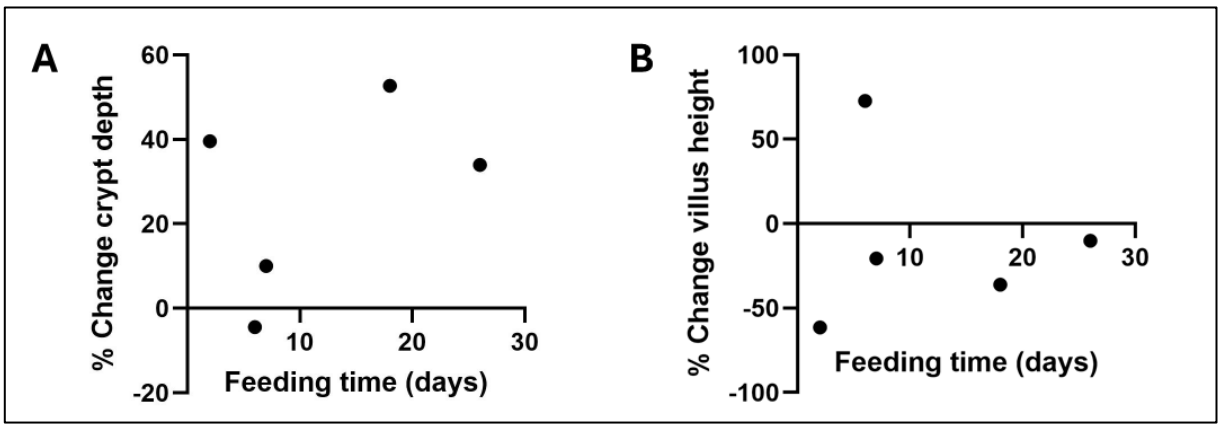

Figure 3.7 - ***Investigating the relationship between prebiotic feeding time and the percentage change in crypt depth and villus height*****. A)** Scatter plot of % change in crypt depth between the proximal and distal segments against the number of days the prebiotic was administered before surgery. **B)** Scatter plot of % change in villus height against feeding time.

However, no correlation was found between the percentage change in crypt depth and the prebiotic feeding time (Figure 3.7A). There may be a slight correlation between feeding time and villus height; for instance, the patient with the shortest feeding time of 2 days had the most significant villus reduction, at 61.46%.

3.2.3 Goblet and proliferative cell quantities in the crypt remained similar after prebiotic feeding

To investigate the effect of prebiotic feeding on specific cell types in the epithelium, goblet cells and proliferative crypt cells were identified using histological staining.

Goblet cells were stained using periodic acid-Schiff's (PAS) reagent, resulting in a pink appearance, as demonstrated

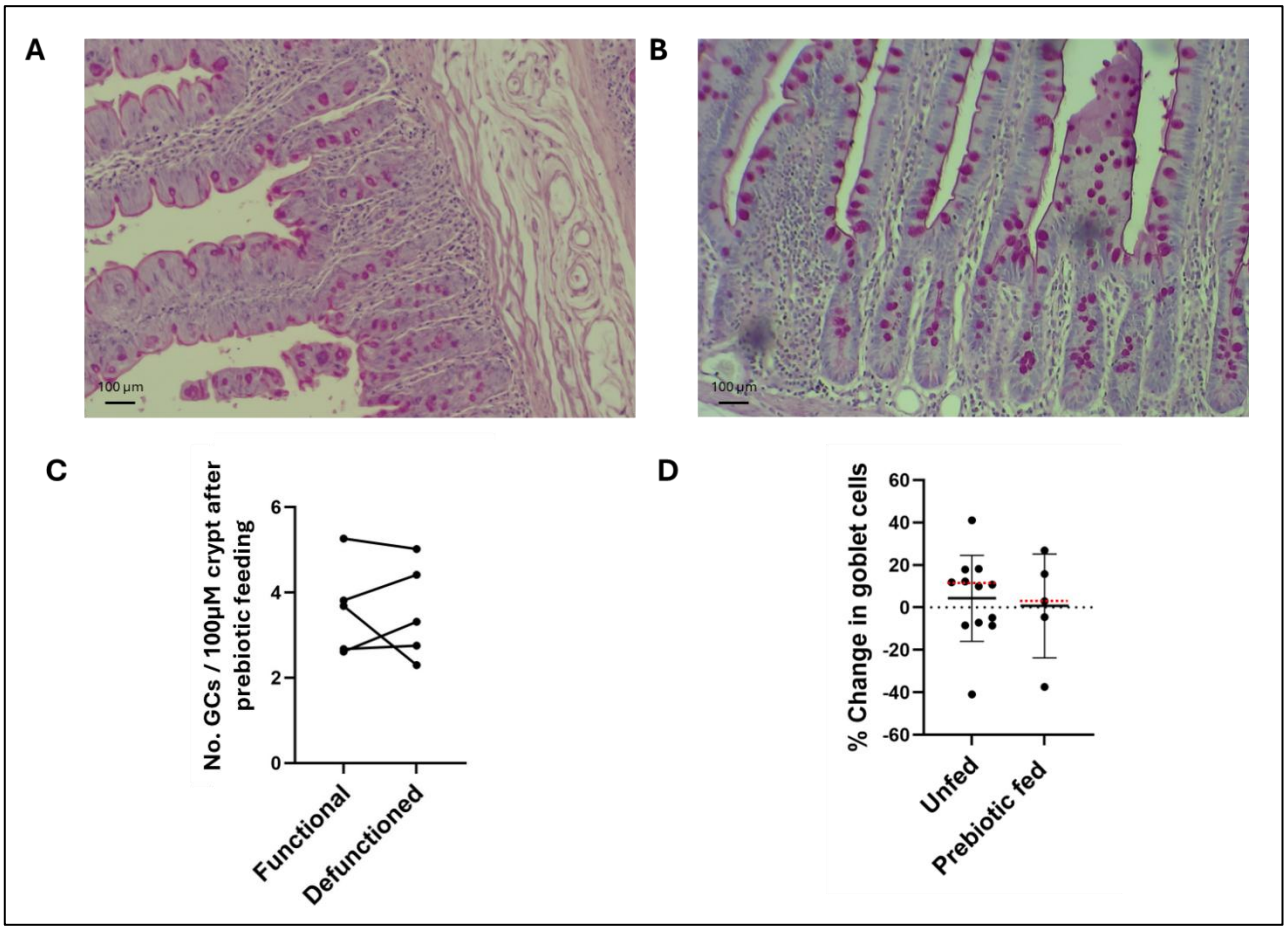

*in Figure 3.8***igure 3.8 -** ***Quantification of goblet cell abundance per 100 µM crypt using PAS-stained intestinal sections.*** Images were taken using a MotiConnect camera, and the number of goblet cells (stained pink) was counted within each crypt. **A)** Representative PAS-stained section of functional intestine, showing goblet cells in pink. **B)** Representative PAS-stained section of prebiotic-fed defunctioned ileum within the same patient (SFS009). **C)** Mean number of goblet cells per 100 µM crypt in the functional and defunctioned segments of the prebiotic-fed patients (N=5) ($p>0.999$). **D)** The percentage change in goblet cell frequency between the proximal and distal limbs was compared between the unfedand prebiotic-fed patient groups (N=12 unfed, 5 fed). The mean and SD are represented in black, and the red dashed line highlights the median ($p=0.959$).

There was no significant difference in goblet cell frequency between the functional and defunctioned ileum, suggesting that prebiotic feeding did not stimulate goblet cell proliferation (Figure 3.8C). The percentage change in goblet cells was highly similar in the unfed and prebiotic-fed ileum, with little variance between the functional and defunctioned limbs (Figure 3.8D).

Crypt stem cell proliferation was approximated by immunofluorescent staining of proliferative cell nuclear antigen (PCNA) positive cells, shown in green (Figure 3.9). The number of proliferative cells per crypt was counted, and the mean number of $PCNA^{+}$ cells per 100 μM crypt was calculated for each sample.

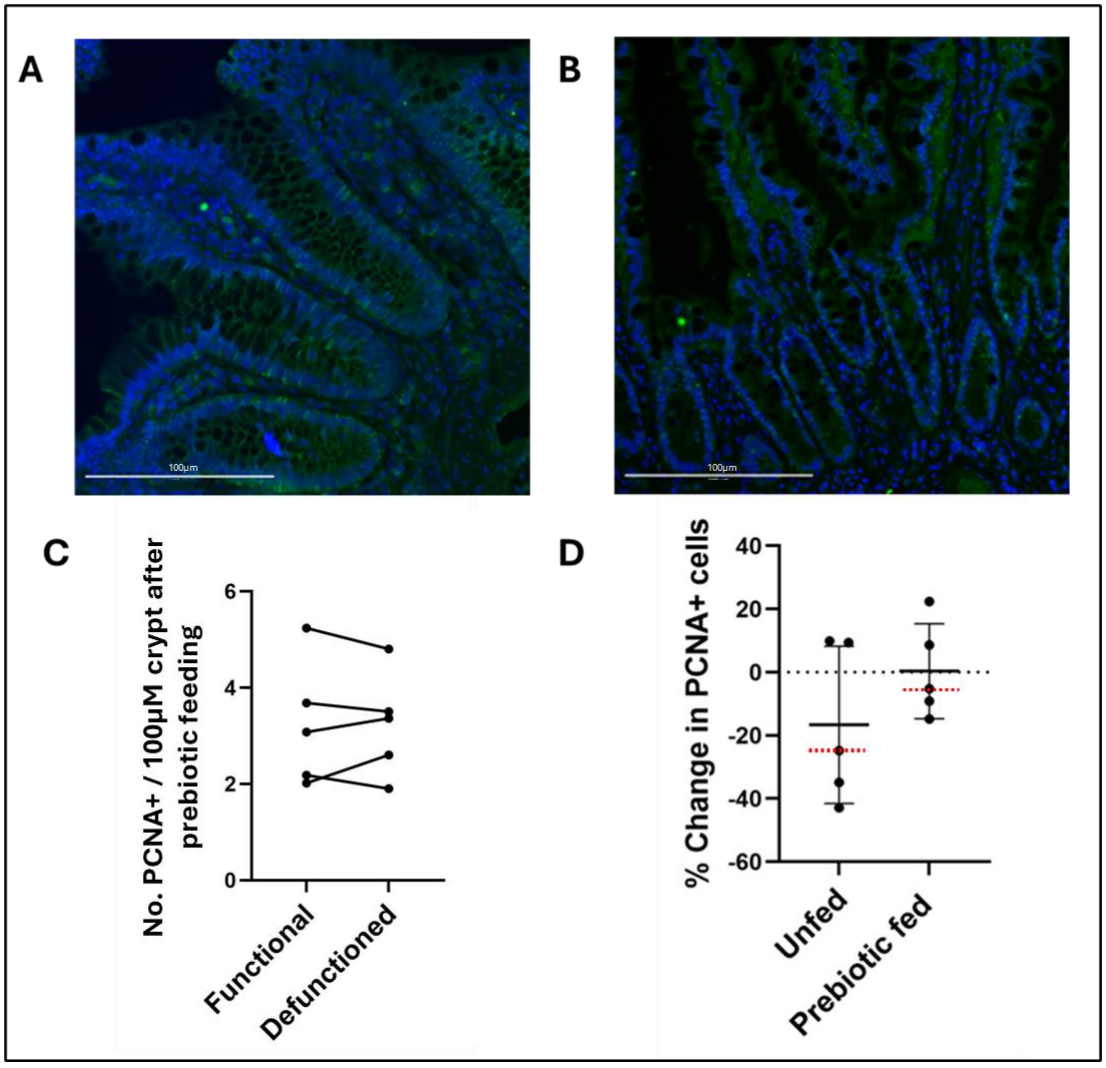

Figure 3.9 - ***Immunofluorescent staining of PCNA-positive cells to estimate crypt stem cell proliferation.*** Representative immunofluorescent PCNA labelling (green) of proliferative cells in A) proximal, healthy bowel and B) prebiotic-fed distal bowel. Nuclei were counterstained with Hoechst 33342 (blue), and images were taken at 20X magnification. C) Mean number of proliferative cells per 100µM crypt in the functional and defunctioned segments after prebiotic feeding (N=5) (p=>0.999). D) Percentage change in proliferative cells between the two limbs of intestine in the unfed vs fed patient cohorts (N=5 unfed, 5 fed). The mean value and SD are represented in black, and the median indicated by red dashed lines (p=0.222).

After prebiotic feeding, there was no significant difference in the number of proliferative cells per 100 µM crypt between the two segments of intestine (p>0.999). The

percentage change in proliferative cell frequency was similar between the unfed and prebiotic-fed groups, with a non-significant increase after feeding (p=0.222).

3.3 Investigating the impact of prebiotic feeding on immune populations in the lamina propria

3.3.1 Prebiotic feeding did not stimulate T helper cells or macrophages

T helper cells and macrophages were identified using flow cytometry, and their frequencies were recorded as a percentage of the total immune cell count ($CD45^+$).

The T helper population was identified by CD4 expression and the absence of CD19, a marker for B lymphocytes (Figure 3.10A). The percentage change in $CD4^+$ T cells between the proximal and distal limbs was recorded and compared between the unfed and prebiotic-fed groups (Figure 3.10B).

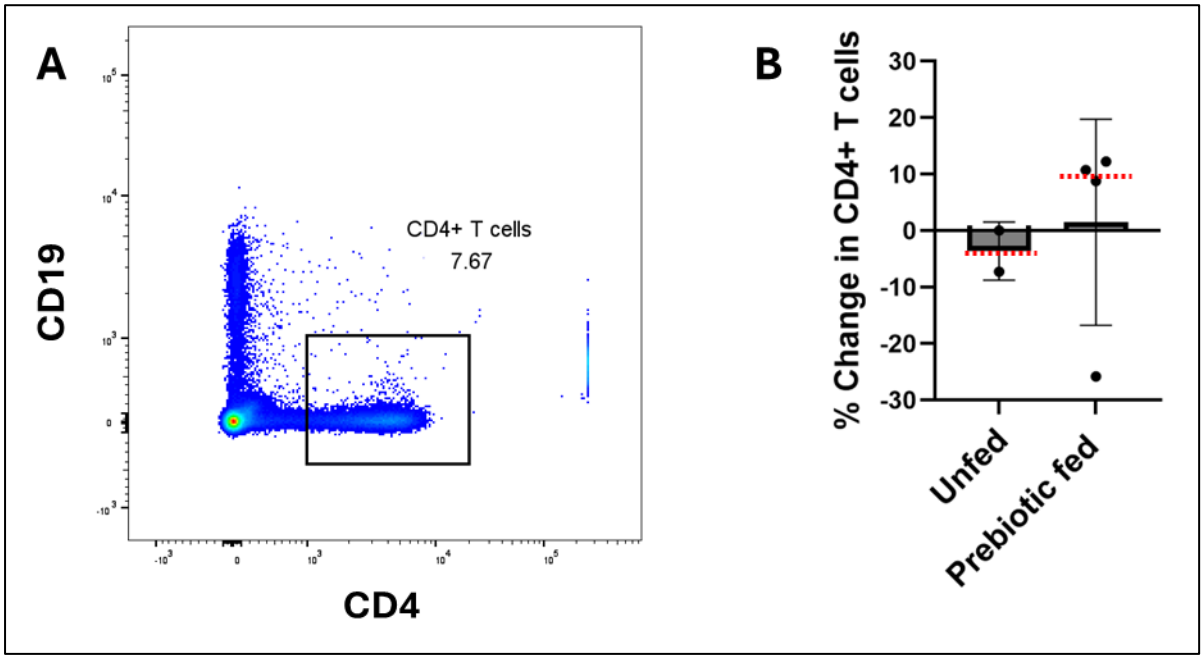

Figure 3.10 - ***Flow cytometry analysis of $CD4^+$ T cells in unfed and prebiotic-fed lamina propria.*** Single cell suspensions were prepared from the mucosa of excess stoma tissue (proximal and distal). A) T helper cells were gated based on $CD4^+$, CD19- within the total $CD45^+$

immune cell population. B) Percentage change in $CD4^+$ T cells between the proximal and distal segments in the unfed (N=2) and the prebiotic-fed (N=4) groups.

The percentage change in $CD4^+$ T cells across the functional and defunctioned tissue was similar between the unfed and prebiotic-fed ileum.

Macrophages were identified based on the expression of CD14 and HLA-DR, and their frequency was recorded as a percentage of the total immune cell count (Figure 3.11A). The percentage change in macrophage frequency between the proximal and distal ileum was compared in unfed and prebiotic-fed patient samples (Figure 3.11B).

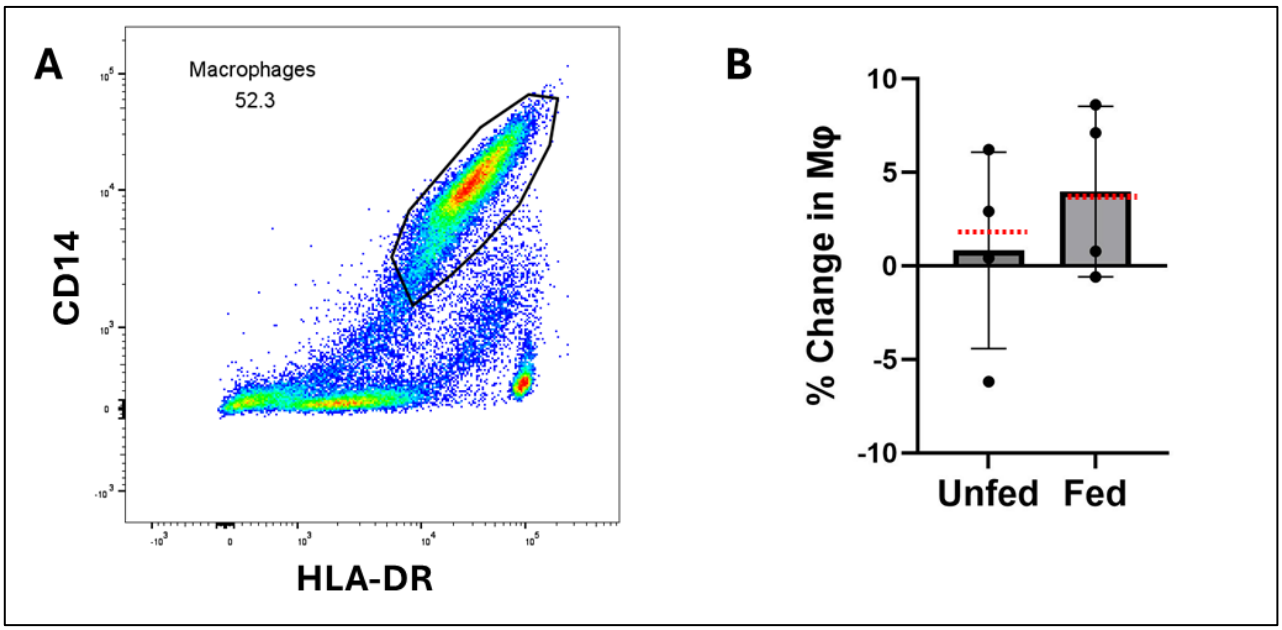

Figure 3.11 - ***Flow cytometry analysis of macrophages in unfed and prebiotic-fed lamina propria.*** Single cell suspensions were prepared from the mucosa of excess stoma tissue (proximal and distal). A) Macrophages were gated based on $CD14^+$ $HLA\text{-}DR^+$ within the total $CD45^+$ immune cell population. B) The percentage change in macrophage frequency between the proximal and distal segments of bowel was compared between the unfed (N=5) and prebiotic-fed (N=4) patient groups. The median values are indicated with red dashed lines (p=0.486.

A slight increase in macrophages was observed after prebiotic feeding, but this was not statistically significant (p=0.486).

3.3.2 CD11c$^+$ dendritic cells were reduced after prebiotic feeding

To investigate differences in CD11c$^+$ DCs after prebiotic feeding, the percentage of CD11c-expressing DCs was compared between unfed and prebiotic-fed patient tissues (Figure 3.12).

CD11c$^+$ DCs were significantly increased in the defunctioned bowel in unfed patients (Figure 3.3), which was reduced after prebiotic feeding (Figure 13.12).

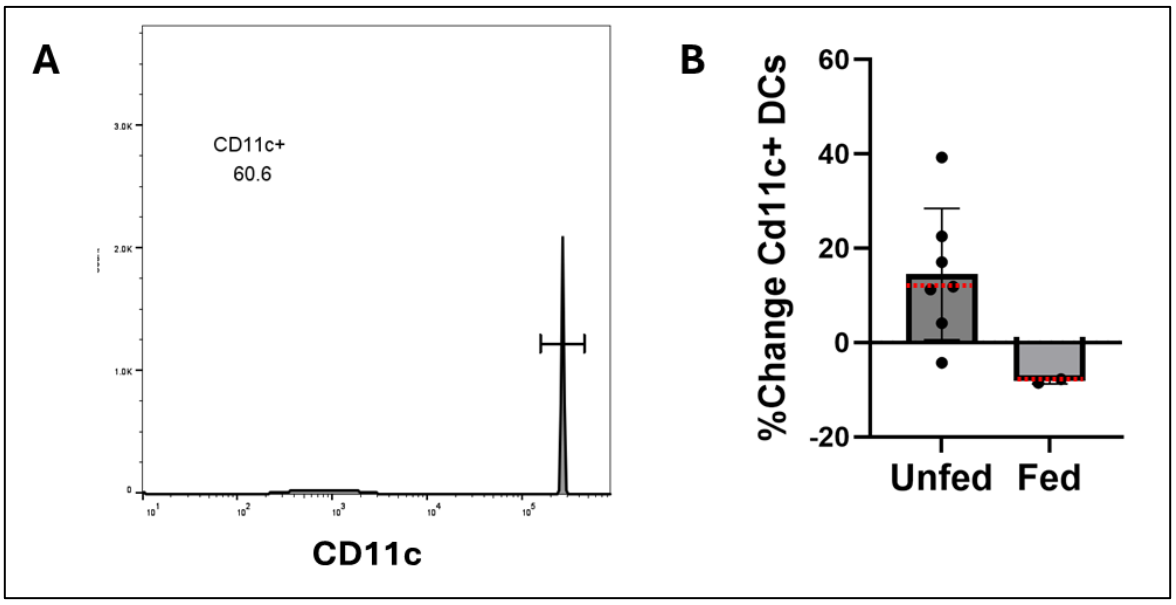

Figure 3.12 - ***Frequency of CD11c$^+$ DCs in unfed and prebiotic-fed ileum.*** Single cell suspensions were prepared from the mucosa of excess stoma tissue (proximal and distal). **A)** The CD11c$^+$ subset was identified within the HLA-DR$^+$ Cocktail$^-$ total DC population, and the frequency of CD11c$^+$ DCs was recorded as a percentage of all DCs. **B)** The percentage change in CD11c$^+$ DCs between the proximal and distal limbs was compared between unfed and prebiotic-fed patient tissues(N=7 unfed, 2 fed). Medians are represented by red dashed lines (p=0.0556)

CD11c$^+$ DCs tended to decrease in the distal ileum of the prebiotic-fed group, relative to the functional bowel within the same patient. A mean reduction of 22.7% as

observed, compared to the unfed patients (p = 0.0556). This was not a significant finding, with only an N=2 in the prebiotic-fed group; however, further analysis may highlight a significant reduction after feeding.

3.4 Phyla-specific 16s-rDNA qPCR

The relative abundance of 4 of the most prominent gut phyla (Firmicutes, Bacteroidetes, γ-Proteobacteria, and Actinobacteria) was estimated using qPCR to quantify phyla-specific regions of 16s-rRNA.

The frequency of each phylum was estimated as a percentage of the total bacterial count, using a universal primer to detect all bacteria present. The percentage change in relative abundance between the proximal and distal ileum after prebiotic feeding was calculated (Figure 3.13).

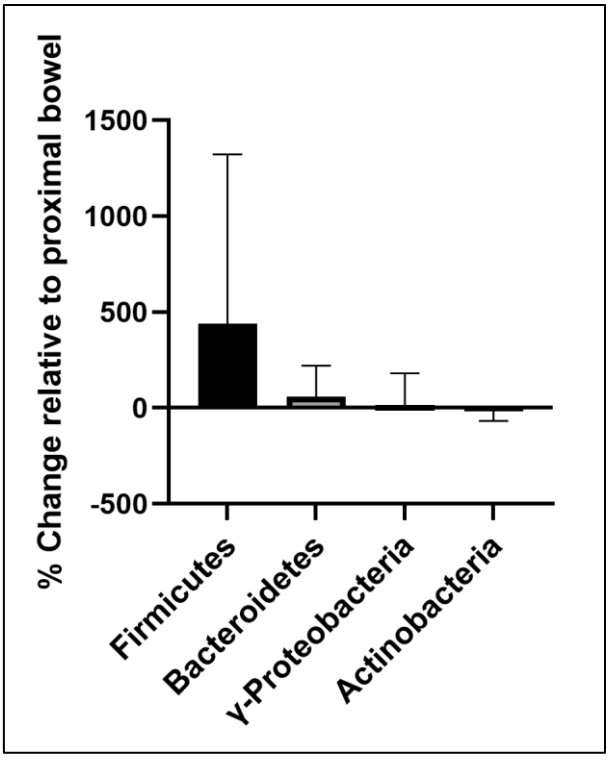

Figure 3.13 - ***Relative percentage change in phyla abundance of Firmicutes, Bacteroidetes, γ-Proteobacteria, and Actinobacteria in prebiotic-fed bowel compared to the functional***

limb. Phyla-specific regions of bacterial r-DNA were detected using RT-qPCR, and the relative abundance of each phylum was recorded as a percentage of the total bacterial count (N=3). The percentage change in phyla abundances between the proximal and distal segments is shown, with standard deviation error bars.

After prebiotic feeding, there was a 439% increase in Firmicutes in the distal bowel, and a 58% increase in Bacteroidetes. The abundance of γ-Proteobacteria and Actinobacteria was similar between the proximal and distal segments, with slight variations of 15.7% (γ-Proteobacteria) and -17.9% (Actinobacteria).

4 Discussion

4.1 The impact of faecal diversion on intestinal immunology

4.1.1 Inflammation may occur initially after stoma formation, but is not present upon stoma reversal

Faecal stream diversion is understood to cause intestinal dysbiosis, with an overall reduction in bacterial load and shifts in dominant phyla (Lee *et al.*, 2023). Dysbiosis has been shown to contribute to the pathogenesis of inflammatory conditions through the dysregulation of immune homeostasis. A similar inflammatory response occurs in the downstream intestine after ileostomy formation, known as diversion colitis (inflamed colon) or pouchitis (inflamed ileal pouch) (Tominaga *et al.*, 2024). Nutrient deprivation leads to depletion of the gut microbiota, which in turn decreases microbe-dependent tolerogenic pathways and promotes a shift towards inflammation. Although diversion colitis is most prevalent in IBD patients, inflammation is likely to occur in most patients to some extent (Tominaga *et al.*, 2018). The impacts of faecal diversion on the intestinal immune system at the time of stoma reversal are not well understood. This study aims to address whether there are any signs of immune imbalance at the time of reversal. Previous work conducted by the Rigby group found that the defunctioned intestinal tissue was fibrotic, indicating an initial inflammatory period upon stoma formation (Beamish *et al.*, 2017)). This aligns with recent single-cell RNA sequencing data that found significant fibrosis with a pro-fibrotic microenvironment in the defunctioned

intestine (Ma *et al.*, 2023). However, there was no evidence of ongoing inflammation at the time of reversal, suggesting that any inflammation had been resolved and a 'dysbiotic equilibrium' was reached over time. To investigate the immunology of faecal diversion, flow cytometry analysis was conducted within the same patient cohort to compare the immune cell populations in the intestinal tissue at the time of reversal. Since histological analysis showed no signs of inflammation, it was hypothesised that there would be no significant difference in immune cell frequencies between the two limbs.

Flow cytometry findings, detailed in Section 3.1, offer further evidence that no significant inflammation was present at the time of reversal, in agreement with histological findings of Beamish *et al,* 2017. The frequency of macrophages, $CD103^+$ DCs, $CD64^+$ cells, and $TLR5^+$ cells was similar between the functioned and defunctioned bowel upon reversal. These cell types were of particular interest due to their role in sampling antigens from commensal bacterial ligands to stimulate T_{reg} cells and activate tolerogenic pathways that are vital in preventing chronic inflammation. During microbial depletion, fewer bacterial ligands are available, leading to a shift towards an inflammatory environment. The frequency of these cell types was very similar in the defunctioned and functioning ileum, suggesting that homeostasis had been restored at the time of reversal.

$CD103^+$ DCs are important mediators of the immune response to commensal bacteria in the intestinal epithelium, supporting the balance of tolerance and immunity by stimulating $iT_{reg}s$ (Ruane and Lavelle, 2011). Figure 3.1B indicates a slight increase in $CD103^+$ DC frequency in the defunctioned ileum upon stoma reversal; however, this was non-significant ($p=0.0938$). This suggests that faecal stream diversion did notsignificantly impact the $CD103^+$ DC subset, and they remained at a similar abundance relative to the total DC population (Figure 3.1A). This small upregulation of $CD103^+$ DCs may have occurred as part of an immune response to the reduced microbial ligands and tissue damage seen during faecal diversion. As CD11c and CD11b expression was not considered in this experiment, the entire $CD103^+$ population was identified, meaning that the phenotype is unknown and explaining the large population size. Despite their varied functions and locations, all $CD103^+$ DCs are involved in maintaining immune balance, making them a good measure of the inflammatory state of the tissue. Therefore, Figure 3.1 suggests that the defunctioned ileum was not inflamed at the time of reversal, as the $CD103^+$ DC frequency was similar to the functional ileum.

Investigating alterations in $CD64^+$ APCs between the functional and defunctioned bowel provides insight into the balance of tolerance and immunity, with high CD64 expression indicating a pro-inflammatory phenotype. Figure 3.1D shows the frequency of $CD64^+$ APCs as a percentage of the total APC count, characterised by HLA-DR expression. The frequency of $CD64^+$ APCs was similar between the two limbs, providing no evidence of inflammation at the time of reversal (p=0.875). Because CD64 is particularly upregulated on DCs during inflammation, it would be useful in the future to look specifically at CD64 expression within the DCs, using the ratio of $CD64^+$ / $CD64^-$ DCs as a measure of the balance between immunity and tolerance (Sánchez-Cerrillo *et al.*, 2023, p. 2).

Moreover, tissue resident macrophages were characterised based on CD163 expression within the $CD14^+HLA\text{-}DR^+$ macrophage population. Overexpression of CD163 is used as a biomarker for inflammatory conditions, indicating the need for tissue repair. There was no significant difference in $CD163^+$ macrophages between the functional and defunctioned portions of bowel, suggesting that there was no inflammatory response after faecal diversion (p=0.750). To investigate this further, it would be useful to identify markers of tissue damage, such as TNFα and IFNγ, using flow cytometry (Menzel *et al.*, 2021).

Under normal conditions, TLR5 is expressed at high levels in the gut due to the substantial number of microbes interacting with the intestinal epithelium. TLR5 expression was investigated within the macrophage and DC populations present in the intestinal tissue at stoma reversal. The frequency of $TLR5^+$ macrophages was highly similar between the two portions of intestine (p=0.875), indicating that the expression of TLR5 is not altered following faecal diversion. Furthermore, the frequency of $TLR5^+$ DCs was slightly increased in the defunctioned DC population, which was interesting due to the reduction in microbial ligands, and could be due to microbial dysbiosis; however, this was non-significant (p=0.0547). These findings may support previous hypotheses that the defunctioned bowel is not inflamed at the time of reversal. However, TLR5 detects both commensal and pathogenic bacteria, stimulating pro- and anti-inflammatory pathways accordingly. Therefore, it is not possible to determine the implications on the intestinal immune environment without assessing cytokine levels.

Interestingly, $CD11c^+$ DCs were significantly increased in the defunctioned segment upon stoma reversal (Figure 3.4) ($p=0.0468$). Since $CD11c^+$ DCs represent a major immune population that can mediate both pro- and anti-inflammatory responses, their role in faecal diversion cannot be fully understood without examining their cytokine production. $CD11c^+$ DCs may be upregulated as part of an inflammatory response; however, such a response would typically be accompanied by fluctuations in additional immune populations such as macrophages, which were not detected in this patient cohort. This suggests that the accumulation of $CD11c^+$ DCs in the defunctioned bowel may instead represent a tolerogenic role aimed at reducing inflammation. For example, IL-10 secreting $CD11c^+$ DCs are known to facilitate the resolution of immune responses by promoting an anti—inflammatory microenvironment (Girard-Madoux *et al.*, 2016). It is possible that $CD11c^+$ DCs were upregulated in the defunctioned segment as a protective mechanism to resolve any inflammation that occurred upon stoma formation. Evaluating cytokine expression would provide a critical insight into whether the observed $CD11c^+$ DC population is involved in driving inflammation or promoting tolerance.

Overall, macrophages and DCs in the defunctioned bowel had similar levels of TLR5 expression as the functional tissue. Paired with the similarity in $CD103^+$ DC, $CD64^+$ APC, and $CD163^+$ macrophage levels between the two limbs, these findings are indicative that there was no ongoing inflammation at the time of reversal. However, further investigation is required to determine the phenotypes of immune cells present, as many of the cell types have multiple roles in the intestinal immune system.

4.2 Prebiotic stoma feeding and intestinal epithelial repair

4.2.1 Prebiotic feeding may stimulate epithelial cell division by targeting gut microbiota

It is well understood that faecal diversion renders the defunctioned limb atrophied, affecting nutrient absorption and barrier function upon reanastomosis, contributing to post-operative morbidities (Chow *et al.*, 2009). This intestinal atrophy is mainly

characterised by a reduction in villus height, with the crypts not significantly shortened in the unfed patient group, as described by Beamish et al. (2017).

Following prebiotic feeding, analysis of the intestinal tissue revealed an increase in crypt depth relative to the functional tissue, indicating that cell division was upregulated in the distal ileum. This suggests that the prebiotic was able to stimulate crypt stem cell division (Markandey *et al.*, 2021). To investigate the rate of crypt stem cell division, the rate of proliferation in each crypt was determined (Figure 3.9).

In the unfed cohort, the rate of proliferation in the crypts was significantly reduced by approximately 20% in the defunctioned tissue (Beamish, 2017). After feeding, however, immunofluorescent PCNA analysis revealed similar levels of proliferation in the defunctioned crypts to the functional portion. This indicates that the defunctioned tissue may be renewing at a similar rate as the healthy tissue after feeding, suggesting that the prebiotic mixture stimulated proliferation. Since the gut microbiota are known to stimulate epithelial renewal and maintain the crypt stem cell niche, increased proliferation is likely driven by replenishment of the microbiota. The importance of prebiotic fibre in maintaining microbe-epithelium interactions in the intestine is well characterised, with fibre deprivation causing barrier dysfunction through the erosion of the mucosa (Desai *et al.*, 2016). For instance, bacterial SCFAs, produced by fermentation of fibre, are an important energy source for IECs, and often contribute to signalling pathways that promote stem cell proliferation (Gehart and Clevers, 2019). The availability of dietary fibre may also alter the mucus layer: the outer mucus layer provides a glycan store which is foraged by microbiota as a food source. In the absence of sufficient dietary fibre, glycan-dependent gut microbiota begin to use the mucus layer as a food source, degrading the mucus layer and impairing barrier function (Tailford *et al.*, 2015).

Alternatively, it is possible that the prebiotic feed directly fed IECs with dietary nutrients, reversing the effects of nutrient starvation and promoting proliferation. Cellular nutrient deprivation during defunctioning may contribute to the atrophy observed, rather than the loss of microbiota being the sole cause (Rock *et al.*, 2022). The prebiotic mixture contains carbohydrates, fats, protein, and essential vitamins and minerals. Therefore, the increased proliferation seen in Figure 3.9D may be due to IECs

directly receiving nutrients from the feeding mixture, rather than depending on microbial metabolites.

4.2.2 Villus height was not restored during the prebiotic feeding period

Despite the increase in crypt depth, the villi remained atrophied in the distal bowel following prebiotic feeding (Figure 3.6). However, the previous study in the unfed patient cohort found a significant reduction in villus height between the functioned and defunctioned bowel. Whereas the villi were no longer significantly atrophied after prebiotic feeding ($p=0.315$). This highlights a slight improvement in the average villus height between the unfed and the prebiotic-fed groups, but likely not enough to significantly improve post-operative nutrient absorption.

Based on these findings, it is likely that the prebiotic feeding period was not long enough to allow for the restoration of villus height. Under normal conditions, ISCs are constantly proliferating in the base of the crypts and migrate upwards towards the villus as they become specialised epithelial cells. IECs continue to move up to the tip of the villus, where they are shed into the intestinal lumen after 3-5 days. During faecal diversion, this process is slowed due to the absence of nutrients and microbiota, leading to the observed atrophy. It may take several days of prebiotic feeding for the gut microbiota to replenish and promote IEC turnover. Therefore, we hypothesise that ISC proliferation began during the feeding period, but there was not sufficient time to see significant improvements in villus height. For future patients, a minimum feeding time of 2-3 weeks is advised.

Scatterplot analysis (Figure 3.7) reveals a slight correlation between feeding time and villus height, with the exception of an outlier who experienced a 72.8% increase in villus height after just 6 days of feeding. The patient with the shortest feeding time experienced the most severe villus atrophy, with a reduced height of 61.4%; whereas the patient with the highest feeding time only had a slight reduction of 10.01%. This supports the theory that increased feeding time reduces the risk of atrophy. However,

only 5 patients were included at this stage, so further investigation into the optimal feeding time is required.

4.2.3 Prebiotic feeding did not stimulate goblet cells in the epithelium

Figure 3.8D highlights that despite the differences in crypt depth between the unfed and prebiotic-fed defunctioned bowel, the abundance of goblet cells per 100 μM crypt was unaffected. This suggests that the absence of gut microbiota in the defunctioned bowel impacts the overall rate of IEC renewal but does not alter goblet cell maturation. However, single-cell RNA sequencing of defunctioned ileum has revealed reduced expression of genes related to mucus secretion, such as *MUC2* (Ma *et al.*, 2023). Therefore, it is possible that goblet cells of the defunctioned tissue were defective and unable to maintain a healthy mucus barrier.

Overall, the frequency of goblet cells was highly similar after prebiotic feeding, indicating that the prebiotic had no impact on goblet cell maturation. RNA sequencing of prebiotic-fed ileum may provide insight into the activity of goblet cells, assessing their ability to secrete mucins and maintain the mucus layer.

4.3 Impact of prebiotic feeding on immune cell populations in the lamina propria

The total $CD4^+$ T cell count is a useful measure of the ability of the intestinal immune system to recognise and respond to immunostimulatory molecules and orchestrate an appropriate response (Brockmann *et al.*, 2023). While there are many subpopulations within the T helper (Th) population, the total frequency provides insight into the gut immune state. The abundance of Th cells may also impact the ability of the gut to self-renew through promoting ISC proliferation and differentiation (Biton *et al.*, 2018).

Flow cytometry analysis of $CD4^+$ T cells present in the mucosa upon stoma reversal revealed no significant difference (p=0.731) between the unfed and prebiotic-fed patients (Figure 3.10). Both cohorts had similar levels of T helper cells in the functional ileum compared to the defunctioned, suggesting that faecal diversion did not impact the overall Th population. This indicates that the depletion of microbiota in the defunctioned bowel did not have a significant impact on the Th cell frequency. However, there was an overall decrease in Th cells between the functional and defunctioned ileum of the unfed group, which may be caused by reduced microbiota (Sun *et al.*, 2023). This was resolved after prebiotic feeding, with highly similar Th cell levels between the functional and defunctioned limb. This indicates that the Th cell population was maintained, suggesting that the intestinal immune system is functioning normally. However, there are many subpopulations of Th cells with various roles in orchestrating tolerance and immunity in the gut. For instance, Th17 cells are crucial IL-10 secretors that promote homeostasis and protect the epithelial barrier (Brockmann *et al.*, 2023). Although the overall population size was similar between the two intestinal limbs, there were likely alterations in the subpopulations present within them. Therefore, it would be beneficial to identify Th cell phenotypes in both the functional and defunctioned bowel by staining for additional surface markers, such as CD25 (T_{reg}s), and examining cytokine expression.

Under homeostatic conditions, macrophages make up a large proportion of intestinal immune cells, with key roles in antigen sampling of luminal contents and stimulating appropriate downstream responses (Bujko *et al.*, 2018). Macrophage infiltration in the gut tissue upon stoma reversal may indicate an inflammatory response to infection or tissue damage. Figure 3.11 compares the percentage change in macrophages between the functional and defunctioned intestine within the unfed and prebiotic-fed patients. The percentage change in macrophages across the two stoma limbs was similar between the patient cohorts, suggesting that the prebiotic feeding did not impact the overall macrophage population frequency (p=0.486). Investigating the various phenotypes of macrophages present within each of the intestinal tissues would provide further insight into the impact of prebiotic feeding on macrophages, as there may be

fluctuations in specific subsets that cannot be determined by total macrophage frequency.

After prebiotic treatment, the frequency of $CD11c^+$ DCs was reduced in the defunctioned bowel, with a mean reduction of 22.7% compared to the unfed cohort ($p=0.0556$). Although this was not statistically significant at N=2 prebiotic-fed patients, it indicates a shift towards homeostatic immune conditions. Further analysis of $CD11c^+$ DC populations may provide further insight into the nature of this finding.

4.4 Prebiotic feeding may replenish commensal bacterial phyla

Faecal stream diversion is associated with a decrease in total bacterial load and a reduction in beneficial bacteria, causing a shift in dominance towards potentially harmful phyla such as Proteobacteria (Lee *et al.*, 2023). Similar shifts in phyla abundance were observed in the unfed patient cohort, with Firmicutes significantly reduced, γ-Proteobacteria increased, and microbial dominance switched to Bacteroidetes (Firmicutes ($n=18$, $p=0.02$), Bacteroidetes ($n=18$, $p>0.05$), γ-Proteobacteria ($n=9$, $p<0.05$)) (Beamish *et al.,* 2017).

The role of prebiotics (dietary fibre) in the composition of the gut microbiota is well established, with low-fibre diets associated with alterations in the microbiota that contribute to poor digestion and nutrient absorption (Gill *et al.*, 2021). Since Firmicutes are key fermenters of fibre, the dysbiosis observed in defunctioned bowel was likely caused by the lack of available fibre, promoting a shift towards species that thrive on amino acids and lipids (Cronin *et al.*, 2021). Therefore, it was hypothesised that prebiotic feeding should replenish the Firmicutes, promoting a shift back to normal phylum dominance.

After prebiotic feeding, Firmicutes were significantly increased by 439% in the defunctioned bowel. This suggests that the prebiotic feeding was successful in providing an energy source for the Firmicutes, promoting their growth. Bacteroidetes were also increased by 58%, suggesting that the phylum dominance had shifted towards normal conditions, with Firmicutes and Bacteroidetes making up the majority. The abundance of γ-Proteobacteria and

Actinobacteria remained similar between the functional and defunctioned limbs. These findings indicate that the prebiotic feeding may allow replenishment of the key phyla Firmicutes and Bacteroidetes in the defunctioned limb, promoting eubiosis.

These findings provide promising evidence that the prebiotic feeding promoted a shift towards beneficial phyla, which are likely to stimulate intestinal repair through microbial metabolite signalling. However, 16S-rDNA qPCR provides only an estimate of the phyla abundances and does not address species-specific alterations in microbiota. Each of the phyla analysed contains a diverse array of bacterial species, including those beneficial to human health and potential pathogens (Rosenberg, 2024). While it is useful to look at the overall fluctuations in phyla abundance between the functional and defunctioned bowel, there may still be dysbiosis at the species level. Therefore, 16S sequencing will allow further insight into species-level changes to the microbial composition.

4.5 Limitations and future directions

4.5.1 Characterising the immune environment in defunctioned bowel

Although flow cytometry can provide insight into the overall immune cell populations in the defunctioned bowel, many cell types of interest have both pro-inflammatory and anti-inflammatory roles. In the intestinal immune system, many cell types such as macrophages and DCs can switch phenotypes and cytokine production in response to different stimuli (Perez-Lopez *et al.*, 2016). Therefore, assessing the frequency of these populations is not sufficient to determine the presence/absence of an inflammatory response. It would be useful to investigate cytokine levels in the tissue samples using flow cytometry to establish the balance between pro- and anti-inflammatory signalling at the time of reversal.

Additionally, it may be beneficial to identify the specific location of immune populations within the mucosa to determine tissue infiltration and link it to regions of atrophy or tissue damage. Immunohistochemical staining can identify specific cell types, such as

macrophages, within sections of intestinal tissue, to investigate regions of potential inflammation.

4.5.2 Morphometric analysis as a measure of epithelial repair

This study assessed epithelial recovery in the defunctioned ileum through histological parameters such as crypt depth, villus height, goblet cell frequency, and proliferative cell frequency. While these figures may provide insight into the morphology of the intestinal epithelium at the time of stoma reversal, they represent static, structural readouts that do not address functionality. For instance, crypt depth and villus height can be influenced by multiple factors, such as inflammation and mechanical stress, and may not be representative of intestinal barrier function. The measurement of villi and crypts may also be subjective, and altered by the orientation of the tissue (Taavela *et al.*, 2013). Despite this, crypt depth: villus height (CD: VH) ratio is commonly used as a measure of intestinal epithelial health, with studies suggesting longer villi and shorter crypts as an indicator of barrier functionality. CD:VH ratio could be calculated in the future to estimate epithelial repair in the defunctioned bowel, instead of analysing crypt depth and villus height separately.

Alternatively, the I see inside (ISI) scoring system uses a numerical score of mucosal health that combines LP thickness, epithelial thickness, enterocyte proliferation, immune cell infiltration, goblet cells, and fibrosis (Belote *et al.*, 2019). ISI scoring was not possible within the scope of this project as it requires more thorough training for histological interpretation. However, similar scoring was utilised in the unfed cohort by Beamish et al (2017), so it would be useful to compare the prebiotic-fed tissues in the future.

Moreover, goblet cell counts cannot determine functionality, as they do not account for the functionality of the secreted mucins or the composition of the mucus layer. Similarly, PCNA immunofluorescence can identify proliferative cells but cannot distinguish between regenerative proliferation and aberrant/dysregulated proliferation caused by inflammation. Overall, while histology is a valuable tool for characterising epithelial structure and cellular composition, the complexity of epithelial health is not determined, with factors such as barrier integrity, permeability, and metabolic functions left unknown.

4.5.3 Confirming the role of the gut microbiota

This study hypothesised that prebiotic stimulation of the distal limb would provide the nutrients necessary to replenish the gut microbiota, increasing microbial interactions with the epithelium, and promoting intestinal repair. However, any improvements in intestinal health may be directly caused by the nutrients in the Ensure® shake, which contains a complete feed of macro and micronutrients. During faecal diversion, intestinal epithelial cells are deprived of nutrients, which may cause cell death, contributing to the atrophy observed in defunctioned tissue. There is substantial evidence supporting the impact of enteral nutrition on the intestinal epithelium, with enteral feeding restoring mucosal atrophy after total parenteral nutrition (TPN) (Yang *et al.*, 2009). Therefore, the improvements in crypt stem cell proliferation detailed in Figure 3.5 may be caused by direct feeding of IECs.

To further investigate the role of microbial interactions in epithelial repair after stoma reversal, future work should profile the bacterial composition at the species level by 16S sequencing. This is crucial for validating the qPCR characterisation of bacterial phyla detailed in Figure 3.13, as well as looking more closely at species-level alterations in bacteria. If 16S sequencing of prebiotic-fed samples shows a shift towards eubiosis in the defunctioned bowel compared to unfed controls, the role of the microbiota will be indicated. It is likely that both the Orafti® prebiotic and Ensure® drink impact epithelial turnover, as microbial regulation and nutrient availability are crucial for maintaining barrier function.

4.6 Conclusions and clinical relevance

This study investigated the effects of faecal diversion on intestinal epithelial morphology, immune cell populations, and microbial composition, and assessed whether prebiotic stimulation of the defunctioned ileum could improve mucosal recovery before ileostomy

reversal. Overall, the findings demonstrate that the defunctioned bowel is not inflamed at the time of reversal, with major immune populations such as macrophages and CD64+ APCs undisrupted. However, an increase in CD11c+ DCs was observed, potentially indicating an anti-inflammatory adaptation to restore homeostasis.

Importantly, prebiotic feeding promoted crypt stem cell proliferation to some extent, with crypt depth and proliferative ISCs restored to levels comparable to functional bowel, indicating reactivation of regenerative pathways. However, villus height remained slightly atrophied compared to the functional ileum, with only a slight improvement compared to the unfed tissue. Goblet cell frequencies remained similar between the functional and defunctioned segments in both the unfed and prebiotic-fed tissues, suggesting that faecal diversion does not impact their proliferation. However, the functionality of the intestinal barrier in terms of mucus composition and permeability is undetermined. Immunological analysis of prebiotic-fed ileum found a reduction in $CD11c^{+}$ DCs compared to unfed, indicating a potential shift towards homeostasis. Moreover, phylum-specific bacterial analysis suggested a trend towards replenishment of commensal phyla such as Firmicutes, supporting the hypothesis that prebiotic stimulation enhances epithelial health by restoring microbe-epithelial crosstalk, improving patient outcomes.

From a clinical perspective, these findings suggest that prebiotics can stimulate crypt renewal and modulate immune populations, providing a rationale for their use in preventing post-operative complications. Of the 5 patients studied so far, no serious complications (e.g. anastomotic leak, ileus, and ileitis) have been reported. Prebiotic stoma feeding is a safe and minimally invasive intervention to improve epithelial repair before reversal surgery, with even very short-term feeding showing some improvements.

While the sample size was limited and villus restoration remained incomplete, these findings demonstrate that prebiotic feeding can activate epithelial turnover and promote a more favourable microbial/immune environment. Future studies should explore optimal feeding durations, validate the role of the gut microbiota in stimulating ISC proliferation, and perhaps attempt combination strategies with probiotics in patients with severe dysbiosis.

5 Appendices

5.1 Patient consent form + ethics approval

Royal Preston Hospital,
Sharoe Green Lane,
Fulwood,
Preston.
PR2 9HT

Date:
Centre Number:
Study Number:
Participant Identification Number for this trial:

CONSENT FORM

Study title: Enteral feeding of fibre to improve microbiota.

Name of Researchers: Mr Arnab Bhowmick, Mr Peter Mitchell and Dr Rachael Rigby

Please initial box

1. I confirm that I have read and understand the information sheet dated 17-08-22 (version.2) for the above study. I have had the opportunity to consider the information, ask questions and have had these answered satisfactorily. ☐

2. I understand that my participation is voluntary and that I am free to withdraw at any time without giving any reason, without my medical care or legal rights being affected. ☐

3. I understand that data collected during the study may be looked at by individuals from Lancaster University, from regulatory authorities or from the NHS Trust, where it is relevant to my taking part in this research. I give permission for these individuals to have access to my records. ☐

4. My tissue may be stored anonymously and used in future research (pending further ethical approval - optional). ☐

5. I agree to take part in the above study. ☐

Name of Patient	Date	Signature
Name of Person taking consent	Date	Signature

Ymchwil Iechyd a Gofal Cymru
Health and Care Research Wales

NHS
Health Research Authority

Dr Rachael Rigby
Senior Lecturer in Biomedicine
Lancaster University
Faculty of Health and Medicine
Biomedical and Life Sciences
Lancaster
LA1 4YQ

Email: approvals@hra.nhs.uk
HCRW.approvals@wales.nhs.uk

27 October 2022

Dear Dr Rigby

HRA and Health and Care Research Wales (HCRW) Approval Letter

Study title:	**Does stoma feeding improve the microflora in the distal limb of loop ileostomy patients and is this linked to a reduction in post-operative complications?**
IRAS project ID:	**315656**
Protocol number:	**n/a**
REC reference:	**22/WM/0222**
Sponsor	**Lancashire Teaching Hospitals NHS Foundation Trust**

I am pleased to confirm that **HRA and Health and Care Research Wales (HCRW) Approval** has been given for the above referenced study, on the basis described in the application form, protocol, supporting documentation and any clarifications received. You should not expect to receive anything further relating to this application.

Please now work with participating NHS organisations to confirm capacity and capability, in line with the instructions provided in the "Information to support study set up" section towards the end of this letter.

How should I work with participating NHS/HSC organisations in Northern Ireland and Scotland?
HRA and HCRW Approval does not apply to NHS/HSC organisations within Northern Ireland and Scotland.

If you indicated in your IRAS form that you do have participating organisations in either of these devolved administrations, the final document set and the study wide governance report

(including this letter) have been sent to the coordinating centre of each participating nation. The relevant national coordinating function/s will contact you as appropriate.

Please see IRAS Help for information on working with NHS/HSC organisations in Northern Ireland and Scotland.

How should I work with participating non-NHS organisations?
HRA and HCRW Approval does not apply to non-NHS organisations. You should work with your non-NHS organisations to obtain local agreement in accordance with their procedures.

What are my notification responsibilities during the study?

The standard conditions document "*After Ethical Review – guidance for sponsors and investigators*", issued with your REC favourable opinion, gives detailed guidance on reporting expectations for studies, including:

- Registration of research
- Notifying amendments
- Notifying the end of the study

The HRA website also provides guidance on these topics, and is updated in the light of changes in reporting expectations or procedures.

Who should I contact for further information?
Please do not hesitate to contact me for assistance with this application. My contact details are below.

Your IRAS project ID is **315656**. Please quote this on all correspondence.

Yours sincerely,
Amber Slack

Approvals Specialist

Email: approvals@hra.nhs.uk

Copy to: *Dr Paul Brown, Lancashire Teaching Hospitals NHS Foundation Trust*

5.2 Nutritional information for Ensure® and Orafti®

Product Sheet

beneo
connecting nutrition and health

Orafti®Synergy1

Description

- Orafti®Synergy1 is a food ingredient (powder) consisting of a unique combination of chicory inulin fractions with selected chain lengths. In Orafti®Synergy1 shorter chain inulin (oligofructose) is combined with longer chain inulin in essentially equal amounts.
- Inulin consists of oligo- and polysaccharides composed of fructose units linked together by ß-(2,1)-linkages. Almost every fructose chain is terminated by a glucose unit. The number of fructose and glucose units in inulin (Degree of Polymerization = DP) ranges mainly between 2 and 60.
- Shorter chain inulin (oligofructose) consists of oligosaccharides obtained by partial enzymatic hydrolysis from inulin. Part of shorter chain inulin is terminated by a glucose unit. The degree of polymerization is less than 10.
- Longer chain inulin consists of inulin of which shorter fractions were removed. Almost every molecule is terminated by a glucose unit and has a DP of 10 or higher.

Specifications

Physical and Chemical Parameters

Parameter	Limit	Unit	Reference method[1]	Frequency
Inulin	92 ± 2	g/100 g d.m.	AOAC 997.08	Each batch[2]
Glucose + fructose + sucrose	8 ± 2	g/100 g d.m.	AOAC 997.08	Each batch[2]
Dry matter (d.m.)	97 ± 2	g/100 g	Vacuum (<35 mbar, 70 °C, 20 h)	Each batch
pH (10 g/100 g)	6 ± 1		Potentiometric (20 °C)	Each batch
Conductivity (15 g/100 g)	max 250	µS/cm	ICUMSA GS2/3/9-17, adapted	Each batch
Ash (sulphated)	max 0.2	g/100 g d.m.	ICUMSA GS3/4/7/8-11, adapted	Monitoring
Arsenic (total)	max 0.03	mg/kg	ICP-MS	Monitoring
Lead	max 0.02	mg/kg	ICP-MS	Monitoring
Mercury	max 0.01	mg/kg	ICP-MS	Monitoring
Cadmium	max 0.01	mg/kg	ICP-MS	Monitoring

1 or validated equivalent
2 CoA: % carbohydrates (HPLC)

Product Sheet

beneo
connecting nutrition and health

Information relevant for Nutrition Declaration

Nutritional information provided in the table shall enable food manufacturers to calculate the contribution of Orafti®Synergy1 in their food products in compliance with the applicable EU/US regulations. More detailed information is available upon request.

Any nutritional claim made using Orafti®Synergy1 is based on an appropriate use level (grams/serving) of commercial product. Please consult your local BENEO contact with any questions.

Nutrient	Unit per 100 g	Typical Value	
		EU	US
Energy/calories[1]	**kJ/kcal**	**866/214**	Not applicable/**214**
Total Fat[2]	**g**	**Negligible**[3]	
Saturates	g	Negligible[3]	
Total carbohydrate[4]	**g**	Not applicable	**97**
Carbohydrate[5]	**g**	**10**	Not applicable
(Total) sugars	g	10	10
Added sugars	g	Not applicable	Not applicable[6]
Dietary fibre[7] (AOAC 997.08)	**g**	**87**	**87**
Protein	**g**	**Negligible**[3]	
Salt (sodium)	**g**	**Negligible**[3]	
Vitamins, minerals	**g**	**Negligible**[3]	

1 Applying the energy conversion factor of 8 kJ/g or 2 kcal/g as laid down for all fibres in the EU and for all soluble non-digestible carbohydrates in the US
2 Applicable to US: trans fats and cholesterol also negligible
3 Negligible means "0" according to applicable rounding rules
4 Applicable to US: Total carbohydrate includes dietary fibre
5 Applicable to EU: Carbohydrate does not include dietary fibre
6 Further information available upon request
7 EU/US dietary fibre definition: non-digestible carbohydrate oligo- or polymers with three or more monomeric units (DP ≥ 3); excludes inulobiose

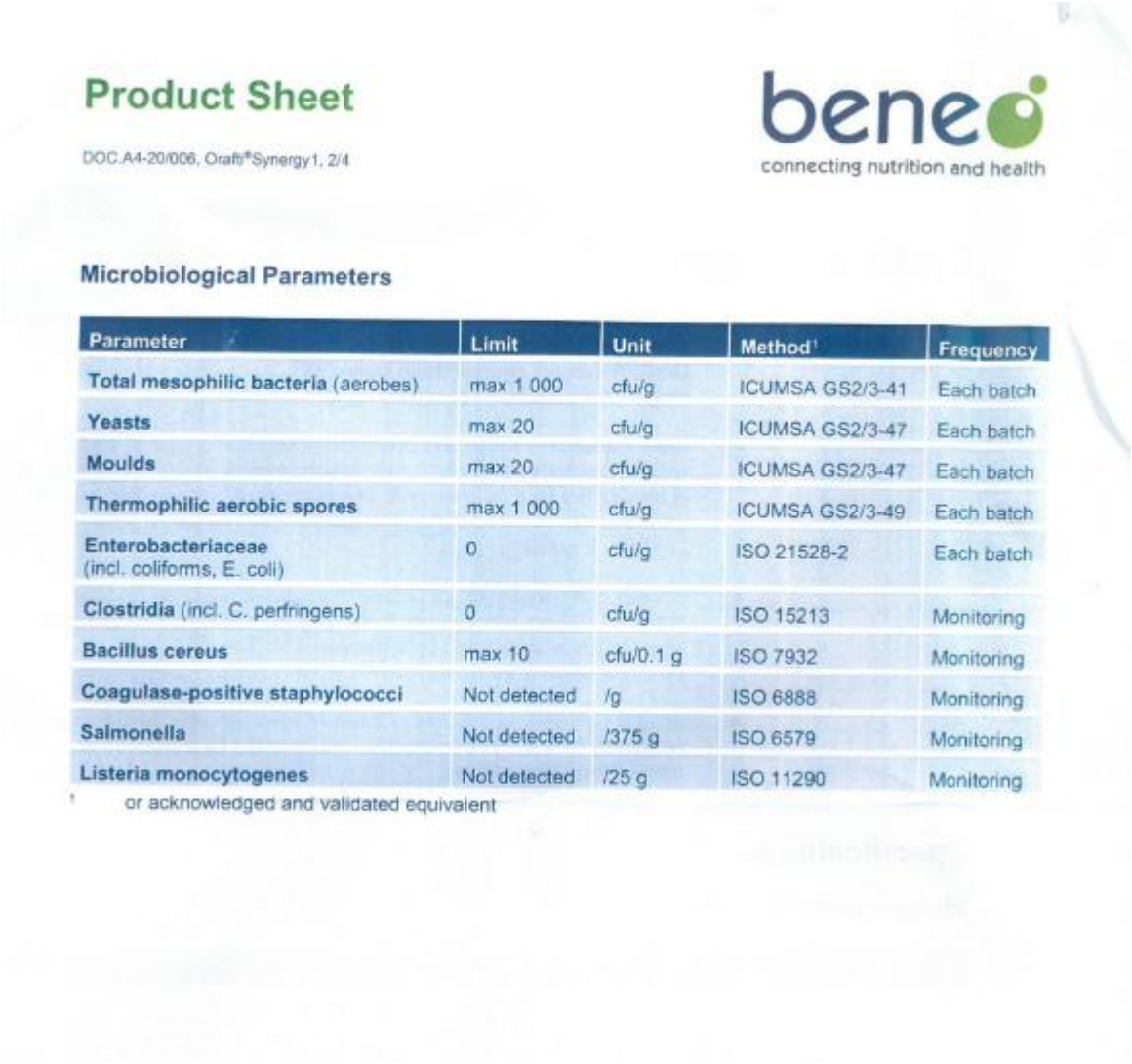

Product Sheet

DOC.A4-20/006, Orafti®Synergy1, 2/4

beneo
connecting nutrition and health

Microbiological Parameters

Parameter	Limit	Unit	Method[1]	Frequency
Total mesophilic bacteria (aerobes)	max 1 000	cfu/g	ICUMSA GS2/3-41	Each batch
Yeasts	max 20	cfu/g	ICUMSA GS2/3-47	Each batch
Moulds	max 20	cfu/g	ICUMSA GS2/3-47	Each batch
Thermophilic aerobic spores	max 1 000	cfu/g	ICUMSA GS2/3-49	Each batch
Enterobacteriaceae (incl. coliforms, E. coli)	0	cfu/g	ISO 21528-2	Each batch
Clostridia (incl. C. perfringens)	0	cfu/g	ISO 15213	Monitoring
Bacillus cereus	max 10	cfu/0.1 g	ISO 7932	Monitoring
Coagulase-positive staphylococci	Not detected	/g	ISO 6888	Monitoring
Salmonella	Not detected	/375 g	ISO 6579	Monitoring
Listeria monocytogenes	Not detected	/25 g	ISO 11290	Monitoring

[1] or acknowledged and validated equivalent

Ensure plus contains 310 calories per bottle, with 5 grams of fibre per (200ml bottle)

Ensure Plus Fibre Milkshake is a complete, balanced nutritional sip feed, with mixed fibre and FOS (fructooligosaccharides), designed for people at risk of disease-related malnutrition. Ensure Plus Fibre is a high energy, high protein liquid supplying extra energy within a limited volume. Ensure Plus Fibre also contains fibre and fructooligosaccharides. Ensure Plus Fibre is ready to use and presented in 200 ml (310 kcal) bottles. Ensure Plus Fibre is available in banana, chocolate, fruits of the forest, raspberry, strawberry and vanilla flavours.

Ensure Plus Fibre may be used as a nutritional supplement or as the sole source of nutrition for patients who cannot or will not eat sufficient quantities of everyday food and drink to meet their nutritional requirements. Ensure Plus Fibre is nutritionally complete for vitamins and minerals in 1000ml*.

Ensure Plus Fibre is a 1.6kcal/ml, ready-to-drink, milkshake style oral nutritional supplement with fibre, for people with, or at risk of developing disease-related malnutrition. Ensure Plus Fibre contains a mix of fibre and FOS (fructo-oligosaccharides).

Malnutrition and weight loss occur when the body is not getting enough of the nutrients and vitamins it needs to stay healthy and it can develop if a person stops eating properly, cannot eat at all, or if the body needs more nutrients than normal (e.g. due to infection or disease). Malnutrition can occur from some of these condition/infections: Mental health condition/ Depression,Ulcerative colitis,Dementia,Vomiting / diarrhoea,Eating disorder / Anorexia nervosa/ Bulimia, Food Poisoning,Cancer/ Oncology,Cow's Milk Allergy,Critical Care/ ICU,Cystic Fibrosis,Diabetes,Epilepsy,Failure to thrive/ Faltering growth, Kidney/ Renal Disease,Liver Disease/ Cirrhosis, Malabsorption/ Maldigestion,Malnutrition/Undernutrition, Pre & Post surgery, Respiratory Disease, Swallowing Problems, Dysphasia, Weight Loss in older adults, Would healing,Throat Reflux, Paediatric-Malnutrition, Gastrointestinal (GI) Intolerance, Stroke, Coma ,Bedsores, Phenylketonuria ,Digestive problems, and Dehydration. Malnutrition can have an impact on both physical and mental health; symptoms include weight loss, tiredness and a lack of energy.

Patients can overcome malnutrition and involuntary weight loss or maintaining nutrients by consulting a nutritionist to determine the level of malnutrition. There are various ways to overcome weight loss. These include nutritional food with additional nutrients, adding snacks to increase nutritional or energy intake, adding extra calories to food. Oral nutritional supplements (ONS) such as Ensure Plus can be a simple way to obtain extra nutrition. In some cases, additional or full nutrition may be given via a feeding tube.

Key Information

Contains Milk	✓	Protein (g)	13 / 200ml
Nutritionally Complete	✓	Calories (kcal)	310 / 200ml
Lactose & Gluten Free	✓	Carbohydrate (g)	40 / 200ml
Flavour	Vanilla		
Preparation	LIQUID		
Age	18 YEARS +		

5.3 Flow cytometry staining panels (Unfed patients)

BCRG004		FL-1	FL-2	FL-3	FL-4	FL-5
prox.	distal	FITC	PE	APC	PE-Cy7	APC-Cy7
1	6	TLR5	CD103	Cocktail	HLA-DR	Dye
2	7	TLR5	CD11c	Cocktail	HLA-DR	Dye
3	8	IgG2a	CD103	Cocktail	HLA-DR	Dye
4	9	IgG2a	CD11c	Cocktail	HLA-DR	Dye
5	10	TLR5	IgG1	Cocktail	HLA-DR	Dye
	Comp. ctrl					
	11	IgG2a	_	_	_	_
	12	_	IgG1	_	_	_
	13	_	_	CD3	_	_
	14	_	_	_	IgG2a	_
blood	15**	_	_	_	_	Dye

BCRG005		FL-1	FL-2	FL-3	FL-4	FL-5
prox.	distal	FITC	PE	APC	PE-Cy7	APC-Cy7
1	7	TLR5	CD163	CD14	HLA-DR	Dye
2	8	TLR5	CD103	Cocktail	HLA-DR	Dye
3	9	IgG2a	CD163	CD14	HLA-DR	Dye
4	10	TLR5	IgG1	CD14	HLA-DR	Dye
5	11	TLR5	CD163	IgG1	HLA-DR	Dye
6	12	IgG2a	CD103	Cocktail	HLA-DR	Dye
	Comp. ctrl					
	13	IgG2a	_	_	_	_
	14	_	IgG1	_	_	_
	15	_	_	CD3	_	_
	16	_	_	_	IgG2a	_

BCRG007		FL-1	FL-2	FL-3	FL-4	FL-5
prox.	distal	FITC	PE	APC	PE-Cy7	APC-Cy7
1	9	TLR5	CD163	CD14	HLA-DR	Dye
2	10	IgG2a	CD163	CD14	HLA-DR	Dye
3	11	TLR5	CD163	IgG1	HLA-DR	Dye
4	12	TLR5	CD103	Cocktail	HLA-DR	Dye
5	13	TLR5	CD11c	Cocktail	HLA-DR	Dye
6	14	IgG2a	CD103	Cocktail	HLA-DR	Dye
7	15	IgG2a	CD11c	Cocktail	HLA-DR	Dye
8	16	TLR5	IgG1	Cocktail	HLA-DR	Dye
	Comp. ctrl					
	17	IgG2a	_	_	_	_
	18	_	IgG1	_	_	_
	19	_	_	CD3	_	_
	20	_	_	_	IgG2a	_

BCRG022		FL-1	FL-2	FL-3	FL-4	FL-5
prox.	distal	FITC	PE	APC	PE-Cy7	APC-Cy7
1	9	CD25	CD4	CD19	CD14	Dye
2	10	IgG1	CD4	CD19	CD14	Dye
3	11	IgG1	IgG1	IgG1	IgG2a	Dye
4	12	_	CD33	CD14	HLA-DR	Dye
5	13	_	IgG1	CD14	HLA-DR	Dye
6	14	_	CD33	IgG1	HLA-DR	Dye
7	15	_	CD11c	Cocktail	HLA-DR	Dye
8	16	_	IgG1	Cocktail	HLA-DR	Dye
	Comp. ctrl					
	17	IgG1	_	_	_	_
	18	_	IgG1	_	_	_
	19	_	_	IgG1	_	_
	20	_	_	_	IgG2a	_
	21	_	_	_	_	Dye
	22	_	_	_	_	_

BCRG018		FL-1	FL-2	FL-3	FL-4	FL-5
prox.	distal	FITC	PE	APC	PE-Cy7	APC-Cy7
1*	8*	TLR5	_	CD3	CD14	Dye
2*	9*	TLR5	CD64	Cocktail	HLA-DR	Dye
3*	10*	IgG2a	_	CD3	CD14	Dye
4*	11*	IgG2a	CD64	Cocktail	HLA-DR	Dye
5	12	_	IgG1	Cocktail	HLA-DR	Dye
6	13	_	_	CD14	IgG2a	Dye
7	14	_	_	IgG1	CD14	Dye
	Comp. ctrl					
	15	IgG2a	_	_	_	_
	16	_	IgG1	_	_	_
	17	_	_	IgG1	_	_
	18	_	_	_	IgG2a	_
	19	_	_	_	_	Dye
	20**	_	_	_	_	_

5.4 Flow cytometry raw data

CD103+ expression in DCs: Percentage / total DCs			
Patient	Functional	Defunctioned	
BCRG003	63	81.9	
BCRG004	41.4	91.5	
BCRG005	20.1	86.2	
BCRG006	71.4	64.3	
BCRG007	67.6	71.7	
BCRG008	18.4	96	
Mean	46.98333333	81.93333333	

	TLR5+ DCs / total DCs		
	Patient	Functional	Defunctioned
	BCRG003	82.2	86.3
	BCRG004	49.1	88.3
	BCRG005	20.2	86.5
	BCRG006	71.7	68.9
	BCRG007	65.9	61.6
	BCRG008	18.4	96
	BCRG021	74.8	86.6
	BCRG022	60.7	83.2
	Mean	55.375	82.175

CD11c+ DCs / total DCs		
Patient	Functional	Defunctioned
BCRG003	82.2	86.3
BCRG004	49.1	88.3
BCRG006	64.1	81.1
BCRG007	65.8	61.5
BCRG021	74.8	86.6
BCRG022	60.7	83.2
BCRG023	85.6	96.8
Mean	68.9	83.4
T test	0.0329004	

CD64+ APCs / total APCs		
Patient	Functional	Defunctioned
BCRG018	69.1	80.5
BCRG019	91.7	83.9
BCRG027	99.8	99.9
BCRG029	80.8	71.8
Mean	85.35	84.025

CD163+ macros / CD14+ HLA-DR+		
Patient	Functional	Defunctioned
BCRG005	78.2	78.6
BCRG006	81.3	75.1
BCRG007	81.3	84.2
BCRG008	86.8	93
Mean	81.9	82.725

5.5 Histology raw data (prebiotic fed)

Crypt	Patient sample num					
	002 prox	002 dist	004 prox	004 dist	005 prox	005 dist
1	1042.01	1014.62	1037.19	1421.43	1487.05	1160.5
2	835.709	1061.98	1042.45	1030.74	907.677	1188.47
3	714.835	903.187	913.908	1783.85	1011.33	1343.63
4	778.74	1209.75	1021.38	1854.93	978.928	1342.07
5	889.579	1008.26	1152.73	1782.38	1470.12	1264.68
6	700.359	1063.15	1262.47	1763.66	1029.69	1533.61
7	1096.97	1211.96	1295.04	1851.41	923.521	1297.92
8	1002.09	1344.97	954.921	1617.11	1434.85	1476.81
9	729.646	859.892	942.378	1036.39	946.571	838.423
10	928.099	1759.59	889.73	1133.75	1818.15	1185.67
11	781.847		1222.66		809.49	1220.06
12	743.734		1402.07		931.098	1272.83
Mean	853.635	1143.74	1094.74	1527.56	1145.71	1260.39
Convert to um	437.761	586.531	561.407	783.367	587.542	646.354
Inc in crypt depth (um)	148.77		221.96		58.812	
% increase in crypt depth	33.984		39.536		10.001	

Villus	Patient sample num					
	002 prox	002 dist	004 prox	004 dist	005 prox	005 dist
1	1032.46	1154.22	1982.65	726.4	2594.59	2038.34
2	1080.89	1336.96	1822.07	1289.72	2138.24	1077.68
3	1408.28	1738.64	2746.23	967.49	1267.6	1935.6
4	1210.27	1272.57	3212.49	933.81	1126.4	1437.49
5	923.87	1365.1	1601.45	829.47	1849.9	1612.87
6	911.07	889.32	2964.77	796.49	1653.27	1502.91
7	1433.52	1316.43	3123.63	829.29	1586.69	1315
8	1319.56	898.32	2184.38	834.04	1441.17	950.02
9	1509.79	845.56	2340.08		1522.21	848.03
10	1762.04	781.04	1785.56		1884.62	1032.58
11	1414.32	699.8	1949.52		1418.6	917.38
12		1452.52				
Mean	1273.28	1145.87	2337.53	900.839	1680.3	1333.45
Convert to um	652.964	587.627	1198.73	461.969	861.692	683.818
Dec villous length	65.337		736.764		117.874	
% decrease	10.006		61.462		20.642	

Villous Height:				
	Height (Image J units)			
Villous	SFS007 proximal	SFS007 distal	SFS009 proximal	SFS009 distal
1	2440.8	1807.8	2398.8	1200.9
2	2256.4	2350	1841.66	1480.6
3	1620.2	4492.9	1986.4	1123.2
4	1736.3	2051.9	2131.6	1307.3
5	467.4	2075.9	2146.5	1113.8
6	400.5	1504.2	2286.8	866.2
7	522.1	2338.9	2274.2	857.4
8	690.3		2471.1	1027.5
9	704.6		2503.4	641.9
10			2010.8	780.9
	Height (microns)			
x4 mag	1251.692308	927.07692	1230.153846	615.84615
Scale = 80 units	1157.128205	1205.1282	944.4410256	759.28205
1um = 1.25 units	830.8717949	2304.0513	1018.666667	576
x10 mag	890.4102564	1052.2564	1093.128205	1045.84
scale = 195 units	373.92	1064.5641	1100.769231	891.04
1um = 1.95 units	320.4	771.38462	1172.717949	692.96
	417.68	1199.4359	1166.25641	685.92
	552.24		1267.230769	822
	563.68		1283.794872	513.52
			1031.179487	624.72
Mean (um)	706.4469516	1220.7436	1130.833846	722.71282
SD	342.2143135	465.23913	112.7706827	160.72363

Crypt depth:				
	Depth (Image J units)			
Crypt	SFS007 proximal	SFS007 distal	SFS009 proximal	SFS009 distal
1	854.06	1231.5	747.3	1372.1
2	1106.1	1175.8	904.8	1471.5
3	1280.2	1366.9	802.2	1882.3
4	1202	1060.4	774.8	1520.9
5	1220.4	1205.9	828.5	1767.5
6	1627.39	1261.9	1002.8	1472.1
7	1527	1390	923.9	655.8
8	1398.4		784.3	704.5
9	1810.6		990.7	589.9
10	621.7		828.7	566.3
			807.5	599
	Depth (microns)			
	437.9794872	631.5384615	383.2307692	703.6410256
	567.2307692	602.974359	464	754.6153846
	656.5128205	700.974359	411.3846154	965.2820513
	616.4102564	543.7948718	397.3333333	779.9487179
	625.8461538	618.4102564	424.8717949	906.4102564
	834.5589744	647.1282051	514.2564103	754.9230769
	783.0769231	712.8205128	473.7948718	524.64
	717.1282051		402.2051282	563.6
	928.5128205		508.0512821	471.92
	497.36		424.974359	453.04
			414.1025641	479.2
Mean (um)	666.461641	636.8058608	438.018648	668.8382284

% Change in Villus Prox vs Dist	
Unfed	Fed
-46.42	-10.01
-22.34	-61.46
-19.51	-20.64
-16.31	72.80
-24.75	-36.09
29.75	
-43.62	
-13.1	
-6.59	
-43.36	
-55.26	
-16.38	

% Change in crypt depth prox vs dist	
Unfed	Fed
21.4438839	33.98
-21.768	39.54
19.188	10
41.222	-4.45
-4.368	52.69
-29.356	
-13.536	
-13.84	
-20.397	
-0.85	
-49.227	
-13.35	

SFS002	Proximal			Distal		
Crypt	Depth	No.goblet	No.goblet per 100um crypt	Depth	No.goblet	No.goblet per 100um crypt
1	521.025641	18	3.454724409	515	11	2.13592233
2	556.41	9	1.617512266	536	16	2.985074627
3	475.38	12	2.524296352	610	19	3.114754098
4	507.69	10	1.969705923			
5	373.33	9	2.41073581			
6	468.72	13	2.773510838			
7	504.62	14	2.774364869			
8	518.97	19	3.661097944			
9	531.28	15	2.823369974			
10						
Mean			2.667702043			2.745250352
SFS004	Proximal			Distal		
Crypt	Depth	No.goblet	No.goblet per 100um crypt	Depth	No.goblet	No.goblet per 100um crypt
1	678.97	22	3.240202071	710.77	21	2.954542257
2	504.62	16	3.170702707	922.56	14	1.517516476
3	662.05	26	3.927195831	625.13	12	1.919600723
4	561.03	25	4.456089692	672.82	18	2.675306917
5	670.26	28	4.177483365	520	7	1.346153846
6	563.08	18	3.196703843	939.49	32	3.406103311
7	651.28	29	4.45276993			
8	635.38	18	2.83295036			
9						
10						
Mean			3.681762225			2.303203922

	A	B	C	D	E	F	G	H
6								
7	SFS005	Proximal			Distal			
8	Crypt	Depth	No.goblet	No.goblet per 100um crypt	Depth	No.goblet	No.goblet per 100um crypt	
9	1	601.03	29	4.82505033	782.051282	34	4.347540984	
10	2	567.69	32	5.636879283	610.25641	36	5.899159664	
11	3	428.21	24	5.604726653	493.333333	24	4.864864865	
12	4	522.05	28	5.363470932	581.538462	27	4.642857143	
13	5	442.56	22	4.971077368	689.74359	37	5.364312268	
14	6	520.51	27	5.187220226			#N/A	
15	7							
16	8							
17	9							
18	10							
19	mean			5.264737465			5.023746985	
20	SFS007	Proximal			Distal			
21	Crypt	Depth	No.goblet	No.goblet per 100um crypt	Depth	No.goblet	No.goblet per 100um crypt	
22	1	753.3333333	35	4.646017699	1014.35897	41	4.041961577	
23	2	713.3333333	25	3.504672897	952.820513	37	3.88320775	
24	3	797.4358974	37	4.639871383	358.461538	19	5.300429185	
25	4	667.1794872	26	3.897002306				
26	5	614.8717949	29	4.716430359				
27	6	514.3589744	21	4.082751745				
28	7	529.7435897	14	2.642787996				
29	8	854.8717949	32	3.74325135				
30	9	839.4871795	20	2.382406842				
31	10							
32	mean			3.806132508			4.408532837	
33								

SFS009	Proximal			Distal		
Crypt	Depth	No.goblet	No.goblet per 100um crypt	Depth	No.goblet	No.goblet per 100um crypt
1	656.9230769	12	1.826697892	858.974359	27	3.143283582
2	536.4102564	7	1.304971319	759.487179	31	4.081701553
3	483.0769231	15	3.105095541	586.153846	25	4.265091864
4	505.1282051	15	2.969543147	649.74359	20	3.078137332
5	583.5897436	16	2.741652021	857.435897	17	1.982655502
6	491.7948718	14	2.846715328			
7	497.9487179	12	2.409886715			
8	353.8461538	11	3.108695652			
9	443.0769231	10	2.256944444			
10	458.4615385	16	3.489932886			
mean			2.606013495			3.310173967

Crypt depth | Feeding time | Villus height | **Goblet cells** | PCNA+ cells | +

	A	B	C	D	E	F	G	H
1	Patient num	proximal				distal		
2		Mean crypt depth	Mean no.PCNA +ve	PCNA+ve per 100um crypt		Mean crypt depth	Mean no.PCNA +ve	PCNA+ve per 100um crypt
3	SFS002	437.76	16.125	3.683525219		586.41	16.25	2.771098719
4	SFS004	561.41	29.4	5.236814449		783.37	23.42857143	2.990741467
5	SFS005	587.542	11.85714286	2.01809281		646.35	14.33333333	2.217580774
6	SFS007	666.46	20.5	3.075953546		636.81	21.42857143	3.364986641
7	SFS009	438.02	9.555555556	2.181534075		668.84	9.5	1.420369595
8								
9								

5.6 Phyla-specific qPCR – raw data

Sample ID	Phyla	Phyla Cq 1	Phyla Cq 2	Universal Cq1	Universal Cq 2	Average P	Average U	Abundance 1	Abundance 2	Av Abundance	Std err
SFS002	Firmicutes	40.21	31.72	28.09		35.965	28.09	0.000224655	0.080772052	0.040498354	0.040274
proximal	Bacteroidetes	36.07	35.83	28.09		35.95	28.09	0.003960779	0.004677651	0.004319215	0.000358
	y-Proteobacteria	37.89	34.04	28.09		35.965	28.09	0.001121776	0.016176014	0.008648895	0.007527
	Actinobacteria	35.63	38.1	28.09		36.865	28.09	0.00537321	0.000969817	0.003171514	0.002202
SFS002	Firmicutes	34.1	29.45	31.65	27.81	31.775	29.73	0.048361406	1.214194884	0.631278145	0.582917
Distal	Bacteroidetes	36.56	35.81	31.65	27.81	36.185	29.73	0.008789519	0.014782151	0.011785835	0.002996
	y-Proteobacteria	37.14	34.15	31.65	27.81	35.645	29.73	0.00587987	0.046714039	0.026296955	0.020417
	Actinobacteria	39.87	39.51	31.65	27.81	39.69	29.73	0.000886249	0.001137435	0.001011842	0.000126
SFS004	Firmicutes	37.57	30.89	33.44	33.46	34.23	33.45	0.057511728	5.897076869	2.977294299	2.919783
Proximal	Bacteroidetes			33.44	33.46	#DIV/0!	33.45				
	y-Proteobacteria	40.03		33.44	33.46	40.03	33.45	0.010452559	11734196456	5867098228	5.87E+09
	Actinobacteria	39.71	38.62	33.44	33.46	39.165	33.45	0.013048249	0.027776334	0.020412291	0.007364
SFS004	Firmicutes	32.21	31.01	30.95	29.82	31.61	30.385	0.282241101	0.648419777	0.465330439	0.183089
Distal	Bacteroidetes			30.95	29.82	#DIV/0!	30.385				#DIV/0!
	y-Proteobacteria	38.55	37.54	30.95	29.82	38.045	30.385	0.003484096	0.007016659	0.005250377	0.001766
	Actinobacteria	34.95	36.88	30.95	29.82	35.915	30.385	0.042247214	0.011086901	0.026667057	0.01558
SFS005	Firmicutes	28.75	27.64	31.43	29.2	28.195	30.315	2.958775018	6.386387091	4.672581055	1.713806
Proximal	Bacteroidetes	39.97		31.43	29.2	39.97	30.315	0.001240382	1335747342	667873670.8	6.68E+08
	y-Proteobacteria		36.94	31.43	29.2	36.94	30.315	1335747342	0.010131559	667873670.9	6.68E+08
	Actinobacteria	37.23	34.05	31.43	29.2	35.64	30.315	0.008286623	0.075102253	0.041694438	0.033408
SFS005	Firmicutes	28.13	28.03	29.54	28.67	28.08	29.105	1.965641197	2.106722072	2.036181635	0.07054
Distal	Bacteroidetes		38.24	29.54	28.67	38.24	29.105	577401654.3	0.001778652	288700827.1	2.89E+08
	y-Proteobacteria		37.87	29.54	28.67	37.87	29.105	577401654.3	0.002298646	288700827.1	2.89E+08
	Actinobacteria	34.74	33.44	29.54	28.67	34.09	29.105	0.02012315	0.049549009	0.034836079	0.014713

5.7 Statistics

Flow cytometry

	Wilcoxon test	
1	Table Analyzed	CD103+ DCs
2		
3	Column B	Defunctioned
4	vs.	vs.
5	Column A	Functional
6		
7	**Wilcoxon matched-pairs signed rank test**	
8	P value	0.0938
9	Exact or approximate P value?	Exact
10	P value summary	ns
11	Significantly different (P < 0.05)?	No
12	One- or two-tailed P value?	Two-tailed
13	Sum of positive, negative ranks	19.00 , -2.000
14	Sum of signed ranks (W)	17.00
15	Number of pairs	6
16	Number of ties (ignored)	0
17		
18	**Median of differences**	
19	Median	34.50
20		
21	**How effective was the pairing?**	
22	rs (Spearman)	-0.9429
23	P value (one tailed)	0.0083
24	P value summary	**
25	Was the pairing significantly effective?	Yes
26		
27		

	Wilcoxon test	
1	Table Analyzed	TLR5+ DCs
2		
3	Column B	Defunctioned
4	vs.	vs.
5	Column A	Functional
6		
7	**Wilcoxon matched-pairs signed rank test**	
8	P value	0.0547
9	Exact or approximate P value?	Exact
10	P value summary	ns
11	Significantly different (P < 0.05)?	No
12	One- or two-tailed P value?	Two-tailed
13	Sum of positive, negative ranks	32.00 , -4.000
14	Sum of signed ranks (W)	28.00
15	Number of pairs	8
16	Number of ties (ignored)	0
17		
18	**Median of differences**	
19	Median	17.15
20		
21	**How effective was the pairing?**	
22	rs (Spearman)	-0.4762
23	P value (one tailed)	0.1215
24	P value summary	ns
25	Was the pairing significantly effective?	No
26		

	Wilcoxon test	
1	Table Analyzed	CD11c+ DCs
2		
3	Column B	Defunctioned
4	vs.	vs.
5	Column A	Functional
6		
7	**Wilcoxon matched-pairs signed rank test**	
8	P value	0.0469
9	Exact or approximate P value?	Exact
10	P value summary	*
11	Significantly different (P < 0.05)?	Yes
12	One- or two-tailed P value?	Two-tailed
13	Sum of positive, negative ranks	26.00 , -2.000
14	Sum of signed ranks (W)	24.00
15	Number of pairs	7
16	Number of ties (ignored)	0
17		
18	**Median of differences**	
19	Median	11.80
20		
21	**How effective was the pairing?**	
22	rs (Spearman)	0.2857
23	P value (one tailed)	0.2780
24	P value summary	ns
25	Was the pairing significantly effective?	No
26		

	Wilcoxon test	
1	Table Analyzed	CD64+ APCs
2		
3	Column B	Defunctioned
4	vs.	vs.
5	Column A	Functional
6		
7	**Wilcoxon matched-pairs signed rank test**	
8	P value	0.8750
9	Exact or approximate P value?	Exact
10	P value summary	ns
11	Significantly different (P < 0.05)?	No
12	One- or two-tailed P value?	Two-tailed
13	Sum of positive, negative ranks	4.000 , -6.000
14	Sum of signed ranks (W)	-2.000
15	Number of pairs	4
16	Number of ties (ignored)	0
17		
18	**Median of differences**	
19	Median	-4.300
20		
21	**How effective was the pairing?**	
22	rs (Spearman)	0.8000
23	P value (one tailed)	0.1667
24	P value summary	ns
25	Was the pairing significantly effective?	No
26		

	Wilcoxon test	
1	Table Analyzed	CD163+ macrophages
2		
3	Column B	Defunctioned
4	vs.	vs.
5	Column A	Functional
6		
7	**Wilcoxon matched-pairs signed rank test**	
8	P value	0.7500
9	Exact or approximate P value?	Exact
10	P value summary	ns
11	Significantly different (P < 0.05)?	No
12	One- or two-tailed P value?	Two-tailed
13	Sum of positive, negative ranks	6.500 , -3.500
14	Sum of signed ranks (W)	3.000
15	Number of pairs	4
16	Number of ties (ignored)	0
17		
18	**Median of differences**	
19	Median	1.650
20		
21	**How effective was the pairing?**	
22	rs (Spearman)	0.6325
23	P value (one tailed)	0.2500
24	P value summary	ns
25	Was the pairing significantly effective?	No
26		

	Wilcoxon test	
1	Table Analyzed	TLR5+ macrophages
2		
3	Column B	Defunctioned
4	vs.	vs.
5	Column A	Functional
6		
7	**Wilcoxon matched-pairs signed rank test**	
8	P value	0.8750
9	Exact or approximate P value?	Exact
10	P value summary	ns
11	Significantly different (P < 0.05)?	No
12	One- or two-tailed P value?	Two-tailed
13	Sum of positive, negative ranks	6.000 , -4.000
14	Sum of signed ranks (W)	2.000
15	Number of pairs	4
16	Number of ties (ignored)	0
17		
18	**Median of differences**	
19	Median	2.350
20		
21	**How effective was the pairing?**	
22	rs (Spearman)	0.8000
23	P value (one tailed)	0.1667
24	P value summary	ns
25	Was the pairing significantly effective?	No
26		

	Mann-Whitney test	
1	Table Analyzed	% change CD11c+unfed vs fed
2		
3	Column B	Fed
4	vs.	vs.
5	Column A	Unfed
6		
7	**Mann Whitney test**	
8	P value	0.0556
9	Exact or approximate P value?	Exact
10	P value summary	ns
11	Significantly different (P < 0.05)?	No
12	One- or two-tailed P value?	Two-tailed
13	Sum of ranks in column A,B	42 , 3
14	Mann-Whitney U	0
15		
16	**Difference between medians**	
17	Median of column A	11.80, n=7
18	Median of column B	-8.200, n=2
19	Difference: Actual	-20.00
20	Difference: Hodges-Lehmann	-20.10
21		
22		
23		
24		
25		
26		
27		

	Mann-Whitney test	
1	Table Analyzed	% change macros unfed vs fed
2		
3	Column B	Fed
4	vs.	vs.
5	Column A	Unfed
6		
7	**Mann Whitney test**	
8	P value	0.4857
9	Exact or approximate P value?	Exact
10	P value summary	ns
11	Significantly different (P < 0.05)?	No
12	One- or two-tailed P value?	Two-tailed
13	Sum of ranks in column A,B	15 , 21
14	Mann-Whitney U	5
15		
16	**Difference between medians**	
17	Median of column A	1.650, n=4
18	Median of column B	3.935, n=4
19	Difference: Actual	2.285
20	Difference: Hodges-Lehmann	3.300
21		
22		
23		
24		
25		

Histology

Table Analyzed	Crypt depth (um)
Column B	Defunctioned
vs.	vs.
Column A	Functional
Wilcoxon matched-pairs signed rank test	
P value	0.1250
Exact or approximate P value?	Exact
P value summary	ns
Significantly different (P < 0.05)?	No
One- or two-tailed P value?	Two-tailed
Sum of positive, negative ranks	14.00 , -1.000
Sum of signed ranks (W)	13.00
Number of pairs	5
Number of ties (ignored)	0
Median of differences	
Median	148.7
How effective was the pairing?	
rs (Spearman)	0.1000
P value (one tailed)	0.4750
P value summary	ns
Was the pairing significantly effective?	No

Wilcoxon test	
Table Analyzed	Villus height
Column B	Defunctioned
vs.	vs.
Column A	Functional
Wilcoxon matched-pairs signed rank test	
P value	0.4375
Exact or approximate P value?	Exact
P value summary	ns
Significantly different (P < 0.05)?	No
One- or two-tailed P value?	Two-tailed
Sum of positive, negative ranks	4.000 , -11.00
Sum of signed ranks (W)	-7.000
Number of pairs	5
Number of ties (ignored)	0
Median of differences	
Median	-346.8
How effective was the pairing?	
rs (Spearman)	0.000
P value (one tailed)	0.5250
P value summary	ns
Was the pairing significantly effective?	No

Wilcoxon test	
Table Analyzed	Goblet cells
Column B	Defunctioned
vs.	vs.
Column A	Functional
Wilcoxon matched-pairs signed rank test	
P value	>0.9999
Exact or approximate P value?	Exact
P value summary	ns
Significantly different (P < 0.05)?	No
One- or two-tailed P value?	Two-tailed
Sum of positive, negative ranks	8.000 , -7.000
Sum of signed ranks (W)	1.000
Number of pairs	5
Number of ties (ignored)	0
Median of differences	
Median	0.08000
How effective was the pairing?	
rs (Spearman)	0.6000
P value (one tailed)	0.1750
P value summary	ns
Was the pairing significantly effective?	No

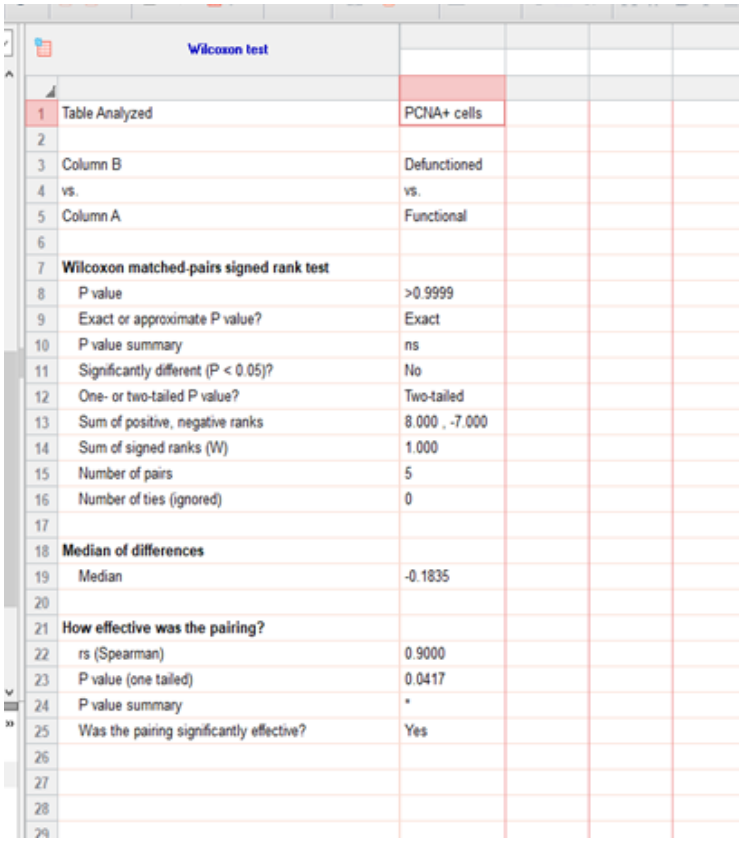

Wilcoxon test	
Table Analyzed	PCNA+ cells
Column B	Defunctioned
vs.	vs.
Column A	Functional
Wilcoxon matched-pairs signed rank test	
P value	>0.9999
Exact or approximate P value?	Exact
P value summary	ns
Significantly different (P < 0.05)?	No
One- or two-tailed P value?	Two-tailed
Sum of positive, negative ranks	8.000 , -7.000
Sum of signed ranks (W)	1.000
Number of pairs	5
Number of ties (ignored)	0
Median of differences	
Median	-0.1835
How effective was the pairing?	
rs (Spearman)	0.9000
P value (one tailed)	0.0417
P value summary	*
Was the pairing significantly effective?	Yes

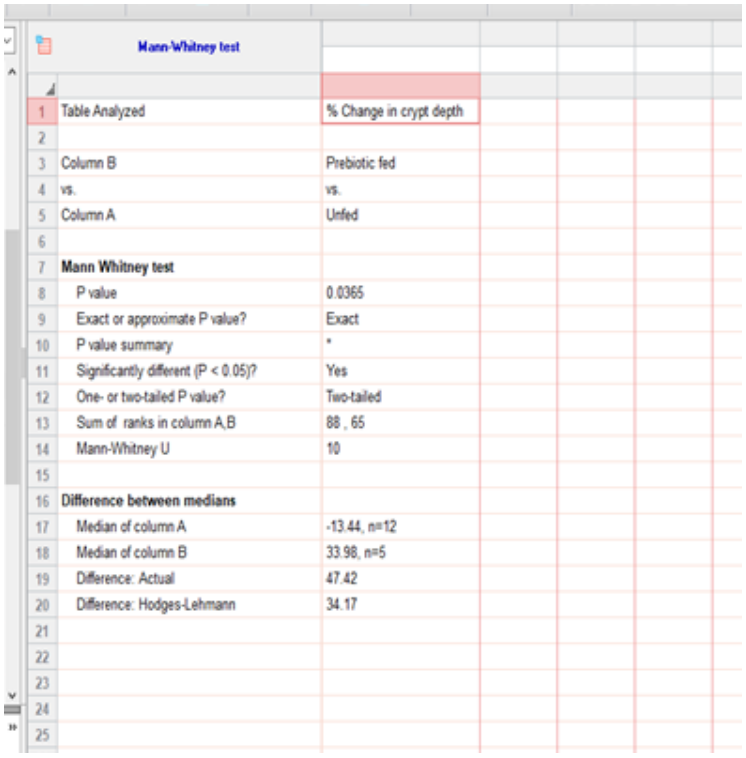

Mann-Whitney test	
Table Analyzed	% Change in crypt depth
Column B	Prebiotic fed
vs.	vs.
Column A	Unfed
Mann Whitney test	
P value	0.0365
Exact or approximate P value?	Exact
P value summary	*
Significantly different (P < 0.05)?	Yes
One- or two-tailed P value?	Two-tailed
Sum of ranks in column A,B	88 , 65
Mann-Whitney U	10
Difference between medians	
Median of column A	-13.44, n=12
Median of column B	33.98, n=5
Difference: Actual	47.42
Difference: Hodges-Lehmann	34.17

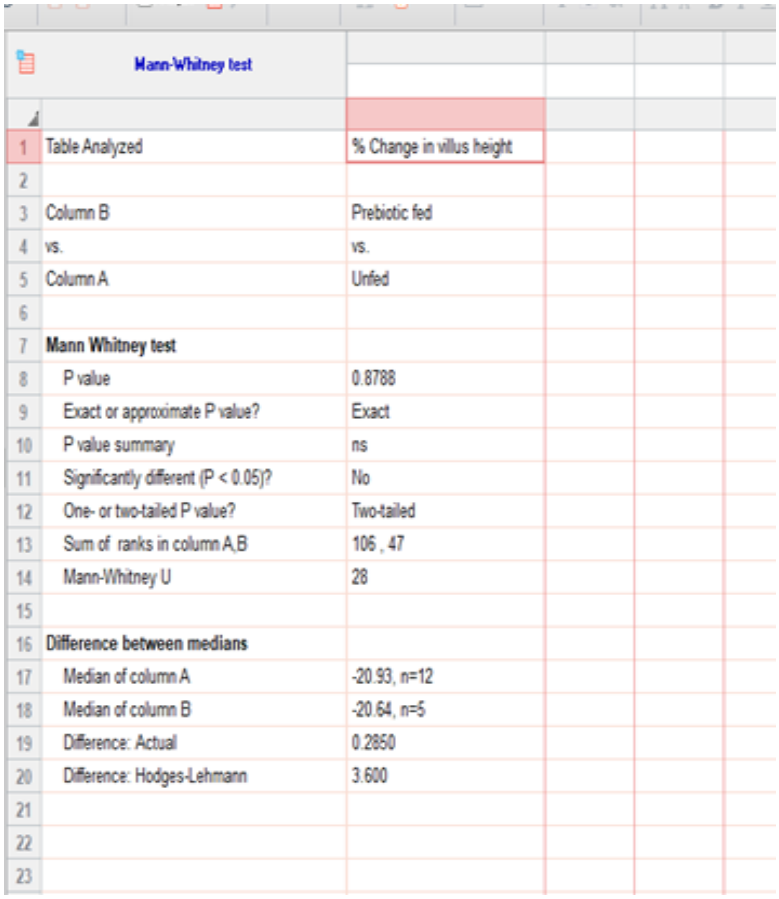

Mann-Whitney test	
Table Analyzed	% Change in villus height
Column B	Prebiotic fed
vs.	vs.
Column A	Unfed
Mann Whitney test	
P value	0.8788
Exact or approximate P value?	Exact
P value summary	ns
Significantly different (P < 0.05)?	No
One- or two-tailed P value?	Two-tailed
Sum of ranks in column A,B	106 , 47
Mann-Whitney U	28
Difference between medians	
Median of column A	-20.93, n=12
Median of column B	-20.64, n=5
Difference: Actual	0.2850
Difference: Hodges-Lehmann	3.600

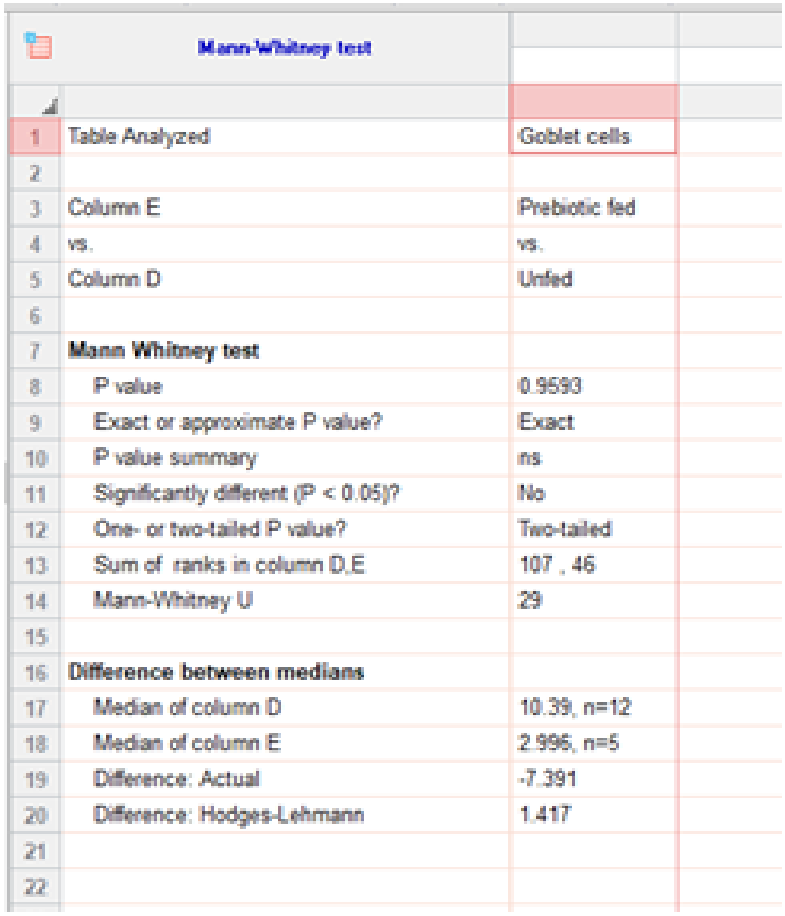

Mann-Whitney test	
Table Analyzed	Goblet cells
Column E	Prebiotic fed
vs.	vs.
Column D	Unfed
Mann Whitney test	
P value	0.9593
Exact or approximate P value?	Exact
P value summary	ns
Significantly different (P < 0.05)?	No
One- or two-tailed P value?	Two-tailed
Sum of ranks in column D,E	107 , 46
Mann-Whitney U	29
Difference between medians	
Median of column D	10.39, n=12
Median of column E	2.996, n=5
Difference: Actual	-7.391
Difference: Hodges-Lehmann	1.417

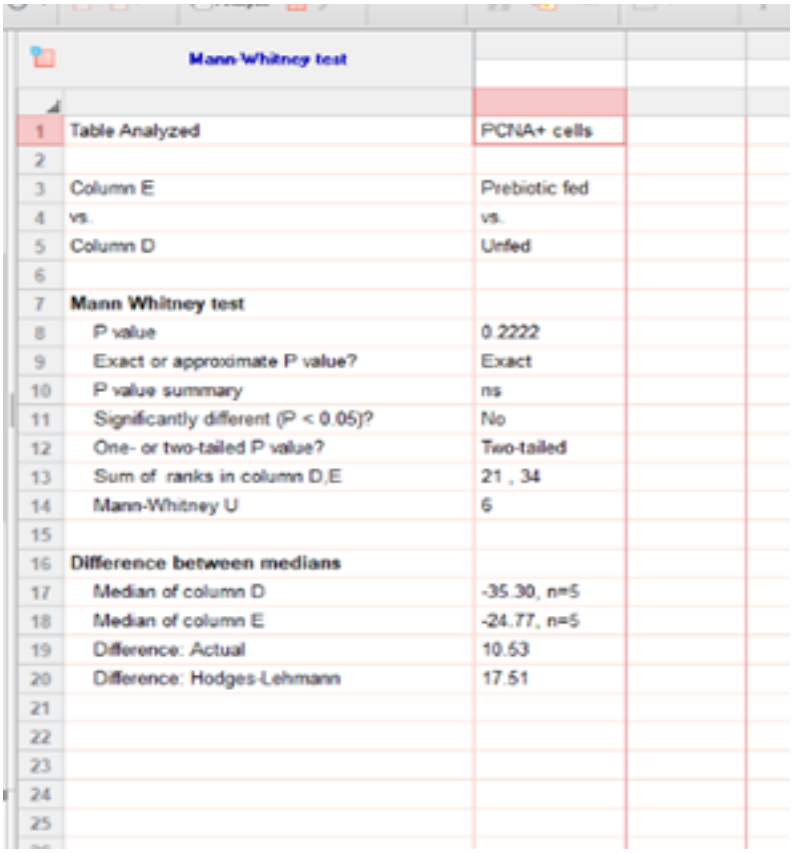

	Mann Whitney test	
1	Table Analyzed	PCNA+ cells
2		
3	Column E	Prebiotic fed
4	vs.	vs.
5	Column D	Unfed
6		
7	**Mann Whitney test**	
8	P value	0.2222
9	Exact or approximate P value?	Exact
10	P value summary	ns
11	Significantly different (P < 0.05)?	No
12	One- or two-tailed P value?	Two-tailed
13	Sum of ranks in column D,E	21 , 34
14	Mann-Whitney U	6
15		
16	**Difference between medians**	
17	Median of column D	-35.30, n=5
18	Median of column E	-24.77, n=5
19	Difference: Actual	10.53
20	Difference: Hodges-Lehmann	17.51
21		
22		
23		
24		
25		

6 References

Abel, A.M. *et al.* (2018) 'Natural Killer Cells: Development, Maturation, and Clinical Utilization', *Frontiers in Immunology*, 9, p. 1869. Available at: https://doi.org/10.3389/fimmu.2018.01869.

Abrisqueta, J. *et al.* (2014) 'Stimulation of the Efferent Limb Before Ileostomy Closure: A Randomized Clinical Trial', *Diseases of the Colon & Rectum*, 57(12), pp. 1391–1396. Available at: https://doi.org/10.1097/DCR.0000000000000237.

Agus, A., Planchais, J. and Sokol, H. (2018) 'Gut Microbiota Regulation of Tryptophan Metabolism in Health and Disease', *Cell Host & Microbe*, 23(6), pp. 716–724. Available at: https://doi.org/10.1016/j.chom.2018.05.003.

Ahluwalia, B., Magnusson, M.K. and Öhman, L. (2017) 'Mucosal immune system of the gastrointestinal tract: maintaining balance between the good and the bad', *Scandinavian Journal of Gastroenterology*, 52(11), pp. 1185–1193. Available at: https://doi.org/10.1080/00365521.2017.1349173.

Aljorfi, A.A. and Alkhamis, A.H. (2020) 'A Systematic Review of Early versus Late Closure of Loop Ileostomy', *Surgery Research and Practice*, 2020, pp. 1–8. Available at: https://doi.org/10.1155/2020/9876527.

Allaire, J.M. *et al.* (2018) 'The Intestinal Epithelium: Central Coordinator of Mucosal Immunity', *Trends in Immunology*, 39(9), pp. 677–696. Available at: https://doi.org/10.1016/j.it.2018.04.002.

Arpaia, N. *et al.* (2013) 'Metabolites produced by commensal bacteria promote peripheral regulatory T-cell generation', *Nature*, 504(7480), pp. 451–455. Available at: https://doi.org/10.1038/nature12726.

Atarashi, K. *et al.* (2011) 'Induction of Colonic Regulatory T Cells by Indigenous *Clostridium* Species', *Science*, 331(6015), pp. 337–341. Available at: https://doi.org/10.1126/science.1198469.

Beamish, E.L. *et al.* (2017) 'Loop ileostomy-mediated fecal stream diversion is associated with microbial dysbiosis', *Gut Microbes*, 8(5), pp. 467–478. Available at: https://doi.org/10.1080/19490976.2017.1339003.

Beamish, E.L. *et al.* (2023) 'Delay in loop ileostomy reversal surgery does not impact upon post-operative clinical outcomes. Complications are associated with an increased loss of microflora in the defunctioned intestine', *Gut Microbes*, 15(1), p. 2199659. Available at: https://doi.org/10.1080/19490976.2023.2199659.

Becker, C., Neurath, M.F. and Wirtz, S. (2015) 'The Intestinal Microbiota in Inflammatory Bowel Disease', *ILAR Journal*, 56(2), pp. 192–204. Available at: https://doi.org/10.1093/ilar/ilv030.

Belote, B.L. *et al.* (2019) 'Applying I see inside histological methodology to evaluate gut health in broilers challenged with Eimeria', *Veterinary Parasitology*, 276, p. 100004. Available at: https://doi.org/10.1016/j.vpoa.2019.100004.

Bevins, C.L. and Salzman, N.H. (2011) 'Paneth cells, antimicrobial peptides and maintenance of intestinal homeostasis', *Nature Reviews Microbiology*, 9(5), pp. 356–368. Available at: https://doi.org/10.1038/nrmicro2546.

Biton, M. *et al.* (2018) 'T Helper Cell Cytokines Modulate Intestinal Stem Cell Renewal and Differentiation', *Cell*, 175(5), pp. 1307-1320.e22. Available at: https://doi.org/10.1016/j.cell.2018.10.008.

Brischetto, C. *et al.* (2021) 'NF-κB determines Paneth versus goblet cell fate decision in the small intestine', *Development*, 148(21), p. dev199683. Available at: https://doi.org/10.1242/dev.199683.

Brockmann, L. *et al.* (2023) 'Intestinal microbiota-specific Th17 cells possess regulatory properties and suppress effector T cells via c-MAF and IL-10', *Immunity*, 56(12), pp. 2719-2735.e7. Available at: https://doi.org/10.1016/j.immuni.2023.11.003.

Burgueño, J.F. and Abreu, M.T. (2020) 'Epithelial Toll-like receptors and their role in gut homeostasis and disease', *Nature Reviews Gastroenterology & Hepatology*, 17(5), pp. 263–278. Available at: https://doi.org/10.1038/s41575-019-0261-4.

Campbell, C. *et al.* (2020) 'Bacterial metabolism of bile acids promotes generation of peripheral regulatory T cells', *Nature*, 581(7809), pp. 475–479. Available at: https://doi.org/10.1038/s41586-020-2193-0.

Cani, P.D. (2018) 'Human gut microbiome: hopes, threats and promises', *Gut*, 67(9), pp. 1716–1725. Available at: https://doi.org/10.1136/gutjnl-2018-316723.

Cariño, R. *et al.* (2022) 'The search for aliens within us: a review of evidence and theory regarding the foetal microbiome', *Critical Reviews in Microbiology*, 48(5), pp. 611–623. Available at: https://doi.org/10.1080/1040841X.2021.1999903.

Chen, L. *et al.* (2024) 'Interactions between toll-like receptors signaling pathway and gut microbiota in host homeostasis', *Immunity, Inflammation and Disease*, 12(7), p. e1356. Available at: https://doi.org/10.1002/iid3.1356.

Chen, W. *et al.* (2003) 'Conversion of Peripheral CD4+CD25− Naive T Cells to CD4+CD25+ Regulatory T Cells by TGF-β Induction of Transcription Factor *Foxp3*', *The Journal of Experimental Medicine*, 198(12), pp. 1875–1886. Available at: https://doi.org/10.1084/jem.20030152.

Chow, A. *et al.* (2009) 'The morbidity surrounding reversal of defunctioning ileostomies: a systematic review of 48 studies including 6,107 cases', *International Journal of Colorectal Disease*, 24(6), pp. 711–723. Available at: https://doi.org/10.1007/s00384-009-0660-z.

Christovich, A. and Luo, X.M. (2022) 'Gut Microbiota, Leaky Gut, and Autoimmune Diseases', *Frontiers in Immunology*, 13, p. 946248. Available at: https://doi.org/10.3389/fimmu.2022.946248.

Coombes, J.L. *et al.* (2007) 'A functionally specialized population of mucosal CD103+ DCs induces Foxp3+ regulatory T cells via a TGF-β– and retinoic acid–dependent mechanism', *The Journal of Experimental Medicine*, 204(8), pp. 1757–1764. Available at: https://doi.org/10.1084/jem.20070590.

Cox, M.J., Cookson, W.O.C.M. and Moffatt, M.F. (2013) 'Sequencing the human microbiome in health and disease', *Human Molecular Genetics*, 22(R1), pp. R88–R94. Available at: https://doi.org/10.1093/hmg/ddt398.

Cronin, P. *et al.* (2021) 'Dietary Fibre Modulates the Gut Microbiota', *Nutrients*, 13(5), p. 1655. Available at: https://doi.org/10.3390/nu13051655.

Crosnier, C., Stamataki, D. and Lewis, J. (2006) 'Organizing cell renewal in the intestine: stem cells, signals and combinatorial control', *Nature Reviews Genetics*, 7(5), pp. 349–359. Available at: https://doi.org/10.1038/nrg1840.

Cummings, R.J. *et al.* (2016) 'Different tissue phagocytes sample apoptotic cells to direct distinct homeostasis programs', *Nature*, 539(7630), pp. 565–569. Available at: https://doi.org/10.1038/nature20138.

David, L.A. *et al.* (2014) 'Diet rapidly and reproducibly alters the human gut microbiome', *Nature*, 505(7484), pp. 559–563. Available at: https://doi.org/10.1038/nature12820.

Delfini, M. *et al.* (2022) 'Macrophages in the gut: Masters in multitasking', *Immunity*, 55(9), pp. 1530–1548. Available at: https://doi.org/10.1016/j.immuni.2022.08.005.

Desai, M.S. *et al.* (2016) 'A Dietary Fiber-Deprived Gut Microbiota Degrades the Colonic Mucus Barrier and Enhances Pathogen Susceptibility', *Cell*, 167(5), pp. 1339-1353.e21. Available at: https://doi.org/10.1016/j.cell.2016.10.043.

Dominika, Ś. *et al.* (2011) 'The study on the impact of glycated pea proteins on human intestinal bacteria', *International Journal of Food Microbiology*, 145(1), pp. 267–272. Available at: https://doi.org/10.1016/j.ijfoodmicro.2011.01.002.

Donohoe, D.R. *et al.* (2011) 'The Microbiome and Butyrate Regulate Energy Metabolism and Autophagy in the Mammalian Colon', *Cell Metabolism*, 13(5), pp. 517–526. Available at: https://doi.org/10.1016/j.cmet.2011.02.018.

Duan, C. *et al.* (2023) 'Fucose promotes intestinal stem cell-mediated intestinal epithelial development through promoting *Akkermansia* -related propanoate metabolism', *Gut Microbes*, 15(1), p. 2233149. Available at: https://doi.org/10.1080/19490976.2023.2233149.

Duncan, S.H. *et al.* (2007) 'Reduced Dietary Intake of Carbohydrates by Obese Subjects Results in Decreased Concentrations of Butyrate and Butyrate-Producing Bacteria in Feces',

Applied and Environmental Microbiology, 73(4), pp. 1073–1078. Available at: https://doi.org/10.1128/AEM.02340-06.

El-Hussuna, A., Lauritsen, M. and Bülow, S. (2012) 'Relatively high incidence of complications after loop ileostomy reversal', *Danish Medical Journal*, 59(10), p. A4517.

Fan, Y. and Pedersen, O. (2021) 'Gut microbiota in human metabolic health and disease', *Nature Reviews Microbiology*, 19(1), pp. 55–71. Available at: https://doi.org/10.1038/s41579-020-0433-9.

Fernández López, F. *et al.* (2019) 'Stimulation the Efferent Limb Before Loop Ileostomy Closure With Short Chain Fatty Acids', *Cirugía Española (English Edition)*, 97(1), pp. 59–61. Available at: https://doi.org/10.1016/j.cireng.2018.12.004.

Ferrebee, C.B. and Dawson, P.A. (2015) 'Metabolic effects of intestinal absorption and enterohepatic cycling of bile acids', *Acta Pharmaceutica Sinica B*, 5(2), pp. 129–134. Available at: https://doi.org/10.1016/j.apsb.2015.01.001.

Foerster, E.G. *et al.* (2022) 'How autophagy controls the intestinal epithelial barrier', *Autophagy*, 18(1), pp. 86–103. Available at: https://doi.org/10.1080/15548627.2021.1909406.

Fu, Y., Lyu, J. and Wang, S. (2023) 'The role of intestinal microbes on intestinal barrier function and host immunity from a metabolite perspective', *Frontiers in Immunology*, 14, p. 1277102. Available at: https://doi.org/10.3389/fimmu.2023.1277102.

Gehart, H. and Clevers, H. (2019) 'Tales from the crypt: new insights into intestinal stem cells', *Nature Reviews Gastroenterology & Hepatology*, 16(1), pp. 19–34. Available at: https://doi.org/10.1038/s41575-018-0081-y.

Gill, S.K. *et al.* (2021) 'Dietary fibre in gastrointestinal health and disease', *Nature Reviews Gastroenterology & Hepatology*, 18(2), pp. 101–116. Available at: https://doi.org/10.1038/s41575-020-00375-4.

Girard-Madoux, M.J.H. *et al.* (2016) 'IL-10 control of CD11c+ myeloid cells is essential to maintain immune homeostasis in the small and large intestine', *Oncotarget*, 7(22), pp. 32015–32030. Available at: https://doi.org/10.18632/oncotarget.8337.

Gordon, H.A. and Pesti, L. (1971) 'The gnotobiotic animal as a tool in the study of host microbial relationships', *Bacteriological Reviews*, 35(4), pp. 390–429. Available at: https://doi.org/10.1128/br.35.4.390-429.1971.

Gustafsson, J.K. and Johansson, M.E.V. (2022) 'The role of goblet cells and mucus in intestinal homeostasis', *Nature Reviews Gastroenterology & Hepatology*, 19(12), pp. 785–803. Available at: https://doi.org/10.1038/s41575-022-00675-x.

Harries, R.L. *et al.* (2017) 'A systematic review of *Clostridium difficile* infection following reversal of ileostomy', *Colorectal Disease*, 19(10), pp. 881–887. Available at: https://doi.org/10.1111/codi.13873.

Hepworth, M.R. *et al.* (2013) 'Innate lymphoid cells regulate CD4+ T-cell responses to intestinal commensal bacteria', *Nature*, 498(7452), pp. 113–117. Available at: https://doi.org/10.1038/nature12240.

Hickey, J.W. *et al.* (2023) 'Organization of the human intestine at single-cell resolution', *Nature*, 619(7970), pp. 572–584. Available at: https://doi.org/10.1038/s41586-023-05915-x.

Hiippala, K. *et al.* (2018) 'The Potential of Gut Commensals in Reinforcing Intestinal Barrier Function and Alleviating Inflammation', *Nutrients*, 10(8), p. 988. Available at: https://doi.org/10.3390/nu10080988.

Hörmann, N. *et al.* (2014) 'Gut Microbial Colonization Orchestrates TLR2 Expression, Signaling and Epithelial Proliferation in the Small Intestinal Mucosa', *PLoS ONE*. Edited by A. Moschetta, 9(11), p. e113080. Available at: https://doi.org/10.1371/journal.pone.0113080.

Hou, Q. *et al.* (2018) 'Lactobacillus accelerates ISCs regeneration to protect the integrity of intestinal mucosa through activation of STAT3 signaling pathway induced by LPLs secretion of IL-22', *Cell Death & Differentiation*, 25(9), pp. 1657–1670. Available at: https://doi.org/10.1038/s41418-018-0070-2.

Johansson, M.E.V. *et al.* (2015) 'Normalization of Host Intestinal Mucus Layers Requires Long-Term Microbial Colonization', *Cell Host & Microbe*, 18(5), pp. 582–592. Available at: https://doi.org/10.1016/j.chom.2015.10.007.

Johansson-Lindbom, B. *et al.* (2005) 'Functional specialization of gut CD103 **+** dendritic cells in the regulation of tissue-selective T cell homing', *The Journal of Experimental Medicine*, 202(8), pp. 1063–1073. Available at: https://doi.org/10.1084/jem.20051100.

Kaiko, G.E. *et al.* (2016) 'The Colonic Crypt Protects Stem Cells from Microbiota-Derived Metabolites', *Cell*, 165(7), pp. 1708–1720. Available at: https://doi.org/10.1016/j.cell.2016.05.018.

Kamdar, K. *et al.* (2018) 'Innate Recognition of the Microbiota by TLR1 Promotes Epithelial Homeostasis and Prevents Chronic Inflammation', *The Journal of Immunology*, 201(1), pp. 230–242. Available at: https://doi.org/10.4049/jimmunol.1701216.

Kao, D. *et al.* (2014) 'Fecal Microbiota Transplantation Inducing Remission in Crohn's Colitis and the Associated Changes in Fecal Microbial Profile', *Journal of Clinical Gastroenterology*, 48(7), pp. 625–628. Available at: https://doi.org/10.1097/MCG.0000000000000131.

Keir, M.E. *et al.* (2020) 'The role of IL-22 in intestinal health and disease', *Journal of Experimental Medicine*, 217(3), p. e20192195. Available at: https://doi.org/10.1084/jem.20192195.

Khoruts, A. and Sadowsky, M.J. (2016) 'Understanding the mechanisms of faecal microbiota transplantation', *Nature Reviews Gastroenterology & Hepatology*, 13(9), pp. 508–516. Available at: https://doi.org/10.1038/nrgastro.2016.98.

Kim, C.H. (2009) 'FOXP3 and Its Role in the Immune System', in K. Maiese (ed.) *Forkhead Transcription Factors*. New York, NY: Springer New York (Advances in Experimental Medicine and Biology), pp. 17–29. Available at: https://doi.org/10.1007/978-1-4419-1599-3_2.

Klemashevich, C. *et al.* (2014) 'Rational identification of diet-derived postbiotics for improving intestinal microbiota function', *Current Opinion in Biotechnology*, 26, pp. 85–90. Available at: https://doi.org/10.1016/j.copbio.2013.10.006.

Kurashima, Y., Goto, Y. and Kiyono, H. (2013) 'Mucosal innate immune cells regulate both gut homeostasis and intestinal inflammation', *European Journal of Immunology*, 43(12), pp. 3108–3115. Available at: https://doi.org/10.1002/eji.201343782.

Kuugbee, E.D. *et al.* (2016) 'Structural Change in Microbiota by a Probiotic Cocktail Enhances the Gut Barrier and Reduces Cancer via TLR2 Signaling in a Rat Model of Colon Cancer', *Digestive Diseases and Sciences*, 61(10), pp. 2908–2920. Available at: https://doi.org/10.1007/s10620-016-4238-7.

Lamkanfi, M. and Dixit, V.M. (2012) 'Inflammasomes and Their Roles in Health and Disease', *Annual Review of Cell and Developmental Biology*, 28(1), pp. 137–161. Available at: https://doi.org/10.1146/annurev-cellbio-101011-155745.

LeBlanc, J.G. *et al.* (2013) 'Bacteria as vitamin suppliers to their host: a gut microbiota perspective', *Current Opinion in Biotechnology*, 24(2), pp. 160–168. Available at: https://doi.org/10.1016/j.copbio.2012.08.005.

Lee, S.Y. *et al.*) 'Dysbiosis of gut microbiota during fecal stream diversion in patients with colorectal cancer', *Gut Pathogens*, 15(1), p. 40. Available at: https://doi.org/10.1186/s13099-023-00566-9.

Lee, Y.-S. *et al.* (2018) 'Microbiota-Derived Lactate Accelerates Intestinal Stem-Cell-Mediated Epithelial Development', *Cell Host & Microbe*, 24(6), pp. 833-846.e6. Available at: https://doi.org/10.1016/j.chom.2018.11.002.

Lombard, V. *et al.* (2014) 'The carbohydrate-active enzymes database (CAZy) in 2013', *Nucleic Acids Research*, 42(D1), pp. D490–D495. Available at: https://doi.org/10.1093/nar/gkt1178.

Lynch, S.V. and Pedersen, O. (2016) 'The Human Intestinal Microbiome in Health and Disease', *New England Journal of Medicine*. Edited by E.G. Phimister, 375(24), pp. 2369–2379. Available at: https://doi.org/10.1056/NEJMra1600266.

Ma, H. *et al.* (2023) 'Dissecting the effect of ileal faecal diversion on the intestine using single-cell sequencing', *Clinical and Translational Medicine*, 13(7), p. e1321. Available at: https://doi.org/10.1002/ctm2.1321.

MacDonald, B.T., Tamai, K. and He, X. (2009) 'Wnt/β-Catenin Signaling: Components, Mechanisms, and Diseases', *Developmental Cell*, 17(1), pp. 9–26. Available at: https://doi.org/10.1016/j.devcel.2009.06.016.

Macfarlane, G.T. and Macfarlane, S. (2012) 'Bacteria, Colonic Fermentation, and Gastrointestinal Health', *Journal of AOAC INTERNATIONAL*, 95(1), pp. 50–60. Available at: https://doi.org/10.5740/jaoacint.SGE_Macfarlane.

Machiels, K. *et al.* (2014) 'A decrease of the butyrate-producing species *Roseburia hominis* and *Faecalibacterium prausnitzii* defines dysbiosis in patients with ulcerative colitis', *Gut*, 63(8), pp. 1275–1283. Available at: https://doi.org/10.1136/gutjnl-2013-304833.

Manichanh, C. *et al.* (2012) 'The gut microbiota in IBD', *Nature Reviews Gastroenterology & Hepatology*, 9(10), pp. 599–608. Available at: https://doi.org/10.1038/nrgastro.2012.152.

Marcelino, M. *et al.* (2023) 'Rectal stimulation with prebiotics and probiotics before ileostomy reversal: a study protocol for a randomized controlled trial', *Trials*, 24(1), p. 31. Available at: https://doi.org/10.1186/s13063-023-07065-x.

Marín, L. *et al.* (2015) 'Bioavailability of Dietary Polyphenols and Gut Microbiota Metabolism: Antimicrobial Properties', *BioMed Research International*, 2015, pp. 1–18. Available at: https://doi.org/10.1155/2015/905215.

Markandey, M. *et al.* (2021) 'Gut microbiota: sculptors of the intestinal stem cell niche in health and inflammatory bowel disease', *Gut Microbes*, 13(1), p. 1990827. Available at: https://doi.org/10.1080/19490976.2021.1990827.

Martyniak, A. *et al.* (2021) 'Prebiotics, Probiotics, Synbiotics, Paraprobiotics and Postbiotic Compounds in IBD', *Biomolecules*, 11(12), p. 1903. Available at: https://doi.org/10.3390/biom11121903.

Mayorgas, A., Dotti, I. and Salas, A. (2021) 'Microbial Metabolites, Postbiotics, and Intestinal Epithelial Function', *Molecular Nutrition & Food Research*, 65(5), p. 2000188. Available at: https://doi.org/10.1002/mnfr.202000188.

Mazmanian, S.K. *et al.* (2005) 'An Immunomodulatory Molecule of Symbiotic Bacteria Directs Maturation of the Host Immune System', *Cell*, 122(1), pp. 107–118. Available at: https://doi.org/10.1016/j.cell.2005.05.007.

McDole, J.R. *et al.* (2012) 'Goblet cells deliver luminal antigen to CD103+ dendritic cells in the small intestine', *Nature*, 483(7389), pp. 345–349. Available at: https://doi.org/10.1038/nature10863.

Menzel, A. *et al.* (2021) 'Common and Novel Markers for Measuring Inflammation and Oxidative Stress Ex Vivo in Research and Clinical Practice—Which to Use Regarding Disease Outcomes?', *Antioxidants*, 10(3), p. 414. Available at: https://doi.org/10.3390/antiox10030414.

MetaHIT Consortium *et al.* (2010) 'A human gut microbial gene catalogue established by metagenomic sequencing', *Nature*, 464(7285), pp. 59–65. Available at: https://doi.org/10.1038/nature08821.

Milani, C. *et al.* (2017) 'The First Microbial Colonizers of the Human Gut: Composition, Activities, and Health Implications of the Infant Gut Microbiota', *Microbiology and Molecular Biology Reviews*, 81(4), pp. e00036-17. Available at: https://doi.org/10.1128/MMBR.00036-17.

Morrison, H. *et al.* (2022) 'Diminished noncanonical NF-κB signaling induces colitis-associated colorectal cancer susceptibility upon de-differentiation of epithelial cells', *The Journal of Immunology*, 208(1_Supplement), p. 178.01-178.01. Available at: https://doi.org/10.4049/jimmunol.208.Supp.178.01.

Mu, C., Yang, Y. and Zhu, W. (2015) 'Crosstalk Between The Immune Receptors and Gut Microbiota', *Current Protein & Peptide Science*, 16(7), pp. 622–631. Available at: https://doi.org/10.2174/1389203716666150630134356.

Murphy, E.A., Velazquez, K.T. and Herbert, K.M. (2015) 'Influence of high-fat diet on gut microbiota: a driving force for chronic disease risk', *Current Opinion in Clinical Nutrition and Metabolic Care*, 18(5), pp. 515–520. Available at: https://doi.org/10.1097/MCO.0000000000000209.

Ni, J. *et al.* (2017) 'Gut microbiota and IBD: causation or correlation?', *Nature Reviews Gastroenterology & Hepatology*, 14(10), pp. 573–584. Available at: https://doi.org/10.1038/nrgastro.2017.88.

Nicholson, J.K. *et al.* (2012) 'Host-Gut Microbiota Metabolic Interactions', *Science*, 336(6086), pp. 1262–1267. Available at: https://doi.org/10.1126/science.1223813.

Ogino, T. and Takeda, K. (2023) 'Immunoregulation by antigen-presenting cells in human intestinal lamina propria', *Frontiers in Immunology*, 14, p. 1138971. Available at: https://doi.org/10.3389/fimmu.2023.1138971.

Östman, S. *et al.* (2006) 'Impaired regulatory T cell function in germ-free mice', *European Journal of Immunology*, 36(9), pp. 2336–2346. Available at: https://doi.org/10.1002/eji.200535244.

Pai, R., Tarnawski, A.S. and Tran, T. (2004) 'Deoxycholic Acid Activates β-Catenin Signaling Pathway and Increases Colon Cell Cancer Growth and Invasiveness', *Molecular Biology of the Cell*, 15(5), pp. 2156–2163. Available at: https://doi.org/10.1091/mbc.e03-12-0894.

Park, J.-H. *et al.* (2016) 'AhR activation by 6-formylindolo[3,2-b]carbazole and 2,3,7,8-tetrachlorodibenzo-p-dioxin inhibit the development of mouse intestinal epithelial cells', *Environmental Toxicology and Pharmacology*, 43, pp. 44–53. Available at: https://doi.org/10.1016/j.etap.2016.02.007.

Park, J.-H. *et al.* (2018) 'Indole-3-Carbinol Promotes Goblet-Cell Differentiation Regulating Wnt and Notch Signaling Pathways AhR-Dependently', *Molecules and Cells*, 41(4), pp. 290–300. Available at: https://doi.org/10.14348/molcells.2018.2167.

Park, J.I. *et al.* (2023) 'Intestinal Peyer's Patches: Structure, Function, and In Vitro Modeling', *Tissue Engineering and Regenerative Medicine*, 20(3), pp. 341–353. Available at: https://doi.org/10.1007/s13770-023-00543-y.

Penders, J. *et al.* (2006) 'Factors Influencing the Composition of the Intestinal Microbiota in Early Infancy', *Pediatrics*, 118(2), pp. 511–521. Available at: https://doi.org/10.1542/peds.2005-2824.

Perez-Lopez, A. *et al.* (2016) 'Mucosal immunity to pathogenic intestinal bacteria', *Nature Reviews Immunology*, 16(3), pp. 135–148. Available at: https://doi.org/10.1038/nri.2015.17.

Perler, B.K., Friedman, E.S. and Wu, G.D. (2023) 'The Role of the Gut Microbiota in the Relationship Between Diet and Human Health', *Annual Review of Physiology*, 85(1), pp. 449–468. Available at: https://doi.org/10.1146/annurev-physiol-031522-092054.

Peterson, L.W. and Artis, D. (2014) 'Intestinal epithelial cells: regulators of barrier function and immune homeostasis', *Nature Reviews Immunology*, 14(3), pp. 141–153. Available at: https://doi.org/10.1038/nri3608.

Pinto, D. *et al.* (2003) 'Canonical Wnt signals are essential for homeostasis of the intestinal epithelium', *Genes & Development*, 17(14), pp. 1709–1713. Available at: https://doi.org/10.1101/gad.267103.

Podolsky, D.K. *et al.* (2009) 'Colitis-Associated Variant of TLR2 Causes Impaired Mucosal Repair Because of TFF3 Deficiency', *Gastroenterology*, 137(1), pp. 209–220. Available at: https://doi.org/10.1053/j.gastro.2009.03.007.

Rakoff-Nahoum, S. *et al.* (2004) 'Recognition of Commensal Microflora by Toll-Like Receptors Is Required for Intestinal Homeostasis', *Cell*, 118(2), pp. 229–241. Available at: https://doi.org/10.1016/j.cell.2004.07.002.

Ramanan, D. *et al.* (2020) 'An Immunologic Mode of Multigenerational Transmission Governs a Gut T_{reg} Setpoint', *Cell*, 181(6), pp. 1276-1290.e13. Available at: https://doi.org/10.1016/j.cell.2020.04.030.

Rinninella, E. *et al.* (2019a) 'What is the Healthy Gut Microbiota Composition? A Changing Ecosystem across Age, Environment, Diet, and Diseases', *Microorganisms*, 7(1), p. 14. Available at: https://doi.org/10.3390/microorganisms7010014.

Rinninella, E. *et al.* (2019b) 'What is the Healthy Gut Microbiota Composition? A Changing Ecosystem across Age, Environment, Diet, and Diseases', *Microorganisms*, 7(1), p. 14. Available at: https://doi.org/10.3390/microorganisms7010014.

Rock, S.A. *et al.* (2022) 'Neurotensin Regulates Proliferation and Stem Cell Function in the Small Intestine in a Nutrient-Dependent Manner', *Cellular and Molecular Gastroenterology and Hepatology*, 13(2), pp. 501–516. Available at: https://doi.org/10.1016/j.jcmgh.2021.09.006.

Rodríguez-Padilla, Á. *et al.* (2021) 'Postoperative Ileus after Stimulation with Probiotics before Ileostomy Closure', *Nutrients*, 13(2), p. 626. Available at: https://doi.org/10.3390/nu13020626.

Rombey, T. *et al.* (2019) 'Preoperative bowel stimulation prior to ileostomy closure to restore bowel function more quickly and improve postoperative outcomes: a systematic review', *Colorectal Disease*, 21(9), pp. 994–1003. Available at: https://doi.org/10.1111/codi.14636.

Rose, E.C. *et al.* (2021) 'Probiotics, Prebiotics and Epithelial Tight Junctions: A Promising Approach to Modulate Intestinal Barrier Function', *International Journal of Molecular Sciences*, 22(13), p. 6729. Available at: https://doi.org/10.3390/ijms22136729.

Rosenberg, E. (2024) 'Diversity of bacteria within the human gut and its contribution to the functional unity of holobionts', *npj Biofilms and Microbiomes*, 10(1), p. 134. Available at: https://doi.org/10.1038/s41522-024-00580-y.

Ruane, D.T. and Lavelle, E.C. (2011) 'The Role of CD103+ Dendritic Cells in the Intestinal Mucosal Immune System', *Frontiers in Immunology*, 2. Available at: https://doi.org/10.3389/fimmu.2011.00025.

Saffarian, A. *et al.* (2019) 'Crypt- and Mucosa-Associated Core Microbiotas in Humans and Their Alteration in Colon Cancer Patients', *mBio*. Edited by J. Parkhill, 10(4), pp. e01315-19. Available at: https://doi.org/10.1128/mBio.01315-19.

Sam, S.W. *et al.* (2024) 'The impact of faecal diversion on the gut microbiome: a systematic review', *Gut Microbiome*, 5, p. e4. Available at: https://doi.org/10.1017/gmb.2024.1.

Sánchez-Cerrillo, I. *et al.* (2023) 'MICA /b-dependent activation of natural killer cells by $CD64^{+}$ inflammatory type 2 dendritic cells contributes to autoimmunity', *The EMBO Journal*, 42(23), p. e113714. Available at: https://doi.org/10.15252/embj.2023113714.

Sartor, R.B. (2006) 'Mechanisms of Disease: pathogenesis of Crohn's disease and ulcerative colitis', *Nature Clinical Practice Gastroenterology & Hepatology*, 3(7), pp. 390–407. Available at: https://doi.org/10.1038/ncpgasthep0528.

Schären, O.P. and Hapfelmeier, S. (2021) 'Robust microbe immune recognition in the intestinal mucosa', *Genes & Immunity*, 22(5–6), pp. 268–275. Available at: https://doi.org/10.1038/s41435-021-00131-x.

Sefik, E. *et al.* (2015) 'Individual intestinal symbionts induce a distinct population of $ROR\gamma^{+}$ regulatory T cells', *Science*, 349(6251), pp. 993–997. Available at: https://doi.org/10.1126/science.aaa9420.

Semin, I. *et al.* (2021) 'Interplay Between Microbiota, Toll-Like Receptors and Cytokines for the Maintenance of Epithelial Barrier Integrity', *Frontiers in Medicine*, 8, p. 644333. Available at: https://doi.org/10.3389/fmed.2021.644333.

Shamjana, U. *et al.* (2024) 'The role of insect gut microbiota in host fitness, detoxification and nutrient supplementation', *Antonie van Leeuwenhoek*, 117(1), p. 71. Available at: https://doi.org/10.1007/s10482-024-01970-0.

Sherman, K. and Wexner, S. (2017) 'Considerations in Stoma Reversal', *Clinics in Colon and Rectal Surgery*, 30(03), pp. 172–177. Available at: https://doi.org/10.1055/s-0037-1598157.

Sniffen, J.C. *et al.* (2018) 'Choosing an appropriate probiotic product for your patient: An evidence-based practical guide', *PLOS ONE*. Edited by L.A. Lobo, 13(12), p. e0209205. Available at: https://doi.org/10.1371/journal.pone.0209205.

Sodhi, C.P. *et al.* (2012) 'Intestinal Epithelial Toll-Like Receptor 4 Regulates Goblet Cell Development and Is Required for Necrotizing Enterocolitis in Mice', *Gastroenterology*, 143(3), pp. 708-718.e5. Available at: https://doi.org/10.1053/j.gastro.2012.05.053.

Sommer, K. *et al.* (2021) 'Intestinal Mucosal Wound Healing and Barrier Integrity in IBD–Crosstalk and Trafficking of Cellular Players', *Frontiers in Medicine*, 8, p. 643973. Available at: https://doi.org/10.3389/fmed.2021.643973.

Sorrentino, G. *et al.* (2020) 'Bile Acids Signal via TGR5 to Activate Intestinal Stem Cells and Epithelial Regeneration', *Gastroenterology*, 159(3), pp. 956-968.e8. Available at: https://doi.org/10.1053/j.gastro.2020.05.067.

Spehlmann, M.E. and Eckmann, L. (2009) 'Nuclear factor-kappa B in intestinal protection and destruction':, *Current Opinion in Gastroenterology*, 25(2), pp. 92–99. Available at: https://doi.org/10.1097/MOG.0b013e328324f857.

Spits, H. and Cupedo, T. (2012) 'Innate Lymphoid Cells: Emerging Insights in Development, Lineage Relationships, and Function', *Annual Review of Immunology*, 30(1), pp. 647–675. Available at: https://doi.org/10.1146/annurev-immunol-020711-075053.

Suez, J. *et al.* (2019) 'The pros, cons, and many unknowns of probiotics', *Nature Medicine*, 25(5), pp. 716–729. Available at: https://doi.org/10.1038/s41591-019-0439-x.

Sun, C.-Y. *et al.* (2023) 'T helper 17 (Th17) cell responses to the gut microbiota in human diseases', *Biomedicine & Pharmacotherapy*, 161, p. 114483. Available at: https://doi.org/10.1016/j.biopha.2023.114483.

Taavela, J. *et al.* (2013) 'Validation of Morphometric Analyses of Small-Intestinal Biopsy Readouts in Celiac Disease', *PLoS ONE*. Edited by K. Sestak, 8(10), p. e76163. Available at: https://doi.org/10.1371/journal.pone.0076163.

Tailford, L.E. *et al.* (2015) 'Mucin glycan foraging in the human gut microbiome', *Frontiers in Genetics*, 6. Available at: https://doi.org/10.3389/fgene.2015.00081.

Tait Wojno, E.D. and Artis, D. (2012) 'Innate Lymphoid Cells: Balancing Immunity, Inflammation, and Tissue Repair in the Intestine', *Cell Host & Microbe*, 12(4), pp. 445–457. Available at: https://doi.org/10.1016/j.chom.2012.10.003.

Takahashi, T. and Shiraishi, A. (2020) 'Stem Cell Signaling Pathways in the Small Intestine', *International Journal of Molecular Sciences*, 21(6), p. 2032. Available at: https://doi.org/10.3390/ijms21062032.

Takiishi, T., Fenero, C.I.M. and Câmara, N.O.S. (2017) 'Intestinal barrier and gut microbiota: Shaping our immune responses throughout life', *Tissue Barriers*, 5(4), p. e1373208. Available at: https://doi.org/10.1080/21688370.2017.1373208.

Tao, R. *et al.* (2007) 'Deacetylase inhibition promotes the generation and function of regulatory T cells', *Nature Medicine*, 13(11), pp. 1299–1307. Available at: https://doi.org/10.1038/nm1652.

Thursby, E. and Juge, N. (2017) 'Introduction to the human gut microbiota', *Biochemical Journal*, 474(11), pp. 1823–1836. Available at: https://doi.org/10.1042/BCJ20160510.

Tominaga, K. *et al.* (2018) 'Diversion colitis and pouchitis: A mini-review', *World Journal of Gastroenterology*, 24(16), pp. 1734–1747. Available at: https://doi.org/10.3748/wjg.v24.i16.1734.

Tominaga, K. *et al.* (2024) 'An updated review on the treatment for diversion colitis and pouchitis, with a focus on the utility of autologous fecal microbiota transplantation and its relationship with the intestinal microbiota', *Bioscience of Microbiota, Food and Health*, 43(3), pp. 162–169. Available at: https://doi.org/10.12938/bmfh.2024-014.

Tremlett, H. *et al.* (2017) 'The gut microbiome in human neurological disease: A review', *Annals of Neurology*, 81(3), pp. 369–382. Available at: https://doi.org/10.1002/ana.24901.

Turnbaugh, P.J. *et al.* (2006) 'An obesity-associated gut microbiome with increased capacity for energy harvest', *Nature*, 444(7122), pp. 1027–1031. Available at: https://doi.org/10.1038/nature05414.

Turnbaugh, P.J. *et al.* (2009) 'The Effect of Diet on the Human Gut Microbiome: A Metagenomic Analysis in Humanized Gnotobiotic Mice', *Science Translational Medicine*, 1(6). Available at: https://doi.org/10.1126/scitranslmed.3000322.

Van Es, J.H. *et al.* (2005) 'Notch/γ-secretase inhibition turns proliferative cells in intestinal crypts and adenomas into goblet cells', *Nature*, 435(7044), pp. 959–963. Available at: https://doi.org/10.1038/nature03659.

Verma, R. *et al.* (2018) 'Cell surface polysaccharides of *Bifidobacterium bifidum* induce the generation of Foxp3$^+$ regulatory T cells', *Science Immunology*, 3(28), p. eaat6975. Available at: https://doi.org/10.1126/sciimmunol.aat6975.

Wang, J.-W. *et al.* (2019) 'Fecal microbiota transplantation: Review and update', *Journal of the Formosan Medical Association*, 118, pp. S23–S31. Available at: https://doi.org/10.1016/j.jfma.2018.08.011.

Williams, L. *et al.* (2007) 'The effect of faecal diversion on human ileum', *Gut*, 56(6), pp. 796–801. Available at: https://doi.org/10.1136/gut.2006.102046.

Wu, H. *et al.* (2024) 'Host-microbiota interaction in intestinal stem cell homeostasis', *Gut Microbes*, 16(1), p. 2353399. Available at: https://doi.org/10.1080/19490976.2024.2353399.

Xu, M. *et al.* (2019) 'Author Correction: c-MAF-dependent regulatory T cells mediate immunological tolerance to a gut pathobiont', *Nature*, 566(7744), pp. E7–E7. Available at: https://doi.org/10.1038/s41586-019-0922-z.

Yin, X. *et al.* (2014) 'Niche-independent high-purity cultures of Lgr5+ intestinal stem cells and their progeny', *Nature Methods*, 11(1), pp. 106–112. Available at: https://doi.org/10.1038/nmeth.2737.

Zeng, H. *et al.* (2019) 'Secondary Bile Acids and Short Chain Fatty Acids in the Colon: A Focus on Colonic Microbiome, Cell Proliferation, Inflammation, and Cancer', *International Journal of Molecular Sciences*, 20(5), p. 1214. Available at: https://doi.org/10.3390/ijms20051214.

Zhao, J. *et al.* (2018) 'Dietary Protein and Gut Microbiota Composition and Function', *Current Protein & Peptide Science*, 20(2), pp. 145–154. Available at: https://doi.org/10.2174/1389203719666180514145437.

Zheng, Y. *et al.* (2008) 'Interleukin-22 mediates early host defense against attaching and effacing bacterial pathogens', *Nature Medicine*, 14(3), pp. 282–289. Available at: https://doi.org/10.1038/nm1720.

Zmora, N., Suez, J. and Elinav, E. (2019) 'You are what you eat: diet, health and the gut microbiota', *Nature Reviews Gastroenterology & Hepatology*, 16(1), pp. 35–56. Available at: https://doi.org/10.1038/s41575-018-0061-2.

Żółkiewicz, J. *et al.* (2020) 'Postbiotics—A Step Beyond Pre- and Probiotics', *Nutrients*, 12(8), p. 2189. Available at: https://doi.org/10.3390/nu12082189.

Zundler, S. *et al.* (2019) 'Immune cell trafficking and retention in inflammatory bowel disease: mechanistic insights and therapeutic advances', *Gut*, 68(9), pp. 1688–1700. Available at: https://doi.org/10.1136/gutjnl-2018-317977.